Universidade do Minho
Escola de Engenharia

Maria João Mogadouro Lopes

Bioinformatics approaches for engineering *L*-tyrosine production in *Escherichia coli*

março de 2022

Bioinformatics approaches for engineering *L*-tyrosine production in *Escherichia coli*
Maria João Lopes
UMinho | 2022

Universidade do Minho
Escola de Engenharia

Maria João Mogadouro Lopes

Bioinformatics approaches for engineering *L*-tyrosine production in *Escherichia coli*

Dissertação de Mestrado
Mestrado em Bioinformática

Trabalho efetuado sob a orientação do
Doutor Óscar Manuel Lima Dias
e da
Doutora Joana Lúcia Lima Correia Rodrigues

março de 2022

DIREITOS DE AUTOR E CONDIÇÕES DE UTILIZAÇÃO DO TRABALHO POR TERCEIROS

Este é um trabalho académico que pode ser utilizado por terceiros desde que respeitadas as regras e boas práticas internacionalmente aceites, no que concerne aos direitos de autor e direitos conexos.

Assim, o presente trabalho pode ser utilizado nos termos previstos na licença abaixo indicada.

Caso o utilizador necessite de permissão para poder fazer um uso do trabalho em condições não previstas no licenciamento indicado, deverá contactar o autor, através do RepositóriUM da Universidade do Minho.

Licença concedida aos utilizadores deste trabalho

Atribuição

CC BY

https://creativecommons.org/licenses/by/4.0/

Acknowledgments

The elaboration of this work would not have been possible without the help and encouragement of several people. I would therefore like to express all my gratitude and appreciation to all of those who contributed to making this task easier.

Firstly, I want to thank my supervisors, Doctor Oscar Dias and Doctor Joana Rodrigues, for their support, motivation, and all the knowledge shared. Thank you for all your guidance and help provided that were essential for the resolution of this dissertation. A special thanks to Alexandre Oliveira and Fernando Cruz for always answering my many doubts.

To all my friends, these past six years would not have been the same without you. To Cenas – Dri, Lobo, Guida, Lobo, Lota, Mass, Rafa e Tina – I hope this friendship never ends, to many more existential crises together. To Tias – Dani, Lena, Sara e Tisco – thank you for all your advice. To Beny and Carol for always being there to make me laugh. And finally, my ride or die, Alexandra e Bárbara, thanks for being there for as long as I can remember, to many more concerts, sleepovers and trips.

I would also like to thank my psychologist for helping me tame my anxiety through this really hard process. On that note, thank you to music and books for being my escapism in the hardest moments.

Lastly, to my parents, for always being there, for being hard on me to never settle for less, for teaching me to never give up, and for all the patience and support shown during my most anxious periods. These were, by far, the hardest couple of years of my life, and it would not have been possible without you. Thank you to the rest of my family for all the care and concern. And, to my grandparents, thank you for being my guardian angels, wherever you are, I hope I made you proud.

STATEMENT OF INTEGRITY

I hereby declare having conducted this academic work with integrity. I confirm that I have not used plagiarism or any form of undue use of information or falsification of results along the process leading to its elaboration.

I further declare that I have fully acknowledged the Code of Ethical Conduct of the University of Minho.

RESUMO

Abordagens bioinformáticas para engenharia da produção de *L*-tirosina em *Escherichia coli*

A *L*-tirosina (*L*-Tyr) tem sido considerada um metabolito apelativo devido à sua ampla variedade de aplicações nas indústrias farmacêutica e química. Este metabolito é um importante precursor de vários metabolitos secundários ou produtos naturais. Estes compostos têm várias propriedades úteis, incluindo antioxidante, anti-inflamatória, anticancerígena, antiviral e antidepressiva. Há vários estudos onde são utilizadas estirpes de *Escherichia coli (E. coli)* sobre-produtoras de *L*-Tyr, mas ainda é necessário aumentar o seu rendimento para tornar o bioprocesso economicamente viável.

Numerosas ferramentas computacionais têm sido desenvolvidas para a conceção de estirpes que identificam estratégias de modificação genética que aumentam a produção de bioquímicos. A construção de um mapa metabólico, e o desenvolvimento de modelos matemáticos e simulações que reproduzem dados experimentais e fenótipos em diferentes condições, permitem o desenho de células com apoio da computação. Os modelos cinéticos contêm um sistema de equações diferenciais que descrevem a evolução temporal das concentrações metabólicas, atividades enzimáticas e fluxos de reação, logo têm a capacidade de captar estas interdependências.

O objetivo deste trabalho foi realizar a inserção *in silico* da via de *L*-Tyr num modelo cinético do metabolismo do carbono central de *E. coli*, o que permitiu identificar os melhores genes alvo para o desenho da estirpe de sobreprodução de *L*-Tyr. Três modelos estequiométricos (iML1515, iJO1366 e iJR904), bem como três modelos cinéticos (Millard, Oliveira e Jahan), foram utilizados para desenhar um modelo cinético que contivesse todas as reações necessárias para produzir *L*-Tyr. Este novo modelo foi, então, utilizado para testar diferentes estratégias de deleção e sobre-expressão para conceber uma estirpe sobre-produtora de *L*-Tyr de *E. coli*.

Com o intuito de desenhar uma estirpe super-produtora de *L*-Tyr, foram utilizadas duas abordagens. Na primeira abordagem, os alvos obtidos pelo Metabolic Course Analysis (MCA) não melhoraram significativamente a produção de *L*-Tyr. Na segunda abordagem foram estudadas a via de produção de *L*-Tyr, bem como diferentes estratégias descritas em literatura que melhoram a produção de *L*-Tyr. Foi possível confirmar que a sobre-expressão dos genes limitadores de fluxo *aroG*, *aroE*, *aroL*, *tyrA* e *tyrB* melhora a produção de L-Tyr.

PALAVRAS-CHAVE

Engenharia Metabólica, *L*-Tirosina, *Escherichia coli*, Modelos Cinéticos, Desenho de Estirpes

ABSTRACT

Bioinformatics approaches for engineering *L*-tyrosine production in *Escherichia coli*

L-tyrosine (*L*-Tyr) has been considered an appealing metabolite due to its wide variety of applications in the pharmaceutical and chemical industries. This metabolite is an essential precursor of various secondary metabolites or natural products. These compounds have various valuable properties, including antioxidant, anti-inflammatory, anti-cancer, antiviral, and anti-depressant. There are several studies where *Escherichia coli (E. coli) L*-Tyr overproducing strains are used, but there is still a need to increase its yield to make the bioprocess economically feasible.

Numerous computational tools have been developed for strain design to identify genetic modification strategies that increase targeted biochemical production. The construction of a biochemical network map, and the development of mathematical models and simulations that reproduce experimental data and phenotypes under different conditions, allow computer-aided cell design. Kinetic models yield a system of ordinary differential equations that describe the time evolution of metabolite concentrations, enzyme activities, and reaction fluxes, therefore potentially capturing these interdependencies.

The aim of this work was to perform the *in silico* insertion of *L*-Tyr pathway in a kinetic model of the central carbon metabolism of *E. coli*, and to identify the best target genes for the design of the *L*-Tyr overproducing strain. Three stoichiometric models (iML1515, iJO1366 and iJR904) and three kinetic models (Millard, Oliveira and Jahan) were used to design an accurate model containing all the necessary reactions to produce *L*-Tyr. The new model was then used to test the different knock-in/out strategies to design an *E. coli L*-Tyr overproducing strain.

In order to design an *L*-Tyr overproducing strain, two optimisation approaches were conducted. In the first approach, the targets obtained in the Metabolic Course Analysis (MCA) did not improve the *L*-Tyr production significantly. In the second approach, the *L*-Tyr production pathway and different strategies described in the literature to improve *L*-Tyr production were tested. It was possible to confirm that the overexpression of rate-limiting genes *aroG*, *aroE*, *aroL*, *tyrA* and *tyrB* improve *L*-Tyr production.

KEYWORDS

Metabolic Engineering, *L*-tyrosine, *Escherichia coli*, Kinetic Models, Strain Design

ÍNDICE

FIGURES INDEX

TABLE INDEX

List of Abbreviations and Acronyms

α-KG	α – Ketoglutarate
AAA	Aromatic Amino Acids
ADP	Adenosine Diphosphate
AroA	5-Enolpyruvylshikimate-3-Phosphate Synthase
AroB	2,4-Dihydroxyquinoline Synthase
AroC	Chorismate Synthase
AroD	2,4-Dihydroxyquinoline Dehydratase
AroE	Shikimate Dehydrogenase
AroG/F/H	3-Deoxy-D-Arabino-Heptulosonic Acid 7-Phosphate Synthase
AroK/L	Shikimate Kinase I/II
ATP	Adenosine Triphosphate
BiGG	Biochemically, Genetically, And Genomically
BPCY	Biomass-Product Coupled Yield
BROs	Biochemical Reaction Operators
CCM	Central Carbon Metabolism
CDRP	1-(2-carboxyphenylamino)-1-deoxy-D-nbulose-5-phosphate
CO_2	Carbon Dioxide
COBRA	COnstraint-Based Reconstruction and Analysis
DAHP	3-Deoxy-D-Arabino-Heptulosonic Acid 7-Phosphate
DHQ	3-Dehydroquinate
E. coli	*Escherichia coli*
EA	Evolutionary Algorithms
E4P	Erythrose 4-Phosphate
EPSP	5-Enolpyruvylshikimate-3-Phosphate

FBA	Flux-Balance Analysis
fbr	Feedback Resistant
FCC	Flux Control Coefficients
FVA	Flux Variability Analysis
G3pP	Glycerol-3-Phosphate Phosphatase
GLC	Glucose
GluD	L-Glutamate Dehydrogenase
GSM	Genome-Scale Metabolic
H_2O	Water
HT	High-Throughput
I3GP	Indole 3-Glycerolphosphate
KEGG	Kyoto Encyclopedia of Genes and Genomes
L-DOPA	3,4-Dihydroxy-L-Phenylalanine
L-Glu	Glutamic Acid
L-Phe	*L*-Phenylalanine
L-Trp	*L*-Tryptophan
L-Tyr	*L*-Tyrosine
LSODA	Solver for Ordinary Differential Equations
LSODAR	Ordinary Differential Equation Solver for Stiff or Non-Stiff System with root-finding
LSODE	Livermore Solver of Ordinary Differential Equations
MA	Mass Action
MAGE	Multiplex Automated Genome Engineering
MCA	Metabolic Control Analysis
MM	Michaelis–Menten
MOMA	Minimization of Metabolic Adjustment

MQO	Malate Quinone Oxidoreductase
NADP	Nicotinamide Adenine Dinucleotide Phosphate
NADPH	Nicotinamide Adenine Dinucleotide Phosphate (reduced)
ODEs	Ordinary Differential Equations
P	Phosphate
PEP	Phosphoenolpyruvate
pFBA	Parsimonious FBA
PheA	Chorismate Mutase - *p* - Prephenate Dehydratase
PP	Pentose Phosphate
PpsA	Phosphoenolpyruvate Synthase
PRAA	n-(5-phospho-β-D-nbosylanthranilate)
PTS	Phosphotransferase System
PYR	Pyruvate
RL	Rate Law
SA	Simulated Annealing
TCA	Tricarboxylic Acid
TktA	Transketolase A
TyrA	Mutase/Prephenate Dehydrogenase
TyrB	Tyrosine Amino-Transferase
TyrR	Tyrosine Repressor
X	Biomass
X5P	Xylulose 5-Phosphate
YdiB	Quinate/Shikimate Dehydrogenase
YIELD	Product Yield with Minimum Biomass

1. INTRODUCTION

1.1 Context and Motivation

Aromatic compounds, such as aromatic amino acids (AAA), petrochemical aromatics, and aromatic polymers, are very important industrial materials. Among them, *L*-tyrosine (*L*-Tyr) has been considered an appealing metabolite to produce due to its wide variety of applications in the pharmaceutical and chemical industries. This metabolite is an important precursor of a diverse number of secondary metabolites or natural products, such as phenylpropanoic acids, benzylisoquinoline alkaloids, flavonoids, curcuminoids, stilbenoids, Parkinson's disease drug 3,4-dihydroxy-L-phenylalanine (L-DOPA) and melanin (Cox & Nelson, 2017; Hernández-Chávez et al., 2019; Kang et al., 2012; Kim et al., 2018; Machado et al., 2014; Menéndez-Perdomo & Facchini, 2018; Rodrigues et al., 2020; Rodrigues, Araújo, et al., 2015; Rodrigues, Prather, et al., 2015; Rodriguez et al., 2014). Several of *L*-Tyr' s derivatives have drawn increased interest due to their useful properties. Phenylpropanoic acids have shown antioxidant, anti-inflammatory, anti-cancer, antiviral, anti-diabetic, and anti-depressant properties (Hernández-Chávez et al., 2019; Rodrigues, Araújo, et al., 2015). Another example are the benzylisoquinoline alkaloids with the evidence of anti-cancer, anti-arrhythmic, anti-HIV, and anti-malarial properties (Menéndez-Perdomo & Facchini, 2018). Curcuminoids also show several beneficial biological activities, including anti-cancer, antioxidant, anti-inflammatory, and antitumor activities (Machado et al., 2014; Rodrigues et al., 2020; Rodrigues, Prather, et al., 2015).

L-Tyr can be synthesised in animals and in plants and bacteria (Cox & Nelson, 2017). However, *Escherichia coli* (*E. coli)* has been shown to be a more cost effective microbial cell factory for recombinant proteins (Rosano et al., 2019). There are several studies where *E. coli L*-Tyr overproducing strains are used, but there is still a need to increase its yield to make the bioprocess economically feasible, as it is observed in the bioprocesses used to synthesise other amino acids (Juminaga et al., 2012; Kim et al., 2018). This optimisation of *L*-Tyr production can be beneficial for the increase of microbial production of many of *L*-Tyr' s derivatives, like caffeic acid and curcuminoids.

Numerous computational tools have been developed for strain design that identify genetic modification strategies that increase targeted biochemicals production (Khodayari et al., 2014). The construction of a biochemical network map, and the development of mathematical models and simulations that reproduce experimental data and phenotypes under different conditions, allow computer-aided cell design (Jahan et al., 2016). Stoichiometric models alone cannot quantitatively measure the effect of concentration levels, enzyme saturation and regulation. Kinetic models yield a system of ordinary

differential equations that describe the time evolution of metabolite concentrations, enzyme activities and reaction fluxes, therefore these interdependencies can be detected (Khodayari et al., 2014, 2015). These types of models can be used to model mutant *E. coli* strains to overproduce *L*-Tyr in a more sustainable and economic manner.

1.2 Goals

The main goal of this thesis was to design an *E. coli* strain that overproduces *L*-Tyr and that could be further used to test the production of other compounds using a known heterologous pathway (e.g., as caffeic acid or curcuminoids) (Hernández-Chávez et al., 2019; Kang et al., 2015; Kim et al., 2018; Rodrigues, Araújo, et al., 2015; Rodrigues, Prather, et al., 2015).

More specifically, this work aimed to:

- Study and understand the *E. coli* metabolism, focusing on the metabolic pathway for *L*-Tyr production;
- Study the impact of certain variables in parameter determination for *in silico* modelling;
- Insert the *L*-Tyr and *L*-Phe pathways into a kinetic model of the central carbon metabolism of *E. coli* and do *in silico* modelling of the *L*-Tyr pathway;
- Identify the best target genes for the design of the *L*-Tyr overproducing strain, including the ones already reported in the literature;
- Optimise the model to allow the highest production of *L*-Tyr.

1.3 Thesis Outline

To address the above-mentioned objectives, this thesis has been structured in 7 chapters:

- **Chapter 1 – Introduction** (Current chapter)
  - This chapter includes a brief mention of the importance of *L*-Tyr and reference to the current demand for more sustainable and economic processes using microbial cell factories and how kinetic modelling can aid in its design. The main motivation for this work is highlighted, and the goals and structure of this thesis are further referenced.

- **Chapter 2 – State of the Art**
  - In chapter 2 the biological relevance of *L*-Tyr, its metabolic pathway and known strategies for its overproduction were revised. In addition, a comprehensive review of metabolic engineering was conducted, touching the basis of systems biology, systems metabolic

engineering, and bioinformatic tools for metabolic modelling. The importance of *E. coli* as a cell factory and the available stoichiometric and kinetic models for this microorganism were reviewed.

- **Chapter 3 – Materials and Methods**
  - This chapter includes a brief overview of the selected model and description of the reactions that need to be inserted into the model and their kinetics, as well information regarding parameter determination. The way time course simulations were performed once the model was assembled is also explained.

- **Chapter 4 – Results and Discussion**
  - In chapter 4 it is included the presentation and discussion of the results obtained through V_{max} calculation, *in silico* simulations of AA production, and comparison with published results for *in vivo* production, and *in silico* optimization of AA yields using the methods that were described in chapter 3.

- **Chapter 5 – Conclusion and Future Perspectives**
  - Finally, chapter 5 presents the conclusions retrieved from the work developed in this thesis and some prospects for future work.

2. State of the Art

2.1 *L* – Tyrosine

Amino acids are relatively simple monomeric subunits that provide the key to thousands of different proteins' structure. There are 20 amino acids and this group of precursor molecules may be seen as the alphabet in which the language of protein structure is written (Cox & Nelson, 2017). These monomers are α-amino acids, with a carboxyl group and an amino group bonded to the same carbon atom. The 20 amino acids differ between them in their side chains (R group), making them vary in structure, size, and electric charge and influence their solubility and chemical properties (Cox & Nelson, 2017).

L-Tyr is considered a conditionally essential amino acid in animals because it can be synthesised from the essential amino acid phenylalanine (*L*-Phe). But, to some degree, it is required in young, growing animals and/or sometimes during illness. As *L*-Tyr has an aromatic R group, it is relatively nonpolar (hydrophobic), and its hydroxyl group makes it significantly more polar than other amino acids with a similar side chain. *L*-Tyr is both a ketogenic and a glucogenic amino acid, having the ability to form ketone bodies in the liver and to be converted to glucose and glycogen (Cox & Nelson, 2017)

The pathway to synthesise *L*-Tyr is different in animals and in plants and bacteria. Animals are able to yield *L*-Tyr directly from *L*-Phe, through hydroxylation at C-4 of the phenyl group by phenylalanine hydroxylase. As for its production in plants and bacteria, both *L*-Tyr and *L*-Phe are synthesised from chorismate, by the common intermediate, prephenate. *L*-tryptophan (*L*-Trp) also is synthesised by chorismite, but in a more complex pathway (Cox & Nelson, 2017).

As previously mentioned, *L*-Tyr has been considered an interesting metabolite, thanks to its broad variety of applications in the pharmaceutical and chemical industries. This metabolite is an important precursor of a diverse number of secondary metabolites or natural products. In plants, one of many compounds produced from *L*-Tyr is the rigid polymer lignin, the second most abundant compound in plant tissues. In animals, some neurotransmitters are synthesised from *L*-Tyr, including epinephrine, norepinephrine, and dopamine. Morphine, a metabolite of the class of benzylisoquinoline alkaloids is also derived from *L*- Tyr (Cox & Nelson, 2017; Hernández-Chávez et al., 2019; Kang et al., 2012; Kim et al., 2018; Machado et al., 2014; Menéndez-Perdomo & Facchini, 2018; Rodrigues et al., 2020; Rodrigues, Araújo, et al., 2015; Rodrigues, Prather, et al., 2015; Rodriguez et al., 2014).

In Table 2.1, the names of the metabolites produced from *L*-Tyr and their respective properties and applications are summarised.

Table 2.1 – Summary of some metabolites that derive from L-Tyr and their respective properties and applications

Class	Compound Examples	Properties and Applications	References
Phenylpropanoic Acids	Caffeic Acid	Antioxidant, Anti-Inflammatory, Anti-Cancer, Antiviral, Anti-Diabetic and Anti-Depressant	(Hernández-Chávez et al., 2019; Rodrigues, Araújo, et al., 2015)
Benzylisoquinoline Alkaloids	Morphine, Noscapine, Glaucine	Anti-Cancer, Anti-Arrhythmic, Anti-HIV, Anti-Malarial, Narcotic Analgesic	(Menéndez-Perdomo & Facchini, 2018)
Curcuminoids	Curcumin, Bisdemethoxycurcumin and Demethoxycurcumin	Antioxidant, Anti-Inflammatory, Cholesterol lowering and Anti-Cancer	(Machado et al., 2014; Rodrigues et al., 2020; Rodrigues, Prather, et al., 2015)
Flavonoids	Flavones, Flavonols, Flavanones, Flavanonols, Flavanols, Anthocyanins and Chalcones	Antioxidant, Anti-Inflammatory, Anti-Mutagenic and Anti-Cancer	(Hernández-Chávez et al., 2019; Kang et al., 2012; Kim et al., 2018; Menéndez-Perdomo & Facchini, 2018; Panche et al., 2016)
Stilbenoids	Resveratrol, Pterostilbene, Gnetol, Piceatannol, Oxyresveratrol	Cardioprotection, Neuroprotection, Anti-Diabetic, Depigmentation, Anti-Inflammatory, Anti-Cancer	(Akinwumi et al., 2018; Hernández-Chávez et al., 2019; Kang et al., 2012; Kim et al., 2018; Menéndez-Perdomo & Facchini, 2018)
Amino acid	L-DOPA	Parkinson's disease drug	(Cox & Nelson, 2017; Hernández-Chávez et al., 2019; Kang et al., 2012; Kim et al., 2018; Menéndez-Perdomo & Facchini, 2018)
Catecholamines	Epinephrine, Norepinephrine, and Dopamine	Changes in blood pressure and Neurotransmitters	(Cox & Nelson, 2017)
Polymer	Melanin	Pigment, Light Absorbance, Redox and Chelating	(Hernández-Chávez et al., 2019; Kang et al., 2012; Kim et al., 2018; Menéndez-Perdomo & Facchini, 2018; Riley, 1997)

2.1.1 Metabolic pathway for the production of *L*-Tyrosine

The AAA, *L*-Trp, *L*-Phe and *L*-Tyr, are the ultimate products of the aromatic biosynthetic pathway containing the shikimate pathway, that connects central carbon metabolism (CCM) with the biosynthesis

of chorismate, which is the last common precursor in the last branches for AAA biosynthesis. These pathways are present in bacteria and in several eukaryotic organisms, like ascomycetes fungi, apicomplexans, and plants (Rodriguez et al., 2014).

The biosynthetic pathway of *L*-Tyr in *E. coli*, from glucose, starts with converting the precursor into three different molecules, pyruvate (PYR), fructose 6-phosphate, and glyceraldehyde 3-phosphate (Figure 2.1). The phosphoenolpyruvate (PEP) synthase (PpsA) converts pyruvate into PEP, and the transketolase A (TktA) converts fructose 6-phosphate and glyceraldehyde 3-phosphate into erythrose 4-phosphate (E4P). These two intermediary products are catalysed by 3-deoxy-D-arabino-heptulosonic acid 7-phosphate (DAHP) synthase (AroG/F/H), synthesing DAHP. Then, DAHP is converted to 3-dehydroquinate (DHQ) by the enzyme DHQ synthase (AroB). Afterwards, DHQ is catalysed by DHQ dehydratase (AroD), generating 3-dehydroshikimic acid. Subsequently, the quinate/shikimate dehydrogenase (YdiB) and the shikimate dehydrogenase (AroE) convert it to shikimate, and shikimate kinase I/II (AroK/L) synthesises shikimate 3-phosphate. The 5-enolpyruvylshikimate-3-phosphate (EPSP) synthase (AroA) allows the synthesis of 5-enolpyruvylshikimate-3-phosphate, which is converted to chorismate by the chorismate synthase (AroC). Prephenate is produced with the help of mutase/prephenate dehydrogenase (TyrA) and chorismate mutase-*p*-prephenate dehydratase (PheA), and, lastly, tyrosine amino-transferase (TyrB) finishes the pathway by synthesising *L*-Tyr (Chávez-Béjar et al., 2012; Juminaga et al., 2012; Rodrigues, Prather, et al., 2015; Rodriguez et al., 2014).

DAHP synthase is encoded by *aroG*, *aroF* and *aroH* genes, whose expression is inhibited by the presence of *L*-Phe, *L*-Tyr, and *L*-Trp, respectively. Each of the isoenzymes contributes differently to the overall activity of the enzyme. AroG contributes for 80%, AroF 15% and AroH 5%, approximately. AroG and AroF are completely inhibited by the *L*-Phe, *L*-Tyr, and *L*-Trp; however, AroH is only partially inhibited by *L*-Trp (Rodriguez et al., 2014). Another regulatory point is present at the chorismate branch point with the enzymes PheA and TyrA. Both these bifunctional enzymes and AroE have shown a feedback regulation by their end products, *L*-Phe, *L*-Tyr, and shikimate (Goldberger, 2012; Rodrigues, Prather, et al., 2015; Wilson, David B.; Sahm, Hermann; Stahmann, Klaus-Peter; Koffas, 2019; C. Zhang et al., 2013). There is a transcriptional control mediated by the protein TyrR (tyrosine repressor), adding to the allosteric inhibition. In case of amino acid overproduction, TyrR can repress *aroF*, *aroG*, *aroL*, *tyrA*, and *tyrB* (Goldberger, 2012; Rodrigues, Prather, et al., 2015; Wilson, David B.; Sahm, Hermann; Stahmann, Klaus-Peter; Koffas, 2019; C. Zhang et al., 2013).

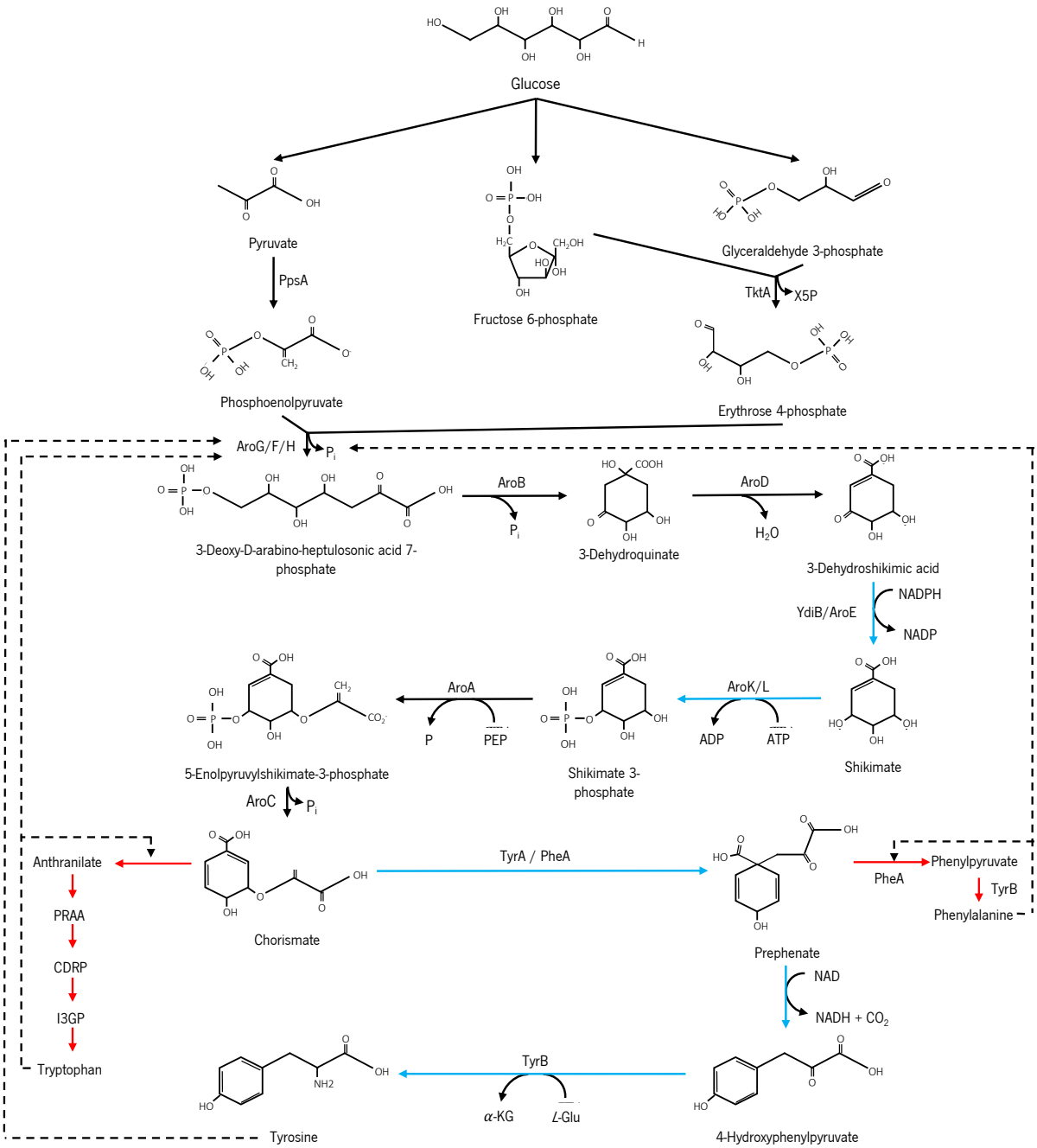

Figure 2.1 - E. coli's L-Tyr biosynthesis pathway. CDRP, 1-(2-carboxyphenylamino)-1-deoxy-D-nbulose-5-phosphate; I3GP, indole 3-glycerolphosphate; L-Glu, glutamic acid; PRAA, n-(5-phospho-β-D-nbosylanthranilate); X5P, xylulose 5-phosphate and α-KG, α-ketoglutarate. The enzymes present in this pathway are as follows: AroA (EPSP synthase), AroB (DHQ synthase), AroC (chorismate synthase), AroD (DHQ dehydratase), AroE (shikimate dehydrogenase), AroF (DAHP synthase, Phospho- 2-dehydro- 3-deoxyheptonate aldolase, Tyr-sensitive), AroG (DAHP synthase, Phospho-2-dehydro-3-deoxyheptonate aldolase, Phe-sensitive), AroH (DAHP synthase, Phospho-2-dehydro-3-deoxyheptonate aldolase, Trp-sensitive), AroK/L (shikimate kinase I/II), PheA (chorismate mutase-p-prephenate dehydratase), PpsA (phospho-enolpyruvate synthase), TktA (transketolase A), TyrA (chorismate mutase/prephenate dehydrogenase), TyrB (tyrosine aminotransferase) and YdiB (quinate/shikimate dehydrogenase) (*Chávez-Béjar et al., 2012;* Goldberger, 2012; Juminaga et al., 2012; Rodrigues, Prather, et al., 2015*; Rodriguez et al., 2014*; Wilson, David B.; Sahm, Hermann; Stahmann, Klaus-Peter; Koffas, 2019; Zhang et al., 2013). *The blue lines show steps of the pathway that can be inhibited by the end product of the reaction in question, the red lines represent deviations from the pathway that also partake in the regulation and the black dashed lines represent the inhibition by L-Tyr, L-Trp and L-Phe* (*Chávez-Béjar et al., 2012;* Goldberger, 2012; Rodrigues, Prather, et al., 2015; Wilson, David B.; Sahm, Hermann; Stahmann, Klaus-Peter; Koffas, 2019; Zhang et al., 2013).

2.1.2 Strategies to increase *L*-Tyr biosynthesis

In the last years, there was an increase in the accessibility to omics-scale data that allowed vigorous developments in metabolic reconstruction and modelling, which resulted in an improved strain design. The amplified use of combinatorial and evolutionary methods, powered by a swift growth of synthetic and molecular biology tools, allowed the opportunity to test new and great combinations of gene expression systems and genetic backgrounds. Furthermore, the efforts made to optimise the fermentation conditions allowed scaling-up the production processes of many AAA while providing important feedback on the engineered strains' physiological performance (Rodriguez et al., 2014).

Practical metabolic engineering approaches for the design of *E. coli* strains capable of overproducing AAA include (Rodriguez et al., 2014):

- Enhancing the availability of the precursors' PEP and E4P;
- Enhancing the enzymatic reaction catalysed by AroG/F/H;
- Enhancing the carbon flow by removing the transcriptional and allosteric regulation and avoiding its loss to competing pathways;
- Identifying and relieving rate-limiting enzymatic reactions;
- Enhancing product export;
- Inhibiting product degradation or re-internalization.

Feedback resistant (fbr) variants AroG^{fbr} and AroF^{fbr} resulted from identifying specific amino acid residues involved in the allosteric sites. Subsequently, intensification and deregulation of AroG/F/H activity are fundamental to overproduce shikimate, therefore aromatic compounds. The introduction of the plasmid-encoded copies of *aroF*^{fbr} and *aroG*^{fbr} in combination with *tktA* gene, or their chromosomal integrations in gene clusters, resulted in an improved carbon flow from the CCM to the shikimate pathway (Rodriguez et al., 2014).

It was possible to increase carbon flux through the shikimate pathway by removing the transcriptional and allosteric control points and alleviating some restrictive enzymatic reactions. The reactions catalysed by AroB, AroK/L and YdiB are some examples, being the last only limiting for the design of *L*-Tyr overproducing strains. To reduce the impact of these rate-limiting steps, during the design of shikimate and AAA production strains there are some techniques that can be used (Rodriguez et al., 2014). These techniques include the overexpression of several genes using plasmids, the co-expression in a modular operon under control of different promoters using plasmids or the expression of supplementary gene copies by chromosomal integration or by engineering the endogenous promoters (Juminaga et al., 2012; Rodriguez et al., 2014).

Metabolic engineering methods to overproduce *L*-Tyr typically include modifications in TyrR and/or *trp* regulons. Inactivation of TyrR-mediated regulation by deletion of *tyrR* and overexpression of *aroG*^{fbr} and *tyrA*^{fbr}, combined with the overexpression of CCM genes, such as *ppsA* and *tktA*, and genes of the *L*-Tyr biosynthetic pathway, such as *tyrB*, *aroC*, and *aroA*, have shown an increase in the production of *L*-Tyr in diverse *E. coli* strains (Rodriguez et al., 2014).

However, in a more recent study (Kim et al., 2018), gene manipulations were made to the wild-type and to *tyrR* knockout strains to conclude whether the *tyrR* knockout is essential to improve *L*-Tyr production. Comparing the individual overexpression of *aroG*^{fbr} and *tyrA*^{fbr}, with the combination of the overexpression of *aroG*^{fbr}, *aroL*, and the gene that encodes cyclohexadienyl dehydrogenase (*tyrC*) through a plasmid in the wild-type managed to get the highest *L*-Tyr production amongst the strains and plasmid constructs observed in this study. This study was able to conclude that the *tyrR* gene knockout was not mandatory to increase *L*-Tyr production (Kim et al., 2018). In the same study, the strains' performance was enhanced by removing the *L*-Tyr specific and/or general AAA transporters, demonstrating that transporters can be potential manipulation targets for further strain optimisation for the *L*-Tyr production (Kim et al., 2018).

Another report (Na et al., 2013) revealed that it was created a synthetic sRNA library for targeted gene expression silencing to aid in the identification and modulation of the expression of target genes for metabolic engineering in *E. coli*. It was possible to confirm the advantages of this approach by overproducing *L*-Tyr through the overexpression of *ppsA*, *tktA*, *aroF*, *aroK*, *tyrC*, *aroG* and *tyrA* genes, and the simultaneous silencing of *tyrR*, *csrA* (enconding a regulatory protein of carbohydrate metabolism), *pgi* (encoding phosphoglucose isomerase) and *ppc* (encoding phosphoenolpyruvate carboxylase) genes generating numerous *E. coli* strains when testing multiple combinations. It was possible to select a strain (*E. coli* S17-1 *tyrR* and *csrA* repressing) that could yield up to 21.9 g/L of *L*-Tyr in high-density (Na et al., 2013; Rodriguez et al., 2014).

Table 2.2 contains a variety of *E. coli* strains engineered for the overproduction of *L*-Tyr published in the last few years.

Table 2.2 – Escherichia coli strains engineered for the overproduction of L-Tyrosine since 2013. ptsG – glucose-specific PTS enzyme IIBC component; pykA - pyruvate kinase 2; pykF – pyruvate kinase 1; glk – glucokinase; feaB – phenylacetaldehyde dehydrogenase; UTR – untranslated region; ptsHI – phosphocarrier protein HPr and PTS enzyme I; galP – galactose:H+ symporter; MAGE – Multiplex Automated Genome Engineering; hpaC – 4-hydroxyphenlacetate 3-hydroxylase; mao-paa – cluster; lacI – DNA-binding transcriptional repressor LacI; tyrP – tyrosine:H+ symporter; tyrC – prephenate dehydrogenase; crr – PTS system glucose-specific EIIA component; ldhA – D-lactate dehydrogenase; adhE – Aldehyde-alcohol dehydrogenase; pflDC – putative formate acetyltransferase 2/pyruvate formate lyase activating enzyme; ascF – β-glucoside-specific PTS enzyme IIBC component

Strain	Related genotype and features	Titer or Yield	Reference
BKT5	*E. coli* BW25113 Δ*ptsG*::FRT Δ*tyrR*::FRT Δ*pykA*::FRT Δ*pykF*::FRT Δ*pheA*::FRT with pYBT5 (pMB1 ori with P_{lacUV5} and P_{trc}; Amp^R P_{lacUV5} *aroG*^{fbr} *tyrA*^{fbr} *aroE*, P_{trc} *ppsA tktA glk*)	0.1071 g/g glucose	(Yao et al., 2013)
BMGA	*E. coli* MG1655 Δ*feaB* Δ*pykA* Δ*pykF* Δ*tyrR* Δ*pheA*	Not mentioned	(Bai et al., 2014; Jiang et al., 2016)
SCK5	*E. coli* K-12 Fλrph-1 IN(*rrnD*,*rrnE*)1 Δ*tyrR aroG*::P_{BBa_J23100}-synUTR$_{aroG}$-*aroG*^{fbr} *tyrA*::P_{BBa_J23100}-synUTR$_{tyrA}$-*tyrA*^{fbr} $P_{aroABCDELtyrB}$-UTR$_{aroABCDELtyrB}$::P_{BBa_J23100}-synUTR$_{aroABCDELtyrB}$ P_{ppsA}-UTR$_{ppsA}$::P_{BBa_J23100}-synUTR$_{ppsA(V4)}$	0.102 g/g glucose	(Kim et al., 2015)
ΔCOS1	*E. coli* C41(DE3); Δ*tyrR*::*tyrA*^{fbr}, *aroG*^{fbr}	450 mg/L	(Kang et al., 2015)
AROM-2 (pQE-hpaBC)	*E. coli* BW25113, Δ*tyrR*, Δ*csrA*, Δ*ptsHI*, Δ*crr*	366.2 mg/L	(Wei et al., 2016)
CFT56	*E. coli* ATCC31882 *ptsHI*::$P_{A1lacO-1}$-*glk-galP* Δ*pykF* Δ*pykA* Δ*pheA* Δ*tyrA* pZA23tyrA^{fbr}	1620 mg/L	(Noda et al., 2016)
DOPA-30 (pQE30-2hpaBC)	*E. coli* BW25113, MAGE strain with the artificial 5′-UTR sequence of the *hpaC*	546.8 mg/L	(Wei et al., 2016)
BAK11	*E. coli* BW25113 Δ*ptsG*, Δ*tyrR*, Δ*pykA*, Δ*pykF*, Δ*pheA* Δ*mao-paa* cluster::P_{lacUV5}-*aroG*^{fbr}-*tyrA*^{fbr}-*aroE* Δ*lacI*::P_{trc}-*ppsA-tktA-glk*	401.5 mg/L	(Zhou et al., 2017)
BTY2.13	*E. coli* BL21(DE3) Δ*tyrP* pBK1::P_{tac}, *aroG*^{fbr}-*aroL*, P_{trc}, *tyrC*	43.14 g/L	(Kim et al., 2018)
HMS174 - Tyr^{OP}	*E. coli* HMS174(DE3) [BBR1 *ori cat Plac-UV5-aroE-aroD-aroBOPT PLtetO-1-aroG*^{fbr}*-ppsA-tktA dbl term*] [p15a *ori bla Plac-UV5-tyrB-tyrA*^{fbr}*-aroC T1 term Ptrc-aroA-aroL dbl term*]	6.23 mM	(Trantas et al., 2019)
LP-7	*E. coli* BL21 Δ*tyrR*-Δ*ptsG*-Δ*crr*-*PT7-galP-glk*-Δ*pheA*-P_{T7}-*aroG*^{fbr}-*tyrA*^{fbr}- P_{T7}-*galp-glk-ppsA-tktA-pykFA*	461.7 mg/L	(Fordjour et al., 2019)
HRP	*E. coli HGX* ΔpheA/tyrR with* pAP-*aroG*^{fbr}-*tyrA*^{fbr} plasmid	5.84 g/L	(Xu et al., 2020)
M-PAR-121	*tyrR*::P_{T7lac}-*aroG*^{fbr} *ldhA*::P_{T7lac}-*tyrA*^{fbr} *adhE*::P_{T7lac}-*ppsA pflDC*::$_{PT7lac(-8TC)}$-*tktA pykF*::P_{T7lac}-*aroALC ascF*::P_{T7lac}-*aroEDB*	0.22 mol/mol glucose	(Koma et al., 2020)

**E. coli* HG (*L*-Tyr auxotrophic, carrying pAP-B03 plasmid with *pheA*^{fbr} and *aro*^{ind} genes, Kan^r) without pAP-B03 plasmid

2.2 Metabolic Engineering

Metabolic engineering covers the analysis and modification of metabolic pathways. This field has gained power over the past few decades in various areas, such as biological and biochemical engineering, cell physiology, and applied microbiology. Even though pathway manipulation was not new, it was Bailey in 1991 that suggested that metabolic engineering was a crucial discipline in its own right, which he defined as the improvement of cellular activities by manipulations of enzymatic, transport, and regulatory functions of the cell with the use of recombinant DNA technology (Bailey, 1991; Keasling, 2010; Nielsen, 2001; Stephanopoulos et al., 1998).

Stephanopoulos defined metabolic engineering as the direct improvement of product formation or cellular properties through the modification of specific biochemical reaction(s) or the introduction of new one(s) with the use of recombinant DNA technology (Stephanopoulos et al., 1998).

Researchers in the biotechnology field have been manipulating metabolic pathways to provide desirable properties to mutant microorganisms. In order to accomplish the expressed goal, molecular biology techniques are used, allowing the amplification, inhibition or deletion, transfer, or deregulation of the genes or enzymes that are involved in the reaction targets (Bailey, 1991; Keasling, 2010; Nielsen, 2001; Stephanopoulos et al., 1998).

Like all fields of engineering, metabolic engineering focuses on analysis, synthesis, and design (Keasling, 2010; Nielsen, 2001; Stephanopoulos et al., 1998). It is necessary to analyse the cellular function to start a metabolic engineering approach. Then, an improved strain is designed and constructed by genetic engineering, taking into account the results (Nielsen, 2001), as illustrated in Figure 2.2.

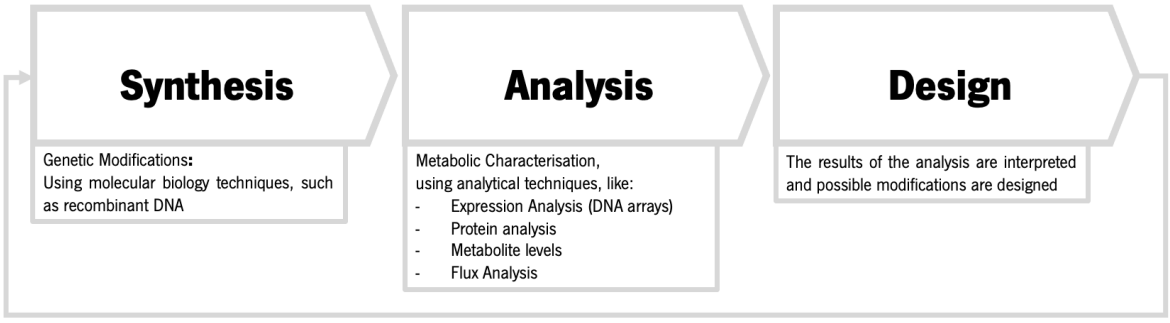

Figure 2.2 – The cycle of metabolic engineering. Adapted from (Nielsen, 2001)

Initially, the predominant technique used for metabolic engineering was DNA recombination. This field was considered the technological manifestation of applied molecular biology (Keasling, 2010; Nielsen, 2001; Stephanopoulos et al., 1998) by using diverse techniques such as the expression of new genes in various host cells, amplification of endogenous enzymes, deletion of genes or modulation of enzymatic activity, transcriptional or enzymatic deregulation (Stephanopoulos et al., 1998). However, as

modern analytical techniques and cloning techniques have evolved rapidly, it has become possible to implement directed genetic changes swiftly and subsequently analyse the effects of the changes implemented at the cellular level (Nielsen, 2001).

Metabolic engineering focuses on joined metabolic pathways instead of individual reactions, examining the broad biochemical networks and their interacting reactions, regarding the pathway synthesis, thermodynamic feasibility, and pathway flux and its control (Nielsen, 2001; Stephanopoulos et al., 1998).

The metabolic fluxes and their control under *in vivo* conditions is the main focus of metabolic engineering. What differentiates this field from others is the combination of analytical methods that quantify fluxes and their control, with molecular biological techniques that implement suggested genetic modifications (Nielsen, 2001; Stephanopoulos et al., 1998).

2.2.1 Systems Biology

The development of more recent high-throughput (HT) technologies enabled the identification of most molecules that compose cells, resulting in high quantities of data available, which allows us to understand the composition of cells and organisms under certain conditions. Understanding the chemical interactions between many of these components allows the reconstruction of the biochemical reaction networks on a genome-scale. The high quantity of data forced the need to integrate various omics data types into a consistent whole and to consider cellular functions as systems (Palsson, 2015).

Klipp et al. defined systems biology as the scientific discipline that studies the systemic properties and dynamic interactions in a biological object, being it a cell, an organism, a virus, or an infected host, in a qualitative and quantitative manner and by combining experimental studies with mathematical modelling (Klipp et al., 2016).

Systems biology has been at the forefront of research and development, focused on life science (Palsson, 2011). The focus of systems biology does not rely only on the components but on how the connecting links and the functional states of the biochemical networks work. Systems biology aims to complete the relationship between all the chemical components of a cell, its genetic bases and physiological functions (Palsson, 2015).

Systems biology allows explaining the whole network, cell, or organism behaviour (Palsson, 2011), which enables the understanding of how the cell adapts to gene disruptions, such as mutations, how the physical structures are built, maintained, and reproduced, how the metabolic state is changing, and how signalling and regulation systems allow cells to adjust to their environment (Klipp et al., 2016).

Reconstructed networks are essential in systems biology because of their multiple usages, like data interpretation, comparing organism capabilities and computing their functional states (Palsson, 2011). However, there is also the need to consider the global dynamics between the networks' components, which is why mathematical models are important (Klipp et al., 2016).

For several years, mathematical modelling has been used in biology, having shaped the discipline differently. Models enable the testing of hypotheses and the development of quantitative predictions or the disclosure of discrepancies or contradictions in previous claims, enabling the understanding of biochemical processes. As previously mentioned, a high amount of biological data (genomic and proteomic) allows the development of computational models of cells, integrating the data into networks and dynamical simulation models (Klipp et al., 2016).

The fundamental paradigm of Systems Biology emerged due to the availability of thorough lists of biological components, their interactions, and genome-wide data sets. The following core sequence of events (Figure 2.3) is the fundamental paradigm of a bottom-up mechanistic methodology to systems biology (Palsson, 2015):

Figure 2.3 – Core sequence of events of the bottom-up mechanistic method of Systems Biology. COBRA stands for COnstraint-Based Reconstruction and Analysis Adapted from (Palsson, 2015).

The fundamental paradigm of systems biology is represented in Figure 2.4.

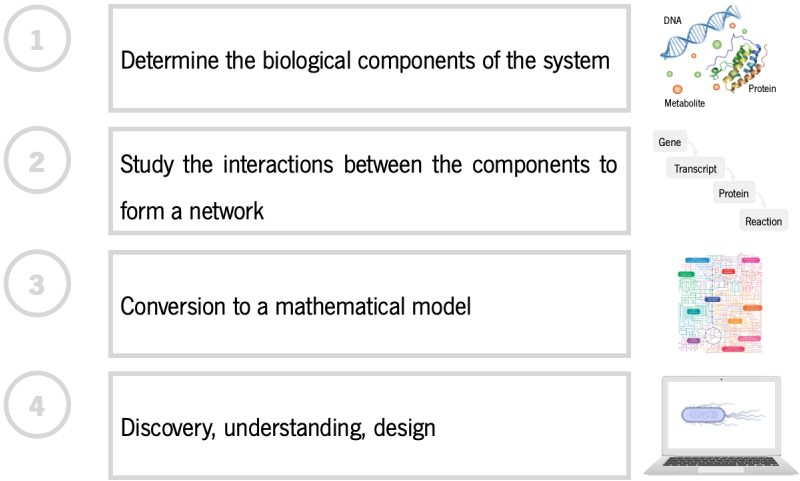

Figure 2.4 – The Systems Biology Paradigm. Adapted from (Palsson, 2015).

The Core Paradigm is constituted of four main steps. Each one of these steps relies on different disciplines (Palsson, 2015) and techniques:

1. **Measuring biological components**

   Define and enumerate the biological components that participate in a cellular process. This step uses omics data sets – genomics, transcriptomics, proteomics, metabolomics, fluxomics, and bibliomics. Such data sets are produced from HT technologies based on miniaturisation, automation, and multiplexing (Palsson, 2015).

2. **Reconstruction of biochemical reactions networks**

   This step is the interface between HT data and *in silico* analysis. The interactions between these components are studied with a comprehensive review of the literature, allowing the reconstruction of the 'wiring diagrams' of genetic circuits and forming genome-scale maps. There are defined procedures for determining which data are included, depending on the components' validation level and their interactions in the target cell. The reconstruction process may follow two different approaches (Palsson, 2015):

   - Bottom-up: mechanistic method to reconstruct the network – characterises all available knowledge from that organism or genome, resulting in a biochemically, genetically, and genomically (BiGG) curated knowledge base (Palsson, 2015).
   - Top-down: this method includes going through the omics data sets, using statistical approaches to interpret the ties between biological components (Palsson, 2015).

3. **Conversion to a mathematical model allowing *in silico* analysis**

   The biochemical network is converted into a mathematical format, becoming an *in silico* model of the knowledge that it represents. These computer models are created to analyse, interpret, and predict the biological functions from reconstructed networks, allowing to determine the properties of the BiGG knowledge base and the consistency of the physiological states with the original data. Several tools, such as topology, constraints, gap-filling, dynamics, sensitivity, noise, and modularisation, are available for this step. A detailed curation and validation of a genome-scale model against available data are also performed (Palsson, 2015).

4. **Prospective uses: discovery, understanding, and design**

   Once an organism-specific knowledge base has been formed, it can be used prospectively. Currently, there are a few main uses and applications. First, to analyse and data-map omics through HT data analysis and the systematic discovery focused on any missing pieces in the

knowledge base. An *in silico* model can help understand a complex biological process, like adaptation or disease progression. Lastly, a predictive *in silico* model can be used to design synthetic biology at the network scale. These *in silico* models of reconstructed networks can be enhanced iteratively (Palsson, 2015).

2.2.2 Systems Metabolic Engineering

The focus of metabolic engineering has been on analysing cellular metabolism and predicting optimal rewiring of metabolic networks through a systems-level view. There have been substantial developments for obtaining high-resolution specifics about the cellular state. In response, this recent skill enabled Systems Metabolic Engineering to emerge as a paradigm that associates metabolic engineering goals with the field of systems biology (Alper, 2013).

Yang and co-workers defined systems metabolic engineering as an interdisciplinary field of study which integrates traditional metabolic engineering with systems biology, synthetic biology, and evolutionary engineering to provide a holistic approach to microbial metabolism for enhanced production of target chemicals while considering upstream to downstream bioprocesses (Yang et al., 2020).

In addition to creative genome-wide engineering, this field integrates large-scale data collection, HT biology and *in silico* modelling efforts to achieve the task of improving a cellular phenotype or pathway flux. There is a continuous expansion of the global system-level view of metabolic engineering through these innovations and initiatives, emphasising individual pathways to the collective, interconnected nature of metabolism and regulation. Due to the improvements of systems biology, there is a growth of the HT collection of genomic, transcriptomic, proteomic, metabolomic, and fluxomic data. However, this vast snapshot of cells creates a great challenge for data collection, integration, interpretation, synthesis, and ultimately perturbation to the cell (Alper, 2013).

Systems Metabolic Engineering's ultimate aim is to systematically and robustly identify the precise perturbations required to modify a cellular phenotype. The desired concrete outcome is a complete cell model capable of simulating cell and metabolic function and predicting phenotypic response to media changes by gene knockouts, under/overexpression, or integration of heterologous pathways (Alper, 2013).

An innovative era of industrial strain engineering – the design of tailor-made overproducers optimised globally – starts with the convergence of system-wide omics, genome-scale modelling and simulation, synthetic biology, and evolutionary engineering (Wittmann & Lee, 2012). This discipline considers the complete metabolic and regulatory networks and the midstream (fermentation) and

downstream (recovery and purification) processes, to establish the engineering objectives. During the metabolic engineering techniques, the effect of the changes on the entire metabolism is examined. Through the iterative mode of operation of metabolic engineering, the developed strain's performance is evaluated, and the ultimate metabolic phenotype desired can be achieved (Park & Lee, 2008).

Numerous systems of metabolic engineering tools have facilitated the design of novel strain engineering tasks to achieve the requirement to design industrially competitive microorganisms. These tools help construct new metabolic pathways, genome-wide identification of metabolic engineering targets, refinement and control of gene expression, multiplex genome engineering, design of synthetic circuits, and growing tolerance to target chemicals or intermediates when desired. Such tools and strategies have been employed for strain development and the optimisation of bioprocess variables such as medium composition, pH, aeration, cultivation mode, and nutrient feeding strategies (Chae et al., 2017).

2.2.3 Bioinformatics in Metabolic Engineering

Biotechnology requires bioinformatics to look for biological "rules" and "principles" on which the design of biological systems can depend. For this, engineering approaches for the operation and design of integrated systems must be used to study the hierarchical relationship between genetics and physiology (Edwards & Palsson, 1998).

In genome-wide research, bioinformatics is essential to understand cell physiology at different cellular levels – genome, transcriptome, proteome, and metabolome. The several bioinformatics fields provide valuable information on the global cellular status and comprehensive cell analysis for system biology and metabolic engineering systems (Chen & Wu, 2013). Some of the computational tools have been developed to aid in the metabolic engineering field by identifying genetic strategies, like strain designs, facilitating the enhancement of chemical production (Long et al., 2015; Patil et al., 2005).

In bioinformatics, genetic knowledge leads to a comparative genomic study that contributes to the systems metabolic biology for genetic circuits targeting and engineering to generate desirable cellular phenotypes. DNA microarrays are used in transcriptome profiling to decipher the expression levels of genes under different biological conditions. Based on the response to genetic variations and environmental changes of regulatory genes when conducting systematic research, this technique can be useful for selecting which genes to use to alter the molecular networks (Chen & Wu, 2013).

These techniques may also be used to recognize new variables in metabolic pathways that enhance heterologous product development. Proteome profiling is used to obtain transcriptome-profiling

data at a protein level. The metabolome contains all the information on metabolites present in and/or out of the cell under detailed conditions. It contributes expressively to understanding the cell and the synthetic circuit engineering in its metabolic pathways (Chen & Wu, 2013). It is possible to model the integration of product biosynthesis pathways with host metabolism with the information acquired and then forecast how metabolic and regulatory changes will affect the yields, titers and productivities of the chemical productions (Long et al., 2015; Yang et al., 2020).

In metabolic engineering, genome-scale constraint-based models have been used to account for a cell's maximum metabolic and regulatory capabilities and do not require precise kinetic parameters to construct them (Long et al., 2015; Patil et al., 2005; Tepper & Shlomi, 2009). Several software packages can swiftly generate Constraint-based models using the organism's genomic, biochemical, and physiological data. Constraint-based models use two types of constraints when defining a metabolic solution space: steady-state mass balances, meaning that the metabolite production and consumption rates are the same, and flux bounds, that set maximum and minimum limits for metabolic fluxes based on an enzyme's capacity and directionality (Long et al., 2015).

Several databases that describe the reactions that known enzymes can catalyse are available, such as KEGG (Kyoto Encyclopedia of Genes and Genomes), BioCyc and BRENDA. These databases can be used to improve reaction networks unique to organisms and full reaction networks comprising known biochemical reactions. Graphical and modelling approaches can be used to discriminate native and non-native pathways leading to product formation from these reaction networks (Long et al., 2015).

For those desirable compounds with no known biological synthesis network, there is a need to find novel routes and enzymes that can catalyse new reactions. Several methods allow us to identify these new reaction pathways and possible enzymes that catalyse them. These approaches use Biochemical Reaction Operators (BROs), which are generic reaction rules that act on a reaction centre. This method targets metabolites and enumerates potential filtered or ranked reactions based on thermodynamics, and other methods suggest enzymes that could catalyse the wanted reactions (Long et al., 2015).

After identifying the biosynthesis pathway, the necessary enzymes are expressed in the host. There may be also the need to adjust other aspects of native host metabolism so that sufficient precursors, ATP (Adenosine Triphosphate), redox carriers, and cofactors can be provided. Experimentally, the modification of the strain metabolism to overproduce a target metabolite can be done using various genetic methods – gene knockout, insertion of heterologous reactions or *de novo* reactions, gene upregulation, and gene downregulation. Thus, several computational strain design algorithms have been

developed to enhance the production of a target metabolite using one or a combination of techniques (Long et al., 2015; Patil et al., 2005; Tepper & Shlomi, 2009; Yang et al., 2020).

2.2.4 Stochiometric Models

A Genome-Scale Metabolic (GSM) model represents the metabolic network in the form of a stoichiometric matrix. Additionally, these models are based on the steady-state supposition and can be used to determine intracellular metabolic fluxes (Orth et al., 2010). The classical principles of chemical engineering, combined with a steady-state approximation that assumes no changes in the system (Edelstein-Keshet, 2005), enable the representation of a biological system's dynamic mass balances as shown in equation 1 (Orth et al., 2010).

$$S.v = 0 \quad (1)$$

Where the S stands for the stoichiometric matrix and the v for the flux vector, most GSM models are underdetermined systems since there are more reactions than metabolites (Orth et al., 2010).

Some algorithms can predict chemical production rates for a set of genetic manipulations using "gene perturbation" constraint-based modelling tools, like flux-balance analysis (FBA) or minimization of metabolic adjustment (MOMA) (Long et al., 2015; Patil et al., 2005; Tepper & Shlomi, 2009; Yang et al., 2020).

FBA, a linear programming strategy that predicts the phenotypic responses forced by environmental elements and factors using metabolic models, is the leading tool for simulating and manipulating cell production *in silico* (Cuevas et al., 2016). This technique maximises or minimises the objective function, for instance, the maximisation of biomass production (Long et al., 2015; Orth et al., 2010; Patil et al., 2005). Parsimonious Flux Balance Analysis (pFBA) derives from FBA and includes a bi-level optimisation. Firstly, the biological objective chosen is optimised like in FBA. Afterwards, under the optimality condition, the sum of all fluxes is minimised by removing the flux distribution of reactions that are not necessary for the cell work or growth (Sá-Correia, 2019; Vilaça et al., 2018).

In order to predict production phenotypes, computational methods, as FBA and pFBA, depend primarily on structural details, like the reaction stoichiometry. So, it is impossible to differentiate between different steps in a linear pathway to find rate-limiting ones. It is also hard to predict how gene expression changes will influence flux using stoichiometric models, as removing a gene will eliminate flux through related reactions (Long et al., 2015; Patil et al., 2005).

Flux Variability Analysis (FVA) is an effective approach, based on linear programming, for calculating the entire range of possible values for each flux to obtain optimal or sub-optimal objective states. This is one of the most common methods for determining the limits of a constraint-based model's viable domain (Vilaça et al., 2018). This method requires selecting a target flux and a pivot flux. The procedure starts by separating the range of all possible pivot flux values into numerous phases. The value of the pivot flux is fixed for each step, and the maximum and minimum values for the target flux are determined (Vilaça et al., 2018).

Heuristic methods, such as EA, are usually computationally less expensive approaches for countless optimisation problems. Even though these methods do not guarantee that the overall optimal solutions are determined, the definition of optimisation frameworks with a set of objective functions is allowed, like biomass-product coupled yield (BPCY) and product yield with minimum biomass (YIELD), encouraging a clear separation of the strain optimisation from the phenotype simulation layers, while allowing optimisation over larger search spaces (Vilaça et al., 2018). The algorithm starts by randomly generating an initial set of candidate solutions, and each is decoded into a set of reaction deletions, which are converted into constraints. Each of these candidate solutions is simulated using one of the phenotype simulations, followed by the assignment of a fitness value by the objective function defined by the user. Then, the algorithm enters an iterative phase, initially with a selection step, selecting solutions as primary candidates for the reproduction in a stochastic way, depending on their assigned fitness, where fitter individuals are more likely to generate offspring solutions. Lastly, a new population is attained and re-evaluated by combining the chosen individuals through crossover or mutation operators. This cycle is repeated until the wanted phenotype is achieved or another termination criterion is met (Vilaça et al., 2018).

2.2.5 Kinetic Models

Metabolism Kinetic models were first assembled for small networks with simplified rate expressions from *in vitro* parameters with low predictive capacity. Recent advances allowed parameterization of genome-scale kinetic models with full mechanistic descriptions only from *in vivo* data. The resulting models can predict reactions operating almost to equilibrium, allosteric control points, catalytic efficiency, and rate-limiting steps across metabolism (Foster et al., 2021).

Kinetic models are based on the principles of biochemical kinetics. Therefore, they rely on the Law of Mass Action and the Michaelis-Menten model for the rate of an irreversible one-substrate reaction (Klipp et al., 2016) or other rates.

Almost all kinetic models are described with coupled differential equations rather than explicit algebraic functions, and the simulators use the appropriate methods to resolve these systems of ordinary differential equations (ODEs) (Mendes & Kell, 1998).

The Law of Mass Action states that the reaction rate is proportional to the probability of a collision of the reactants. This probability is proportional to the concentration of reactants to the molecularity's power, which is the number in which the molecule species enters the reaction. For a simple reaction like Equation 2, the reaction rate is like Equation 3. The basic quantities are the concentration of a substrate S, and the concentration of a product P (Klipp et al., 2016).

$$S_1 + S_2 = 2P \tag{2}$$

$$v = v_+ - v_- = k_+ S_1 \cdot S_2 - k_- P^2 \tag{3}$$

In Equation 3, v is the net rate, and v_+ and v_- are the rates of the forward and backward reactions, respectively. k_+ and k_- are the kinetic or rate constants, meaning, the respective proportionality factors (Klipp et al., 2016).

Michaels-Menten (Michaelis & Menten, 1913) kinetics are represented by Equation 4. K_m value is a major characteristic of the interaction between enzyme and substrate (Klipp et al., 2016).

$$v = \frac{V_{max} \cdot S}{K_m + S} \tag{4}$$

Equation 5 was proposed by Brown (Brown, 1902), and it comprises a reversible formation of an enzyme-substrate complex, ES, from the free enzyme, E, and the substrate, S, and an irreversible product P (Klipp et al., 2016).

$$E + S \underset{k_{-1}}{\overset{k_1}{\rightleftarrows}} ES \xrightarrow{k_2} E + P \tag{5}$$

The ODE system for the reaction dynamics represented in Equation 5 is represented in Equations 6 to 9 (Klipp et al., 2016).

$$\frac{dS}{dt} = k_{-1} E \cdot S + k_{-1} ES \tag{6}$$

$$\frac{dES}{dt} = k_1 E \cdot S - (k_{-1} + k_2) ES \tag{7}$$

$$\frac{dE}{dt} = -k_1 E \cdot S + (k_{-1} + k_2) ES \tag{8}$$

$$\frac{dP}{dt} = k_2 ES \tag{9}$$

The reaction rate is equal to the substrate's negative decay rate and the rate of product formation (Equation 10) (Klipp et al., 2016).

$$v = -\frac{dS}{dt} = \frac{dP}{dt} \tag{10}$$

This ODE system (Equations 6 to 10) cannot be solved analytically. Thus, it must be solved graphically instead (Klipp et al., 2016). Different assumptions have been used to simplify this ODE system. Michaelis and Menten (Michaelis & Menten, 1913) considered a *quasi-equilibrium* between the free enzyme and the enzyme-substrate complex, meaning that the reversible conversion of E and S to ES is much faster than the decomposition of ES into E and P ($k_1, k_{-1} \gg k_2$) (Klipp et al., 2016).

Briggs and Haldane (Briggs & Haldane, 1925) assumed that throughout a reaction, a state is reached where the concentration of the ES complex remains constant, the quasi-steady state. This assumption can only be justified if the initial substrate concentration is greatly superior than the enzyme concentration, $S(t = 0) \gg E$, otherwise such a state will never be reached (Klipp et al., 2016).

Deriving an expression for the reaction rate from the ODE system (Equations 6 to 9) and assuming the quasi-steady-state assumption for ES, it is possible to obtain Equation 11 representing the reaction rate (Klipp et al., 2016).

$$v = \frac{k_2 E_{total} \cdot S}{((k_{-1} k_2)/k_1) + S} \tag{11}$$

Comparing equation 11 with the one that follows the Michaelis-Menten kinetics (Equation 4), it is possible to obtain the parameters for the maximal velocity (Equation 12) – the maximal rate attained when the enzyme is completely saturated with substrate – and the Michaelis constant (K_m) (Equation 13) – equal to the substrate concentration that yields the half-maximal reaction rate (Klipp et al., 2016).

$$V_{max} = k_2 E_{total} \tag{12}$$

$$K_m = \frac{k_{-1} + k_2}{k_1} \tag{13}$$

For the *quasi-equilibrium* assumption, $K_m = k_{-1}/k_1$. The maximum velocity divided by the enzyme concentration ($k_2 = V_{max}/E_{total}$) is often called the turnover number, k_{cat} (Klipp et al., 2016).

Recent advances have allowed the development of kinetic models using a variety of kinetic formalisms. Figure 2.5 provides an overview of the generalized workflow (Foster et al., 2021).

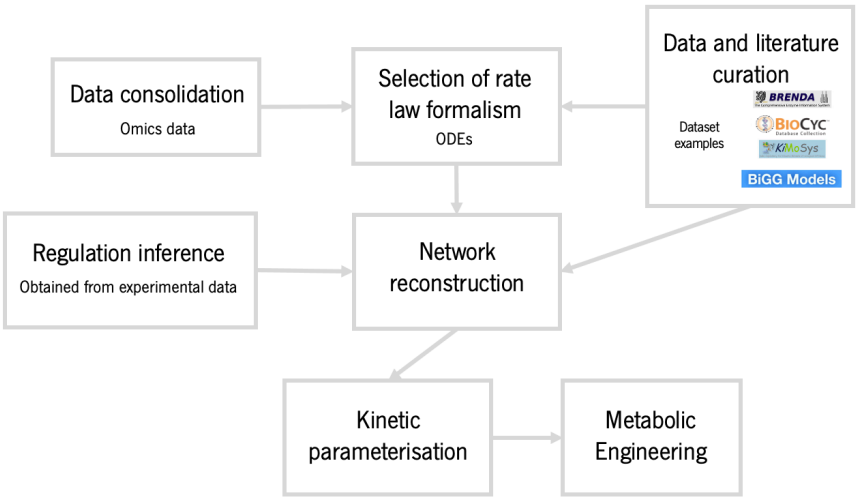

Figure 2.5 – Generalised workflow for Metabolic Kinetic Model construction and use in Metabolic Engineering. First, datasets and literature are used to select kinetic rate law formalisms. A systematic regulatory inference using experimental data is also necessary because it gives the metabolic response to different metabolite concentrations. The final metabolic/regulatory network involves a reaction network based on metabolic reconstructions from literature, regulations gathered from databases, and newly defined regulations. A kinetic model is parameterised using the network and chosen kinetic formalisms. To define engineering methods for a desired metabolic outcome, the parameterized model is then used. ODEs stands for Ordinary Differential Equations. Adapted from Foster et al. (2021).

The development of kinetic models allows strain design algorithms to be improved, enabling the rapid construction, evaluation and improvement of metabolically engineered strains (Long et al., 2015; Patil et al., 2005).

Kinetic simulation software measures internal metabolite concentration values based on kinetic functions, parameter values and external metabolite concentration values. Two different types of simulations can be used with kinetic models: time courses that value the variables determined in a time series and steady states in which the values of the variables are calculated for a state with no metabolite concentration changes. These simulations allow for an efficient analysis of the model's behaviour's reliance on its parameters, thus becoming more effective in predicting the effect of parameter alterations (Mendes & Kell, 1998).

The simulation is carried along with optimisation techniques to obtain the parameters' values as the desired optimum. Parameter estimation, a well-established field of biochemical kinetics where enzyme kinetic parameters are regularly estimated in many laboratories, is used to solve the problem when most kinetic parameters are unknown (Mendes & Kell, 1998).

Kinetic models establish mechanistic relations between metabolic reaction rates, enzyme levels, and metabolite concentrations, allowing the quantitative description of metabolic phenotypes. Therefore,

kinetic models offer more effective metabolic interventions than stoichiometric methods. The used methods are not limited to gene knockouts or up/downregulations but also include optimally tuning enzyme levels, detecting reactions operating close to equilibrium and modifying the concentration and, consequently, the strength of allosteric regulators (Foster et al., 2021).

Stoichiometric models only require reaction stoichiometry and directionality constraints when doing FBA. However, kinetic models require significant upfront investment to identify the proper kinetic formalisms for each reaction and data for parameterization (Foster et al., 2021).

2.2.6 Optimisation

The use of these tools enables the development of engineered strains, for instance, *E. coli*, that can more cost-effectively produce diverse natural products (Yang et al., 2020).

There are several tools available, such as COPASI (Hoops et al., 2006), OptimModels (Correia et al., 2017) and MEWpy (Pereira et al., 2021) able to design and optimise the desired strain for the systems biology purpose.

2.2.6.1 OptimModels

OptimModels is a Python package that implements Evolutionary Algorithms (EA)-based strain design methods on large-scale kinetic models. It has been shown to find which genes should be knocked out or/and their optimum up/down-regulation levels (Correia et al., 2017).

2.2.6.2 MEWpy

MEWpy is a metabolic engineering Python workbench that covers various approaches to metabolic and regulatory modelling and algorithms for phenotype simulation and computational strain optimization. This tool enables the modelling and optimisation of microbial production on GSM by defining gene-protein-reaction associations and transcriptional and translational layers that improve the models. Metaheuristics, like EA, Simulated Annealing (SA) and multi-objective methods, allow the choice of the best set of enzymes, genes or reactions to under/overexpress or delete to optimise the maximisation of the production of a target compound (Pereira et al., 2021).

2.2.6.3 COPASI

COPASI is a user-friendly software for biochemical simulation that combines generic numerical methods with computational systems biology. This tool provides an easier way to shift between distinctive simulation approaches (stochastic and deterministic). It contains features like hybrid deterministic–

stochastic methods, parameter scans, optimisation of arbitrary expressions, and calculation of parameters simultaneously using time course and steady-state data (Hoops et al., 2006).

To simulate the dynamics of any given model, COPASI can employ two different methods: deterministic and stochastic approaches and hybrid methods (COPASI, 2020g). It may also divide reversible reactions into forward and backward directions to help users adapt deterministic rate equations to stochastic equivalents and perform stochastic corrections on rate equations (Bergmann et al., 2017; Hoops et al., 2006).

COPASI uses as default the deterministic methods LSODA (Solver for Ordinary Differential Equations) or LSODAR (Ordinary Differential Equation Solver for Stiff or Non-Stiff System with root-finding), both present in the ODEPACK library (Hindmarsh, 1983). These approaches are modified versions of the Livermore Solver of Ordinary Differential Equations (LSODE). LSODA automatically selects between non-stiff and stiff methods, monitoring the data to decide which method to use to obtain more efficient results. LSODAR also has root-finding capabilities that detect the exact time point to each event (COPASI, 2020a; Petzold, 1983). COPASI automatically selects the most suited approach (COPASI, 2020a).

COPASI offers multiple methods that use stochastic formalisms to determine the system solution (COPASI, 2020f; Pahle, 2009), such as the Next-Reaction (Gibson & Bruck, 2000), the Direct (Daniel T Gillespie, 1976), τ-Leap (D. T. Gillespie, 2001), or adaptive SSA/τ-leap (Cao et al., 2007).

In addition, COPASI includes algorithms that combine deterministic and stochastic methods in a more time-efficient way. These hybrid approaches are the Hybrid RungeKutta, the Hybrid LSODA, and the Hybrid RK-45 (COPASI, 2020b). The Hybrid RungeKutta and the Hybrid LSODA determine the particle number for each reaction, using a deterministic approach if it is below a threshold and a stochastic approach if it is above. The Hybrid RK-45, on the other hand, allows the user to choose which method to employ for each reaction (Bergmann et al., 2017).

Metabolic Control Analysis (MCA) develops a method for quantitatively determining the degree of control that a specific enzyme exerts on flux and metabolite concentrations, thus replacing the intuitive, qualitative concept of rate-limiting steps. Furthermore, MCA aids in understanding the methods by which a given enzyme exerts high or low control and why numerous enzymes and transporters share the pathway's control. MCA identifies which steps should be changed in biotechnological or clinical pathways to change flux or metabolite concentration successfully.

The MCA identifies the critical steps by calculating three different metrics: the elasticity coefficients, flux control coefficients (FCC), and concentration control coefficients (Almquist et al., 2014; COPASI, 2020c). The FCC is the most critical indicator for strain optimising out of the three. FCC is

defined as the degree of control each enzyme exerts on a metabolic pathway flux (Saavedra & Moreno-Sánchez, 2013). This metric assesses a single reaction and returns a value for each of the system's remaining reactions, representing how affected its flux was. However, even if the results are not indisputable and precise, the FCC acts as a guideline for identifying prospective genetic alteration targets, facilitating the optimisation (Almquist et al., 2014).

COPASI can perform optimisation tasks to minimise or maximise a user-defined objective function by scanning one or more parameters over a given range. To meet the objective function, any parameter of a reaction, or even from multiple reactions, can be minimised or maximised. In addition, COPASI also informs to which extent such parameters should be modified (COPASI, 2020d). To achieve this, COPASI supports several different optimisation methods to find the best values toward the set goal (COPASI, 2020d): Evolutionary Programming (Fogel, 1994), Evolutionary Strategy (SRES) (Runarsson & Yao, 2000), Genetic Algorithm (Bäck & Schwefel, 1993), Genetic Algorithm SR (Runarsson & Yao, 2000), Hooke & Jeeves (Hooke & Jeeves, 1961), Levenberg – Marquardt (Kennedy & Eberhart, 1963; Levenberg, 1944), Nelder – Mead (Nelder & Mead, 1965), NL2SOL (Dennis et al., 1981), Particle Swarm (Kennedy & Eberhart, 1963), Praxis (Brent, 1974), Random Search (COPASI, 2020e), Simulated Annealing (Kirkpatrick et al., 1983), Steepest Descent (Fogel, 1994), and Truncated Newton (Nash, 1984).

2.3 *Escherichia coli*

In the last years a huge amount of omics-scale data have been published, allowing for major advances in metabolic reconstruction and modelling, which encouraged a better strain development. Furthermore, with the growing use of combinatorial and evolutionary methods, coupled with the rapid expansion of synthetic molecular methods, new and sizable combinations of gene expression systems and genetic backgrounds have been tested (Rodriguez et al., 2014).

Prokaryotic cells are excellent models to study many essential biochemical and molecular biological aspects. *E. coli* is the preferred organism to study molecular genetics' fundamental processes (Cooper, 2019; Yang et al., 2020). This choice is justified by its relative simplicity and ease of study in the laboratory. Moreover, the small size of the *E. coli*'s genome, which consists of approximately 4.6 million base pairs and contains about 4000 genes, provides advantages for genetic analysis. For instance, *E. coli* is three times less complex than the yeast *Saccharomyces cerevisiae* (Cooper, 2019).

Molecular genetic experiments are further facilitated by *E. coli*'s swift growth under well-defined laboratory conditions, duplicating every 20 minutes (Cooper, 2019). As the cells can be easily isolated as a colony, it is straightforward and rapid to select and analyse different genetic variants of an *E. coli* strain

using different culture mediums. Besides, *E. coli*'s ability to carry out biosynthetic reactions in simple defined media is advantageous to elucidate the involved heterologous pathways (Cooper, 2019; Rosano et al., 2019; Yang et al., 2020).

Regarding the production of AAA, like *L*-Tyr, the physiological and molecular knowledge, as well as the availability of well-established operational tools and techniques for metabolic engineering is not distributed equally among the microorganisms currently used (Rodriguez et al., 2014; Yang et al., 2020).

Such characteristics and available information have rendered *E. coli* the organism with the most recorded success cases and has contributed to a large range of well-characterised strains for AAA overproduction (Rodriguez et al., 2014; Yang et al., 2020). The use of *E. coli* as a microbial cell factory for recombinant proteins has shown to lower the cost of production and improve the yields (Rosano et al., 2019) and, since it is the best-studied organism, there are available several systems metabolic engineering tools and strategies, including the best-curated GSM models (Yang et al., 2020).

2.3.1 Review of stoichiometric models

BiGG (King et al., 2016) database lists several GSM models that can be used to optimize the production of a specific metabolite in *E. coli*. Table 2.3 presents several options of GSM models of *E. coli*.

Table 2.3 – GSM models of E. coli and their features.

BiGG id	Number of metabolites	Number of reactions	Number of genes	References
iJR904	761	1075	904	(BiGG, 2019b; Reed et al., 2003)
iJO1366	1805	2583	1367	(BiGG, 2019a; Orth et al., 2011)
IML1515	1877	2712	1516	(BiGG, 2019c; Monk et al., 2017)

2.3.2 Review of kinetic models

BioModels (Le Novère et al., 2006) and KiMoSys (Mochão et al., 2020) databases list several kinetic models that can be used to optimize the production of a specific metabolite in *E. coli*. Table 2.4 presents several options of kinetic models of *E. coli*.

Table 2.4 – Kinetic models of E. coli and their features.

Model	Number of metabolites	Number of reactions	Number of parameters	References
Chassagnole2002	18 + 7 co-metabolites	48	125	(Chassagnole et al., 2002; KiMoSys (https://kimosys.org), 2014a)
Singh2006	12	11	45	(KiMoSys (https://kimosys.org), 2018d; Singh & Ghosh, 2006)
Kadir2010	23 + 9 co-metabolites	30	173	(Kadir et al., 2010; KiMoSys (https://kimosys.org), 2018a)
Khodayari2014	93	138	1474	(Khodayari et al., 2014; KiMoSys (https://kimosys.org), 2014b)
Maria2014	Not mentioned	Not mentioned	17	(Maria, 2014)
Mannan2015	30	37	214	(KiMoSys (https://kimosys.org), 2018c; Mannan et al., 2015)
Jahan2016	52	129	341	(Jahan et al., 2016; KiMoSys (https://kimosys.org), 2018b)
Millard2017	62	68	449	(Millard et al., 2017)
Kurata2018	27	44	351	(KiMoSys (https://kimosys.org), 2018e; Kurata & Sugimoto, 2018)
Oliveira2020	88	87	Not mentioned	(Oliveira et al., 2021)

The Chassagnole2002 model represents the glycolysis and the pentose-phosphate pathway in *E. coli*. This dynamic model facilitated the CCM exploration and was designed and validated with measured metabolite concentrations at transient conditions. This model's structure was the first to link the kinetics of phosphotransferase system (PTS) – sugar transporter – with the CCM for *E. coli* (Chassagnole et al., 2002). In addition to the features present in Table 2.4, this model contains two compartments and 11 regulators – six activations and seven inhibitions (KiMoSys (https://kimosys.org), 2014a).

The Singh2006 model was developed to help develop anti-tuberculous drugs to target the persistent tubercule bacilli. This dynamic model consists of the glyoxylate bypass in *E. coli,* and it validates the pathway modelling protocol and demonstrates that it is possible to estimate changes in metabolic flux from gene expression data (Singh & Ghosh, 2006). In addition to the features present in Table 2.4, this model contains one compartment (KiMoSys (https://kimosys.org), 2018d).

The model Kadir2010 considers the primary metabolism of *E. coli,* therefore helping with the simulation of the metabolic changes in response to alterations of the environment and specific gene knockouts. This dynamic model includes pathways like glycolysis, pentose phosphate (PP) pathway and

tricarboxylic acid (TCA) cycle, allowing to estimate the ATP, NADPH and CO_2 production rates, which allowed the estimation of growth rate, flux of the oxidative PP pathway and cell yield, respectively (Kadir et al., 2010). In addition to the features present in Table 2.4, this model contains one compartment and 15 regulators (KiMoSys (https://kimosys.org), 2018a).

The Khodayari2014 model represents the core metabolism of *E. coli* using ensemble modelling concepts to fulfil the wild-type and seven mutant strains fluxomic data. This dynamic model includes the glycolysis/gluconeogenesis, PP pathway, TCA cycle, pyruvate metabolism, anaplerotic reactions and several other reactions of the metabolism (Khodayari et al., 2014). In addition to the features present in Table 2.4, this model contains two compartments and 60 regulators (Khodayari et al., 2014; KiMoSys (https://kimosys.org), 2014b).

The Maria2014 model represents a simplified but versatile version of a glycolysis model. This reduced model contains the necessary information to simulate the cell energy potential using the A(MDT)P level, and also simulate the role of ATP/ADP ratio in glycolysis (Maria, 2014).

The Mannan2015 model represents the whole CCM of *E. coli*, containing the whole glycolysis, the PP pathway, the TCA cycle, the glyoxylate shunt, and anaplerotic and acetate production reactions. This dynamic model incorporates all the available knowledge about the kinetic mechanism and the metabolic of every enzyme, and it was built adopting the bottom-up approach (Mannan et al., 2015). Besides the features present in Table 2.4, this model contains 37 regulators (KiMoSys (https://kimosys.org), 2018c; Mannan et al., 2015).

The Jahan2016 model represents the CCM of *E. coli* in a batch culture, containing: the glycolytic pathway, TCA cycle, PP pathway, Entner-Doudoroff pathway, anaplerotic pathway, glyoxylate shunt, oxidative phosphorylation, PTS, non-PTS and four protein transcription factors (cAMP receptor, catabolite repressor/activator, pyruvate dehydrogenase complex repressor and isocitrate lyase regulator), responsible for the metabolic gene regulations (Jahan et al., 2016). In addition to the features present in Table 2.4, this model contains one compartment (KiMoSys (https://kimosys.org), 2018b).

The Millard2017 model represents the central metabolism of *E. coli* cultivated on glucose under aerobic conditions. This dynamic model contains: the glucose PTS, glycolysis and gluconeogenesis, pentose phosphate and Entner-Doudoroff pathways, anaplerotic reactions, TCA cycle, glyoxylate shunt, acetate metabolism, nucleotide interconversion reactions and oxidative phosphorylation. A reaction was included to account for metabolic precursors' consumption, reducing equivalents and energy, thus connecting metabolism with cell proliferation. Besides the features present in Table 2.4, this model

contains 34 regulators and three compartments – environment, periplasm and cytoplasm (Millard et al., 2017).

The Kurata2018 model was developed to solve some problems of the model Jahan2016, therefore representing: the CCM of *E. coli*, containing the glycolytic pathway, PP pathway, Entner-Doudoroff pathway, anaplerotic pathway, TCA cycle, glyoxylate cycle and oxidative phosphorylation, alongside with the transcription factors of catabolite repressor/activator, cAMP receptor protein, pyruvate dehydrogenase complex repressor and acetate operon repressor. The improvements made on the Jahan2016 model were: adding missing typical dynamics of the TCA and glyoxylate cycles (Kurata & Sugimoto, 2018). Besides the features present in Table 2.4, this model contains one compartment (KiMoSys (https://kimosys.org), 2018e).

The Oliveira2020 model is an extension of the Millard2017 model to include Glycerol, Malonyl-CoA, and Beta-Alanine production. The purpose of this dynamic model was to use as a base to insert three independent heterologous pathways for 3-hydroxypropionate and acrylic acid production (Oliveira et al., 2021).

The Chassagnole2002, Kadir2010, Mannan2015, Jahan2016 and Kurata2018 models also integrate biomass production rate equations in their features (Chassagnole et al., 2002; Jahan et al., 2016; Kadir et al., 2010; Kurata & Sugimoto, 2018; Mannan et al., 2015).

.

*

3. Materials And Methods

3.1 Model Selection

From the ten previously described models, the Oliveira2020 metabolic model (Oliveira et al., 2021) (Figure 3.1) was selected. This model extends the Millard2017 (Millard et al., 2017) model (Figure 3.2) to include glycerol, malonyl-CoA, and β-alanine production. Therefore, it offers a detailed description of the CCM and side reactions that are important for AAA production, like the conversion of α-KG to *L*-Glu. The Oliveira2020 model contains 88 metabolites, 90 reactions, 34 regulators and three compartments – environment, periplasm and cytoplasm (Oliveira et al., 2021). The SBML version of the metabolic models used is available for download in the BIOMODELS database (Le Novère et al., 2006) with the identifiers MODEL2010030001 (Oliveira, 2020) and MODEL1505110000 (Millard et al., 2017).

This model does not contain the biosynthesis of *L*-Tyr, which is commonly synthesized by *E. coli*. Therefore, the first step toward *in silico* overproduction of *L*-Tyr is the extension of the CCM to synthesize this AAA. Also, with the intent to experiment with biomass production rate equations, the Jahan2016 (Jahan et al., 2016) model was used. This model is available for download in KiMoSys (Mochão et al., 2020) with the identifier Model EntryID 44 (KiMoSys (https://kimosys.org), 2018d).

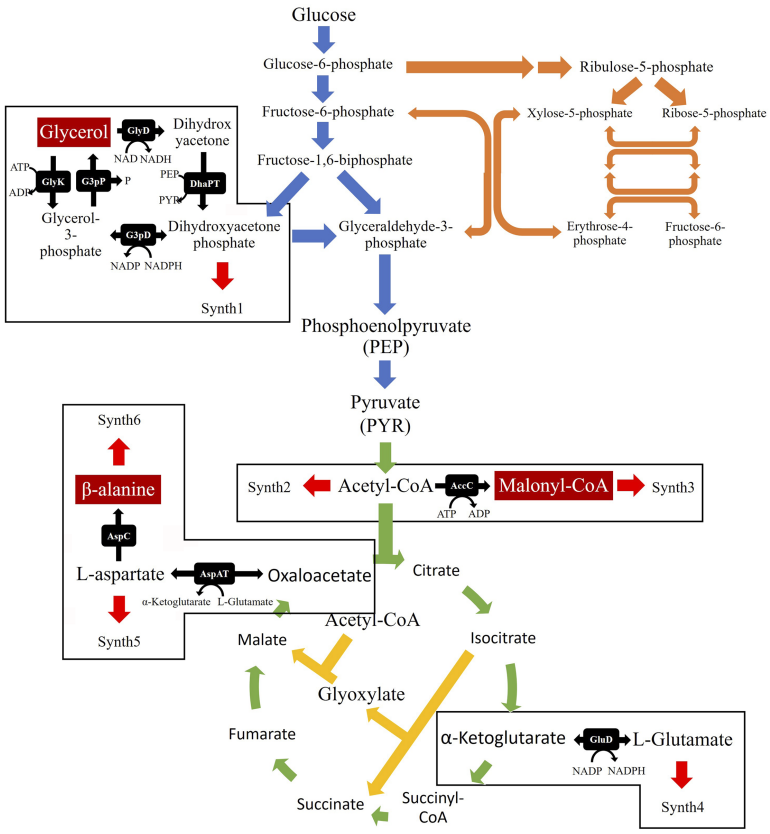

Figure 3.1 – Representation of the dynamic model of E. coli central carbon metabolism developed by Oliveira et al. (2021), based on Millard2017 model (Millard et al., 2017). The reactions portrayed by the blue, orange, green and yellow arrows represent, respectively, the glycolysis, pentose Phosphate pathway, tricarboxylic acid and the glyoxylate shunt, which are all present in the Millard2017 model. The black arrows represent the nine reactions added by Oliveira et al. The red arrows denote the Synth reactions that simulate the presence of the new metabolites in other pathways. Retrieved from Oliveira et al. (2021).

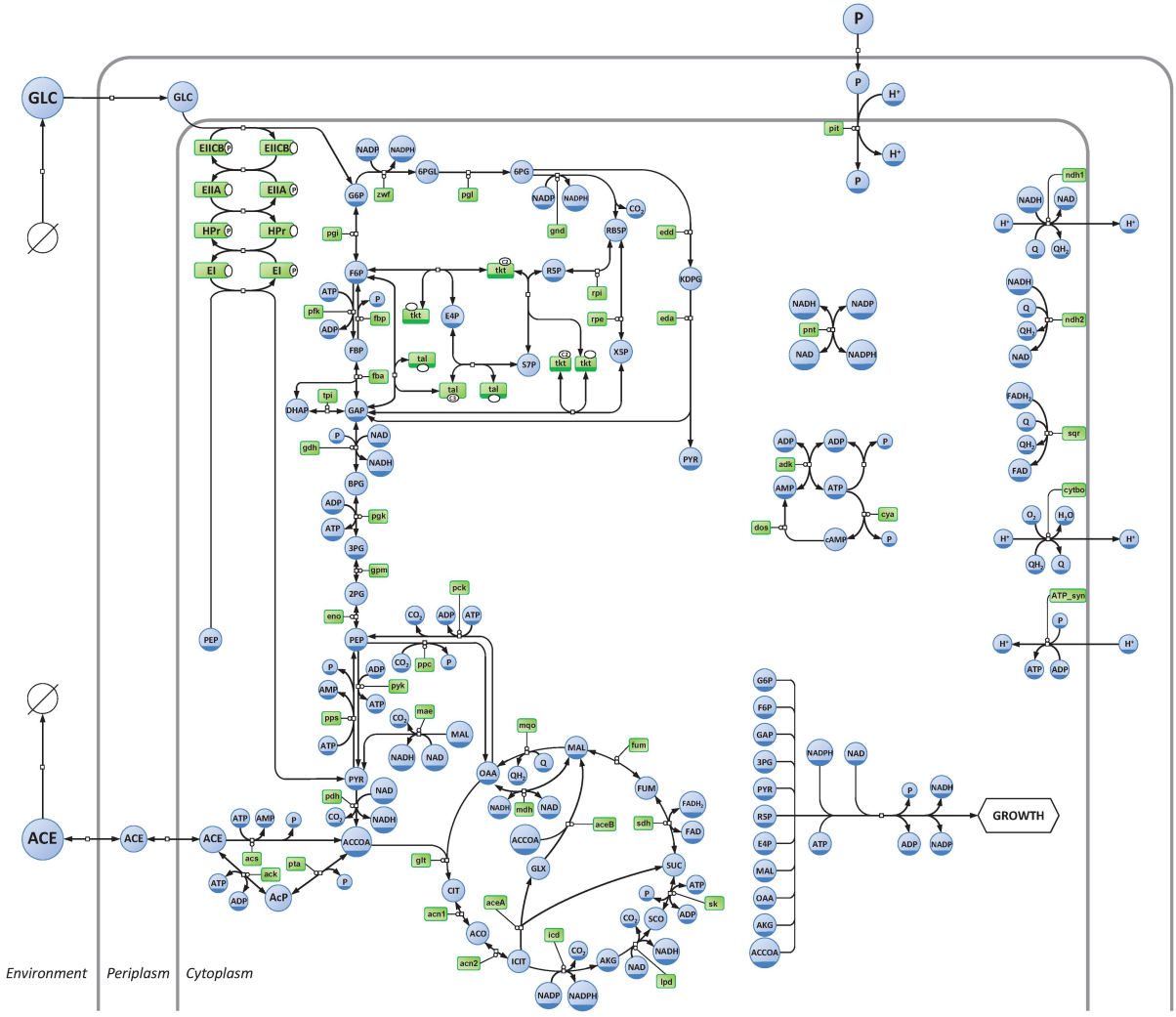

Figure 3.2 – Representation of the dynamic model of E. coli central carbon metabolism developed by Millard et al. (2016). Metabolites are shown in blue and enzymes in green. This model has a total of 62 metabolites and 68 reactions. Retrieved from Millard et al. (2017).

3.2 Kinetic Modelling

The model's development was divided into three phases: the extension of the CCM to include the production of *L*-Tyr, the production of *L*-Phe and the integration of the biomass production rate equation.

3.2.1 Parameter Selection and Determination

Online databases and available literature were used to find kinetic equations and the respective parameters for the reactions of interest. BioCyc (Karp et al., 2018) and BRENDA (Placzek et al., 2017) databases were used to obtain K_m and K_I values. Additionally, the equilibrium constants (K_e) needed for the reversible reactions were determined with eQuilibrator (Flamholz et al., 2012).

Due to its high specificity for the enzyme concentration, the V_{max} parameter is not usually available in the literature. Consequently, a method was designed to estimate the V_{max} of reactions

present in the native metabolism of *E. coli*. This designed method was similar to the one used by Chassagnole et al. (2002). Thus, to predict the flux of the reactions added to the model, a study was conducted to analyse the effects of different variables on the reactions' flux and the resulting kinetic model. The first step was to determine the steady-state flux distribution of the Millard2017 model using COPASI (Hoops et al., 2006) since it was the base model of Oliveira2020. The fluxes obtained were used to set the environmental conditions on the common reactions between the kinetic and stoichiometric models when performing an FVA with MEWpy (Pereira et al., 2021). The FVA allowed estimating flux (v) of the reactions to be added to the kinetic model. Equation 14 was used to determine the V_{max} of the reaction by equalizing v to the reaction's rate law:

$$v = V_{max} \cdot F(X, K) \leftrightarrow V_{max} = \frac{v}{F(X,K)} \quad (14)$$

in which, X is a vector of parameters and K a vector of steady-state concentrations for the metabolites. The steady-state concentration for the new metabolites was assumed to be $1\ \mathrm{mM}$.

3.2.1.1 Variables Impact on Parameter Determination

For this study, five variables important to determine the V_{max} of reactions present in the native metabolism of *E. coli* were evaluated, including:

1) The stoichiometric model;
2) The interval for the environmental conditions
3) The objective function;
4) The optimisation method used for the FVA;
5) The kinetic mechanism of the Synth Reactions.

Regarding 1), three different GSM models of *E. coli* K-12 MG1655 were compared, iML1515 (Monk et al., 2017), iJO1366 (Orth et al., 2011) and iJ904 (Reed et al., 2003). All selected models represent *E. coli* K-12 MG1655 and contain all *L*-Tyr and *L*-Phe pathways' genes. These models were selected to assess the influence of the model characteristics (number of metabolites, reactions, and genes) in this process.

Regarding 2), the environmental conditions were established with three different approaches: a) intervals of +1% for the Upper Bound and -1% for the Lower Bound; b) +10% for the Upper Bound and -10% for the Lower Bound; and c) +0.1 mM for the Upper Bound and -0.1 mM for the Lower Bound.

Variable 3) allowed evaluating the relevance of three different objective functions: a) biomass maximisation; b) *L*-Tyr maximisation; and c) chorismate maximisation, which involved adding the reaction representing the chorismate drain to all stoichiometric models. Whereas variable 4) assessed two optimisation methods, FBA and pFBA.

Finally, variable 5) allowed assessing the two kinetic mechanisms for the Synth reactions. Two different approaches were found in literature, Oliveira et. al (2021) used the Mass Action mechanism (Equation 15), and Machado et. Al (2014) used Michaelis-Menten kinetics (Equation 4) with K_m equal to 1 (Machado et al., 2014).

$$v = k_1 \cdot S \tag{15}$$

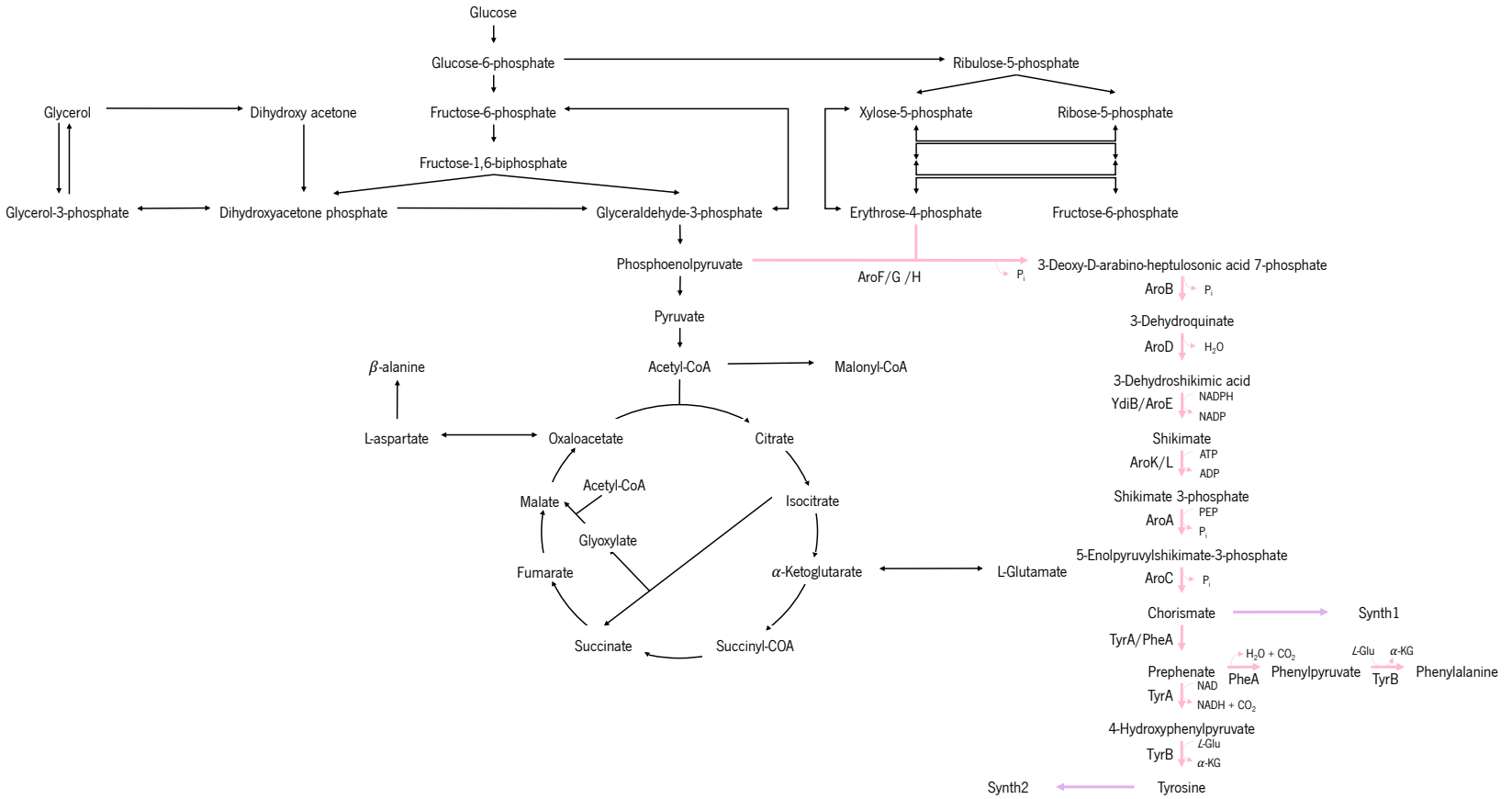

Figure 3.3 – Representation of the TyrOpt Model. This dynamic model contains the central carbon metabolism of E. coli and the addiction of the L-Tyr and L-Phe production pathaway. The reactions represented in black are all present in the original model (Oliveira2020). The pink arrows represent the twelve reactions that were added to obtain L-Tyr and L-Phe. The purple arrows show the Synth reactions. AroA (EPSP synthase), AroB (DHQ synthase), AroC (chorismate synthase), AroD (DHQ dehydratase), AroE (shikimate dehydrogenase), AroF (DAHP synthase, Phospho- 2-dehydro- 3-deoxyheptonate aldolase, Tyr-sensitive), AroG (DAHF synthase, Phospho-2-dehydro-3-deoxyheptonate aldolase, Phe-sensitive), AroH (DAHP synthase, Phospho-2-dehydro-3-deoxyheptonate aldolase, Trp-sensitive), AroK/L (shikimate kinase I/II), PheA (chorismate mutase-p-prephenate dehydratase), PpsA (phospho-enolpyruvate synthase), TktA (transketolase A), TyrA (chorismate mutase/prephenate dehydrogenase), TyrB (tyrosine aminotransferase) and YdiB (quinate/shikimate dehydrogenase), P (Phosphate), H_2O (Water), NADPH (Nicotinamide Adenine Dinucleotide Phosphate reduced), NADP (Nicotinamide Adenine Dinucleotide Phosphate), ATP (Adenosine Triphosphate), ADP (Adenosine Diphosphate), PEP (Phosphoenolpyruvate), CO_2 (Carbon Dioxide), L-Glu (Glutamic Acid) and α-KG (α-ketoglutarate).

3.2.2 Model Extension

After determining the V_{max} values using the previously described method, the Oliveira2020 model was extended to include the *L*-Tyr and *L*-Phe production pathway and the biomass production rate equations, creating the TyrOpt model (Figure 3.3). When a kinetic mechanism of a certain reaction is not specified in literature, the Michaelis-Menten kinetics was used for single substrate reactions, and Bi Bi kinetics for two substrates reactions.

3.2.2.1 *L*-Tyr Production

Considering the pathway for *L*-Tyr production (Figure 2.1) and the model composition, it was necessary to add the substrates and the reactions after the PEP formation to the model.

The reactions and their respective stoichiometry are shown below:

AroF/G/H	PEP + E4P → DAHP + P	(16)
AroB	DAHP → DHQ + P	(17)
AroD	DHQ ↔ 3-Dehydroshikimic acid + H_2O	(18)
YdiB/AroE	3-Dehydroshikimic acid + NADPH + H → Shikimate + NADP	(19)
AroK/L	Shikimate + ATP → Shikimate 3-Phosphate + ADP	(20)
AroA	Shikimate 3-Phosphate + PEP ↔ EPSP + P	(21)
AroC	EPSP → Chorismate + P	(22)
TyrA/PheA	Chorismate → Prephenate	(23)
TyrA	Prephenate + NAD → 4-Hydroxyphenylpyruvate + CO2 + NADH	(24)
TyrB_Tyr	4-Hydroxyphenylpyruvate + Glutamic Acid ↔ *L*-Tyr + α-Ketoglutarate	(25)

AroF/G/H These isoenzymes catalyse the conversion of PEP and E4P to DAHP (Equation 16). Therefore, to assess this dynamic in the kinetic model, three separate reactions were included in this model. The kinetic properties of AroF/G/H were fully characterized in the work of Ahmad and colleagues (Ahmad et al., 1987). They did not identify the kinetic mechanism of the enzymes. However, to accommodate the kinetic properties documented, the Random Bi Bi mechanism equation was adapted.

AroF showed values of K_m of 0.16 mM (K_{m_a}) and 0.33 mM (K_{m_b}), for PEP and E4P, respectively (Ahmad et al., 1987). *L*-Tyr inhibition was mixed-type when PEP was the variable substrate and the K_I value was 18 $\mu\mathrm{M}$ (K_{I_a}). Since the K_I' parameter was not reported nor possible to estimate, the inhibition was considered non-competitive in the kinetic equation. *L*-Tyr was considered an uncompetitive inhibitor against E4P, and the K_I value was 32 $\mu\mathrm{M}$ (K_{I_b}).

AroG showed K_m values of 0.32 mM (K_{m_a}) and 1.1 mM (K_{m_b}), for PEP and E4P, respectively (Ahmad et al., 1987). *L*-Phe inhibition was considered non-competitive against PEP as the variable substrate and uncompetitive against E4P as the substrate. K_I values of 9 $\mu\mathrm{M}$ (K_{I_a}) and 4 $\mu\mathrm{M}$ (K_{I_b}) were obtained with respect to PEP and E4P, respectively.

AroH has K_m values of 0.9 mM (K_{m_a}) and 0.3 mM (K_{m_b}), for PEP and E4P, respectively (Ahmad et al., 1987). *L*-Trp was a non-competitive inhibitor with PEP as the variable substrate and an uncompetitive inhibitor with E4P as the variable substrate. K_I values of 0.48 mM (K_{I_a}) and 0.56 mM (K_{I_b}) were obtained with respect to PEP and E4P, respectively.

AroB AroB catalyses the irreversible transformation of DAHP to DHQ (Equation 17). According to (Mehdi et al., 1987), the K_m for DAHP is reported to be between 33 and 50 $\mu\mathrm{M}$. To accommodate this range, the mean of these values (41.5 $\mu\mathrm{M}$) was used, as well as a single substrate Michaelis-Menten kinetics, as in the literature the mechanism was not mentioned.

AroD AroD catalyzes the conversion of DHQ to 3-dehydroshikimic acid (Equation 18). Liu and colleagues (Liu et al., 2015) presented a K_m for DHQ of 187.68 $\mu\mathrm{M}$. Even tought this reaction is described as reversible (Mitsuhashi & Davis, 1954), the K_m for 3-dehydroshikimic acid was not found. Therefore, a single substrate Michaelis-Menten kinetics was used.

YdiB/AroE YdiB/AroE catalyses the irreversible transformation of 3-dehydroshikimic acid to shikimate (Equation 19). This enzyme has been described by Dell and Frost (Dell & Frost, 1993). They reported a K_m for DHS of 0.072 mM (K_{m_a}) and for NADPH of 0.03 mM (K_{m_b}). Shikimate was a mixed-type inhibitor and the K_I value was 0.16 mM. However, since the parameter K_I' was not reported nor possible to estimate, the inhibition was considered non-competitive in the kinetic equation. There was no reference to a kinetic mechanism, so the Random Bi Bi was used.

AroK/L The AroK/L catalyses the conversion of shikimate to shikimate 3-phosphate (Equation 20). The kinetic parameters of this enzyme were described by Noble and colleagues (Noble et al., 2006), in which they reported a K_m of 0.028 mM (K_{m_a}) for shikimate and of 0.19 mM (K_{m_b}) for ATP. In their study, the kinetic equation for the Order BiBi mechanism and the inhibition constant for both products of the reaction was represented – 0.12 mM (K_{I_p}) for shikimate 3-phosphate and 0.09 mM (K_{I_q}) for ADP.

AroA AroA catalyses the conversion of shikimate 3-phosphate and PEP to EPSP (Equation 21). Shuttleworth and Evans (Shuttleworth & Evans, 1996) presented a kinetic description of this enzyme, in which K_m values of 0.135 mM (K_{m_b}), 0.1 mM (K_{m_a}), 0.011 mM (K_{m_p}), and 4.6 mM (K_{m_q}), were reported for shikimate 3-phosphate, PEP, EPSP, and phosphate, respectively.

eQuilibrator (Flamholz et al., 2012) was used to estimate the K_{eq} (860) for this reaction. Unfortunately, the underlying mechanism of this enzyme was not specified in this study. Therefore, a Reversible Ping-Pong Bi Bi mechanism was used.

AroC The AroC catalyses the irreversible transformation of EPSP to chorismate (Equation 22). According to Macheroux and colleagues (Macheroux et al., 1999), the K_m for EPSP is reported to be between 1.3 and 2.2 $\mu\mathrm{M}$. To accommodate this range, the mean of these values (1.75 $\mu\mathrm{M}$) was used, as well as a single substrate Michaelis-Menten kinetic, as in literature, the mechanism was not mentioned.

TyrA/PheA TyrA/PheA catalyse the conversion of chorismate to prephenate (Equation 23). Zhang and colleagues (S. Zhang et al., 2003) presented a K_m for chorismate of 296 $\mu\mathrm{M}$. Unfortunately, the underlying mechanism of these enzymes was not specified in this study, so a single substrate Michaelis-Menten kinetic was used.

TyrA TyrA also catalyses the irreversible transformation of prephenate to 4-hydroxyphenylpyruvate (Equation 24). This reaction has been described by Christendat and Turnbull (Christendat & Turnbull, 1999). They reported a K_m of 0.044 mM (K_{m_a}) for prephenate and of 0.103 mM (K_{m_b}) for NAD. The study referred a random mechanism, thus Random Bi Bi was used.

TyrB_Tyr The TyrB also catalyses the reversible transformation of 4-hydroxyphenylpyruvate and glutamic acid to *L*-Tyr and α-ketoglutarate (Equation 25). Powell and Morrison (Powell & Morrison, 1978) presented a kinetic description of this enzyme in which K_m values of 0.032 mM (K_{m_b}), 0.28 mM (K_{m_a}), 0.042 mM (K_{m_p}), and 0.23 mM (K_{m_q}), were reported for 4-hydroxyphenylpyruvate, glutamic acid, *L*-Tyr, and α-ketoglutarate, respectively. Furthermore, they also reported that this enzyme exhibited a Reversible Ping-Pong Bi Bi kinetics. Since K_{eq} was not found in literature, eQuilibrator (Flamholz et al., 2012) was used to estimate this reaction's equilibrium constant (0.9).

All relevant information regarding reactions is condensed in Table 3.1

Table 3.1 – Rate Law (RL), equations, and respective parameters of the reactions that belong to the L-Tyr pathway. The following abbreviations were used: RBB - Random Bi Bi; MM - Michaelis-Menten; OBB - Order Bi Bi and PPBB - Ping-Pong Bi Bi.

Reaction	RL	Equation	Parameters	Reference
AroF/G/H (AroF)	RBB	$\frac{V_{max} \cdot A}{\left(K_{m_a} + A\right) \cdot \left(1 + \frac{I}{K_{I_a}}\right)} + \frac{V_{max} \cdot B}{K_{m_b} + B \cdot \left(1 + \frac{I}{K_{I_b}}\right)}$	K_{m_a}= 0.16 mM K_{m_b} = 0.33 mM K_{I_a}= 0.018 mM K_{I_b}= 0.032 mM	(Ahmad et al., 1987)
AroF/G/H (AroG)	RBB	$\frac{V_{max} \cdot A}{\left(K_{m_a} + A\right) \cdot \left(1 + \frac{I}{K_{I_a}}\right)} + \frac{V_{max} \cdot B}{K_{m_b} + B \cdot \left(1 + \frac{I}{K_{I_b}}\right)}$	K_{m_a}= 0.32 mM K_{m_b} = 1.1 mM K_{I_a}= 9 µM K_{I_b}= 4 µM	(Ahmad et al., 1987)
AroF/G/H (AroH)	RBB	$\frac{V_{max} \cdot A}{\left(K_{m_a} + A\right) \cdot \left(1 + \frac{I}{K_{I_a}}\right)} + \frac{V_{max} \cdot B}{K_{m_b} + B \cdot \left(1 + \frac{I}{K_{I_b}}\right)}$	K_{m_a}= 0.9 mM K_{m_b} = 0.3 mM K_{I_a}= 0.48 mM K_{I_b}= 0.56 mM	(Ahmad et al., 1987)
AroB	MM	$\frac{V_{max} \cdot A}{K_m + A}$	K_m = 0.0415 mM	(Mehdi et al., 1987)
AroD	MM	$\frac{V_{max} \cdot A}{K_m + A}$	K_m = 0.18768 mM	(Liu et al., 2015)
AroE	RBB	$\frac{\frac{V_{max}}{1 + \frac{P}{K_I}} \cdot A \cdot B}{K_{m_a} \cdot K_{m_b} + A \cdot K_{m_b} + B \cdot K_{m_a} + A \cdot B}$	K_{m_a}= 0.072 mM K_{m_b} = 0.03 mM K_I = 0.16 mM	(Dell & Frost, 1993)

Table 3.1 – Rate Law (RL), equations, and respective parameters of the reactions that belong to the L-Tyr pathway. The following abbreviations were used: RBB - Random Bi Bi; MM - Michaelis-Menten; OBB - Order Bi Bi and PPBB - Ping-Pong Bi Bi (continuation).

AroK/L	OBB	$\frac{V_{max} \cdot A \cdot B}{\left(K_{m_a} \cdot \left(1 + \frac{P}{K_{I_p}}\right) + A\right) \cdot \left(K_{m_b} \cdot \left(1 + \frac{Q}{K_{I_q}}\right) + B\right)}$	K_{m_a} = 0.028 mM K_{m_b} = 0.19 mM K_{I_p} = 0.12 mM K_{I_q} = 0.09 mM	(Noble et al., 2006)
AroA	PPBB	$\frac{V_{max} \cdot \left(B \cdot A - \frac{P \cdot Q}{K_{eq}}\right)}{K_{m_b} \cdot B + K_{m_a} \cdot A + K_{m_a} \cdot K_{m_b} \cdot \frac{P}{K_{m_p}} + K_{m_a} \cdot K_{m_b} \cdot \frac{Q}{K_{m_q}} + B \cdot A + \frac{B \cdot P \cdot K_{m_b}}{K_{m_p}} + \frac{A \cdot Q \cdot K_{m_a}}{K_{m_q}} + \frac{K_{m_a} \cdot K_{m_b} \cdot P \cdot Q}{K_{m_p} \cdot K_{m_q}}}$	K_{m_a} = 0.1 mM K_{m_b} = 0.135 mM K_{m_p} = 0.011 mM K_{m_q} = 4.6 mM K_{eq} = 860	(Shuttleworth & Evans, 1996)
AroC	MM	$\frac{V_{max} \cdot A}{K_m + A}$	K_m = 0.00175 mM	(Macheroux et al., 1999)
TyrA/PheA	MM	$\frac{V_{max} \cdot A}{K_m + A}$	K_m = 0.296 mM	(S. Zhang et al., 2003)
TyrA	RBB	$\frac{V_{max} \cdot A \cdot B}{K_{m_a} \cdot K_{m_b} + A \cdot K_{m_b} + B \cdot K_{m_a} + A \cdot B}$	K_{m_a} = 0.044 mM K_{m_b} = 0.103 mM	(Christendat & Turnbull, 1999)
TyrB_Tyr	PPBB	$\frac{V_{max} \cdot \left(B \cdot A - \frac{P \cdot Q}{K_{eq}}\right)}{K_{m_b} \cdot B + K_{m_a} \cdot A + K_{m_a} \cdot K_{m_b} \cdot \frac{P}{K_{m_p}} + K_{m_a} \cdot K_{m_b} \cdot \frac{Q}{K_{m_q}} + B \cdot A + \frac{B \cdot P \cdot K_{m_b}}{K_{m_p}} + \frac{A \cdot Q \cdot K_{m_a}}{K_{m_q}} + \frac{K_{m_a} \cdot K_{m_b} \cdot P \cdot Q}{K_{m_p} \cdot K_{m_q}}}$	K_{m_a} = 0.28 mM K_{m_b} = 0.032 mM K_{m_p} = 0.042 mM K_{m_q} = 0.23 mM K_{eq} = 0.9	(Powell & Morrison, 1978)

3.2.2.2 *L*-Phe Production

As *L*-Phe is an inhibitor for AroG and prephenate is converted to *L*-Phe, reactions associated with *L*-Phe synthesis were included in the model to obtain more accurate results. This pathway consists of two steps catalysed by enzymes present in the previously described reactions.

The reactions and their respective stoichiometry are shown below:

PheA Prephenate → Phenylpyruvate + CO_2 + H_2O (26)

TyrB_Phe Phenylpyruvate + Glutamic Acid ↔ *L*-Phe + α-Ketoglutarate (27)

PheA PheA, in addition to converting chorismate to prephenate, also catalyses the irreversible transformation of prephenate to phenylpyruvate (Equation 26). This enzyme is characterised by a single substrate Michaelis-Menten kinetic, with a K_m of 0.559 mM (S. Zhang et al., 2000).

TyrB_Phe The TyrB also catalyses the reversible transformation of phenylpyruvate and glutamic acid to *L*-Phe and α-Ketoglutarate (Equation 27). Powell and Morrison (Powell & Morrison, 1978) presented a kinetic description of this enzyme in which K_m values of 0.056 mM (K_{m_b}), 0.28 mM (K_{m_a}), 0.06 mM (K_{m_p}), and 0.23 mM (K_{m_q}), were reported for phenylpyruvate, glutamic acid, *L*-Phe, and α-ketoglutarate, respectively. Furthermore, they reported that this enzyme exhibited a Reversible Ping-Pong Bi Bi kinetics. As K_{eq} was not found in literature, eQuilibrator was used to estimate the reaction's equilibrium constant (0.9).

All the relevant information regarding all the reactions is condensed in Table 3.2.

Table 3.2 – Rate Law (RL), equations, and respective parameters of the reactions that belong to the L-Phe pathway. The following abbreviations were used: MM - Michaelis-Menten and PPBB - Ping-Pong Bi Bi.

Reaction	RL	Equation	Parameters	Reference
PheA	MM	$\frac{V_{max} \cdot A}{K_m + A}$	K_m = 0.559 mM	(S. Zhang et al., 2000)
TyrB	PPBB	$\frac{V_{max} \cdot \left(B \cdot A - \frac{P \cdot Q}{K_{eq}}\right)}{K_{m_b} \cdot B + K_{m_a} \cdot A + K_{m_a} \cdot K_{m_b} \cdot \frac{P}{K_{m_p}} + K_{m_a} \cdot K_{m_b} \cdot \frac{Q}{K_{m_q}} + B \cdot A + \frac{B \cdot P \cdot K_{m_b}}{K_{m_p}} + \frac{A \cdot Q \cdot K_{m_a}}{K_{m_q}} + \frac{K_{m_a} \cdot K_{m_b} \cdot P \cdot Q}{K_{m_p} \cdot K_{m_q}}}$	K_{m_a} = 0.28 mM K_{m_b} = 0.056 mM K_{m_p} = 0.06 mM K_{m_q} = 0.23 mM K_{eq} = 0.9	(Powell & Morrison, 1978)

3.2.2.3 Biomass

The biomass equation present in Jahan2016 (Jahan et al., 2016) model was adapted to add the biomass production rate equations.

The reaction and its respective stoichiometry are shown below:

$$\text{Biomass} \leftrightarrow \text{X} \tag{28}$$

All the relevant information regarding this reaction is shown in Table 3.3.

Table 3.3 – Equation and respective parameters of the reaction that represents the Biomass.

Reaction	Equation	Parameters	Reference
Biomass	$\frac{mu \cdot X}{Volume}$	$kATP = 1.317324$ e-5	(Jahan et al., 2016)

Here, X represents the concentration of biomass, mu is a variable dependent on the concentration of ATP and $kATP$ is an adjustable constant (Equation 29).

$$mu = [ATP] \cdot kATP \tag{29}$$

3.2.2.4 Synth Reactions

The Synth reactions were added to the model to simulate the drain of metabolites to alternative pathways. These reactions' parameters were determined following the method mentioned in Section 3.2.1, by adding up the fluxes of all reactions that metabolize the intermediary metabolites in the stoichiometric model.

Five metabolites required adding these reactions: DHQ, Chorismate, Prephenate, *L*-Tyr, and Phenylpyruvate.

3.2.2.5 Exchange Reactions

Exchange reactions allow *L*-Tyr (LTYRex) and *L*-Phe (LPHEex) to be transported from the cytoplasm to the extracellular compartment. As it was impossible to find kinetic data for these transport reactions, as in previous studies (Millard et al., 2017; Oliveira et al., 2021), reactions representing the outer membrane diffusion were included in the model (Mendes et al., 2015). Additionally, as per (Millard et al., 2017), reversible Michaelis-Menten kinetics (Equation 4) with a V_{max} of 100 $\mathrm{mM/s}$ and a K_m of 10 mM were used.

3.3 Time Course Simulation

The time course simulations were conducted to calculate the AAA, *L*-Tyr and *L*-Phe production, the biomass, and the consumption of the precursor, glucose. COPASI (Hoops et al., 2006) was used, following a deterministic method (LSODA) and a duration of ten thousand and eight hundred seconds (approximately 3 hours), the time necessary to consume all the carbon source. The initial glucose concentration was 55.5 mM (10 $\mathrm{g/L}$) (Millard et al., 2017).

3.4 Optimisation Strategies

With the TyrOpt model, two new models that represent the first mutant strain (Mutant 0) were created. The first was an identical replica of the model used to run the optimisation and the AAA production simulation, and it was named TyrOpt_SIM_M0. The other one is the same model but converted to a chemostat system to perform the MCA, and it was named TyrOpt_MCA_M0.

As mentioned in Chapter 2, genetic engineering primarily uses gene over/under expressions and knockouts to optimise a pathway. Performing these changes in kinetic models requires adjusting the V_{max}. According to Equation 12, to allow a gene to be overexpressed ten times, the concentration of the corresponding enzyme should have a tenfold increase, which demands a tenfold higher V_{max}. Similarly, a tenfold under expression is characterised by a tenfold lower V_{max}. Knockouts, on the other hand, are replicated by establishing the V_{max} as zero, however, it is crucial to confirm whether the reaction belongs to the list of essential reactions of the organism as their knock-out *in vivo* may completely limit the organism's growth.

Hence, to begin the optimisation process, the FCC was calculated through an MCA, using the chemostat models. The control each reaction has over AAA formation is shown through these coefficients. As a result, the reaction with the greatest influence was selected and modified to enhance the pathway yields, resulting in novel mutant strains.

Then, the optimisation task in COPASI (Hoops et al., 2006) was used to maximise the *L*-Tyr production, now using the batch models. Thus, new *in silico* mutant strains were created (Mutant 1). In the optimisation, the method used was random search, which identifies the best solution by comparing the objective function's value to random values for the adjustable parameters within the user-defined bounds. As the probability of finding a solution for the objective function is correlated to the number of iterations, it is necessary to have a large number of iterations to attain good results (COPASI, 2020e).

Furthermore, it is essential to mention that this method aims to identify reactions that could be optimized and not to predict the greatest *L*-Tyr yield precisely. As a result, over/under expressions were limited to 50 times the initial V_{max} value in the lower or upper bound and a limit of 1000 iterations.

Lastly, this approach was repeated to optimise mutant strains with the new mutant models until the glucose feed restricted AAA synthesis.

4. Results And Discussion

4.1 V_{max} Calculation

The parameter V_{max} is not usually available in the literature due to its high specificity for the enzyme concentration. Consequently, stoichiometric models were used to determine the V_{max} of the enzymes that catalyse reactions from the native metabolism of *E. coli*.

4.1.1 Variables Impact on Parameter Determination

A study was performed de on the impact of five variables – 1) Objective Function; 2) Optimisation Method; 3) Kinetic Mechanism; 4) Stoichiometric Models; and 5) Environmental Conditions – on the reaction fluxes and the kinetic model. For this study, a total of 108 models (Appendix 1) were created, the outcome was compared to assess differences and which combination of variables created the model best suited for *in vivo* laboratory experiments. The selected variables consisted of all existing variables when performing an FVA.

The values of V_{max} obtained for the twelve reactions necessary to produce *L*-Tyr and *L*-Phe and the five synth reactions can be found in Appendix 2. The overall observations and final *L*-Tyr concentration obtained for each kinetic model designed are presented in Appendix 3.

The first variable - objective function - allowed to make some conclusions. Besides *L*-Tyr, chorismate was the only precursor of *L*-Tyr with flux in the Synth reaction. Therefore, it was important to test the maximization of its concentration. When maximising *L*-Tyr and chorismate concentrations, a condition for the biomass flux was added to the environmental conditions, namely the biomass flux obtained with the biomass maximisation (adding or subtracting the same interval as the rest of the environmental conditions). The maximisation of *L*-Tyr concentration provided 10 (over 36), functional models, as the FVA showed in higher fluxes for most reactions, resulting in higher V_{max} for each reaction causing the model to fail due to lack of factors essential for cell survival, such as ATP. The same issue was not observed to the same extent when chorismate concentration was maximised, as the reactions that lead to the synthesis of chorismate have the same flux in both maximisations, but the fluxes of the following reactions were lower when chorismate concentration is maximised, allowing 20 (over 36) models to function. The biomass maximisation allowed obtaining 24 (out of 36) functional models and is thus the most accurate objective function (Appendix 3).

The other three variables – Optimisation Method, Kinetic Mechanism, and Stoichiometric Models – did not significantly impact the final kinetic models. For the optimization method, FBA and pFBA

methods were compared. As detailed in Section 2.1.3, pFBA starts with a standard FBA, but then minimization of the sum of all the reaction fluxes is performed, removing the flux distribution of reactions that are not necessary for the cell to grow (Vilaça et al., 2018). Therefore, a difference was expected between the fluxes obtained through FBA and pFBA, but it was not observed, probably due to the level of constraint that the environmental conditions provide. Out of 54 pairs of models, only eight showed differences, in four pairs it was the difference between being a functional or not functional model (Appendix 3).

For the kinetic mechanism used when the synth reactions were added to the kinetic models, Mass-Action and Michaelis-Menten kinetics were compared. The differences between the results obtained through these models were small, almost non-existent, except in four out of 54 pair of models where it was the difference between a functional or not functional model (Appendix 3).

Three different stoichiometric models were evaluated (iML1515, iJO1366 and iJR904). Kinetic models created with fluxes obtained from the iML1515 model led to higher *L*-Tyr production (average of 41.67 $\mathrm{mg/L}$), whereas the iJR904 model led to the lowest (average of 33.19 $\mathrm{mg/L}$). These results (Appendix 3) seem proportional to the number of reactions in the stoichiometric model, where a higher number of reactions results in higher production of *L*-Tyr.

Regarding the environmental condition's interval variable (Appendix 3), it was possible to observe that the interval +/-0.1 mM seems to be too wide, designing models with high fluxes that do not allow the models to run for very long, probably due to lack of co-factors, providing only four (out of 36) functional models. On the contrary, when using the interval +/-1%, the problem seems to be the narrowness, with 20 (out of 36) functional models. In this case, not only did the models stop running before hour three, but *L*-Tyr did not stabilise probably because of a particularly high flux for the synth reaction. The interval that seemed to provide more precise and analytically more working models was +/-10%, with 30 (out of 36) functional models, showing that this interval provides the ideal gap to obtain reactions' fluxes.

After all variables were assessed and the results evaluated, three kinetic models that better represented the *in vivo* production of *L*-Tyr, out of the 108 designed were selected. All models obtained with the environmental conditions' interval of +/-0.1 mM and designed through the maximisation of *L*-Tyr were ignored as these exhibit higher concentrations of *L*-Tyr (average of 44.16 $\mathrm{mg/L}$). The models obtained for the chorismate maximisation resulted in lower concentrations of *L*-Tyr (average of 31.88 $\mathrm{mg/L}$) and were therefore discarded.

The chosen models and respective variables are presented in Table 4.1. For an easier distinction between models, the three selected models were renamed to TyrOpt1, TyrOpt2 and TyrOpt3. All models are constituted of 113 reactions and 121 metabolites.

Table 4.1 – Kinetic models developed to produce L-Tyr and L-Phe from glucose and respective variables used in its design.

	TyrOpt1	**TyrOpt2**	**TyrOpt3**
Previous name	TyrOpt_3A_Bi_a	TyrOpt_1A_Bii_c	TyrOpt_2B_Bi_c
1) Objective Function	Biomass	Biomass	Biomass
2) Optimisation Method	FBA	FBA	pFBA
3) Kinetic Mechanism	Mass-Action	Michaelis-Menten	Mass-Action
4) Stoichiometric Model	iJR904	iML1515	iJO1366
5) Environmental Conditions' Interval	+/- 1%	+/- 10%	+/- 10%

4.1.2 Models TyrOpt1, TyrOpt2 and TyrOpt3

Out of the five synth reactions, only one, for TyrOpt1 (Synth Chorismate), and two, for TyrOpt2 and TyrOpt3 (Synth Chorismate and Synth *L*-Tyr), have a flux; thus, the other three were discarded. For an easier distinction Synth Chorismate and Synth *L*-Tyr were renamed to Synth1 and Synth2, respectively).

The values obtained for the 12 reactions required to produce *L*-Tyr and *L*-Phe and the synth reactions for the three models are presented in Table 4.2 and 4.3.

Table 4.2 – V_{max} values calculated for the reactions necessary to produce L-Tyr and L-Phe in TyrOpt1, TyrOpt2 and TyrOpt3 models.

	TyrOpt1	**TyrOpt2**	**TyrOpt3**
Reaction	V_{max} (mM/s)	V_{max} (mM/s)	V_{max} (mM/s)
AroF/G/H (AroF)	0.1210	0.1487	0.1486
AroF/G/H (AroG)	0.5183	0.6371	0.6365
AroF/G/H (AroH)	0.0112	0.0138	0.0138
AroB	0.0058	0.0071	0.0071
AroD	0.0066	0.0081	0.0081
YdiB/AroE	0.0445	0.0547	0.0546
AroK/L	0.0231	0.0284	0.0284
AroA	0.0660	0.0811	0.0810
AroC	0.0056	0.0068	0.0068
TyrA/PheA	0.0054	0.0075	0.0075

Table 4.2 – V_{max} values calculated for the reactions necessary to produce L-Tyr and L-Phe in TyrOpt1, TyrOpt2 and TyrOpt3 models (continuation).

	TyrOpt1	TyrOpt2	TyrOpt3
Reaction	V_{max} (mM/s)	V_{max} (mM/s)	V_{max} (mM/s)
TyrA	0.0021	0.0029	0.0028
TyrB_Tyr	0.1504	0.2072	0.2070
PheA	0.0037	0.0052	0.0052
TyrB_Phe	0.1641	0.2305	0.2303

Table 4.3 – V_{max} and k_1 values calculated for the synth reactions necessary to produce L-Tyr and L-Phe in TyrOpt1, TyrOpt2 and TyrOpt3 models.

	TyrOpt1	TyrOpt2	TyrOpt3
Synth Reaction	k_1 (1/s)	V_{max} (mM/s)	k_1 (1/s)
Synth1	0.0014	0.0021	0.0010
Synth2	0	7.995 e-06	3.994 e-06

4.2 AAA Production

Before proceeding to the model optimisation, it was essential to analyse how the model performs with the new reactions.

All models were capable of consuming the 10 g/L of glucose in simulated time frame (3 h). Figures 4.1, 4.2 and 4.3 represent the time course for each model.

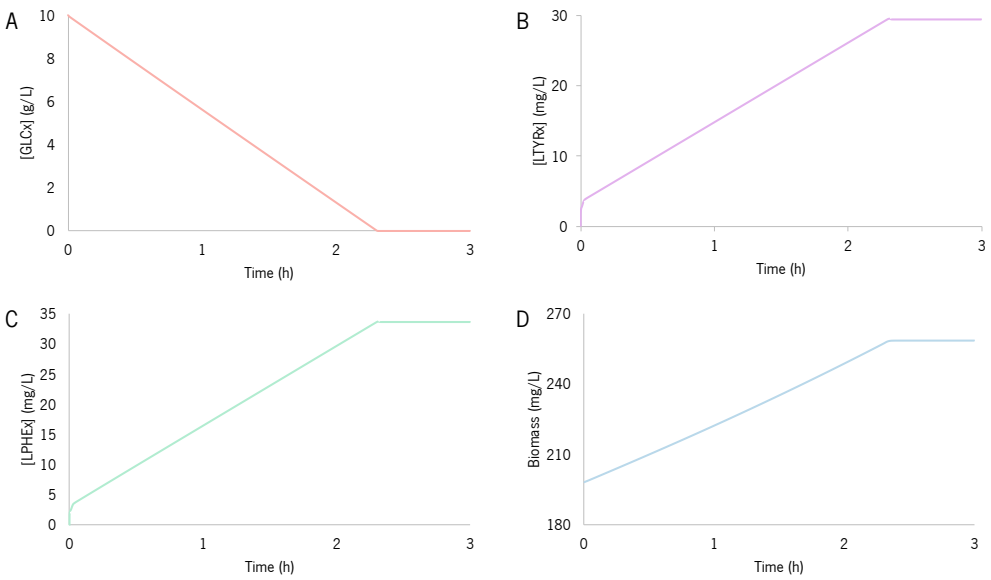

Figure 4.1 – Results of the TyrOpt1 model regarding glucose (GLC) consumption (A), and the production of L-Tyr (LTYR) (B), L-Phe (LPHE) (C), and Biomass (D).

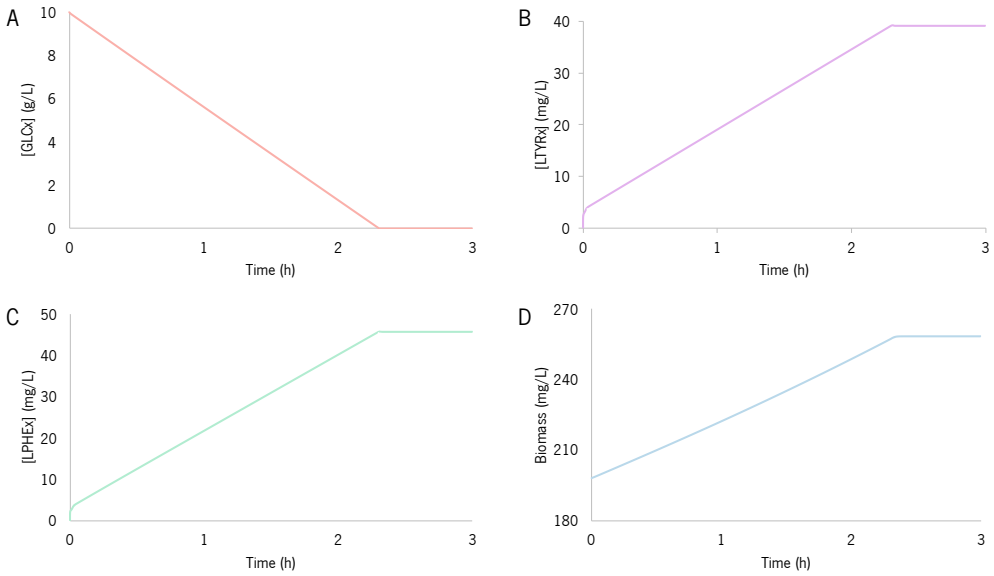

Figure 4.2 – Results of the TyrOpt2 model regarding glucose (GLC) consumption (A), and the production of L-Tyr (LTYR) (B), L-Phe (LPHE) (C), and Biomass (D).

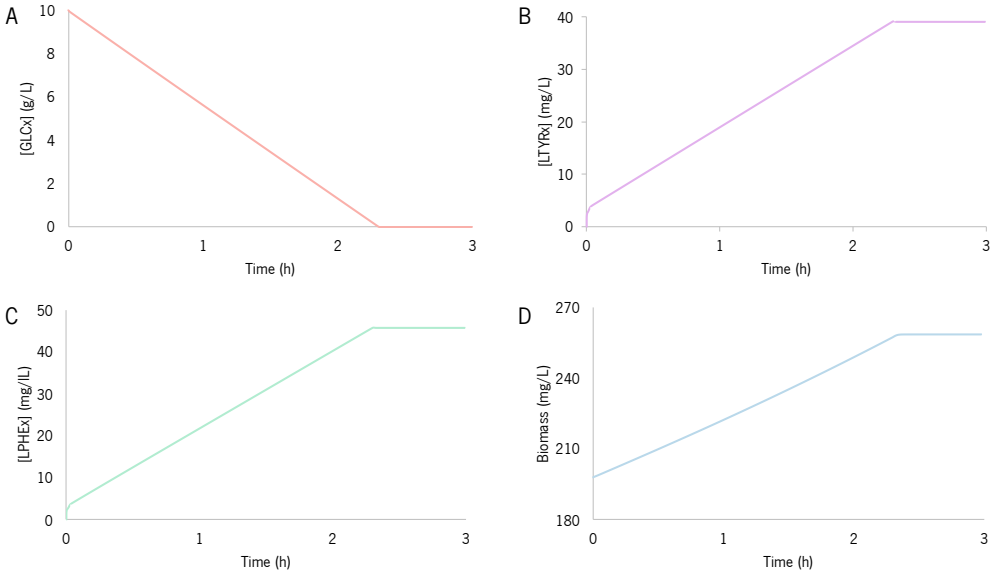

Figure 4.3 – Results of the TyrOpt3 model regarding glucose (GLC) consumption (A), and the production of L-Tyr (LTYR) (B), L-Phe (LPHE) (C), and Biomass (D).

The concentrations of *L*-Tyr, *L*-Phe and Biomass obtained for each model are presented in Table 4.4.

Table 4.4 – Concentrations of L-*Tyr,* L-*Phe and Biomass obtained for each model in the 3h Time Course.*

	TyrOpt1	TyrOpt2	TyrOpt3
[*L*-Tyr] (mg/L)	29.395	39.126	39.112
[*L*-Phe] (mg/L)	33.606	45.676	45.740
[Biomass] (mg/L)	258.560	258.456	258.455

The higher *L*-Tyr and *L*-Phe concentration in TyrOpt2 and TyrOpt3 compared to TyrOpt1, probably, is the effect of the different environmental conditions' interval used in the parameter determination, where TyrOpt1 were more constrained. This difference resulted in higher V_{max} values, and, consequently, higher concentrations.

It is worth noting that when all the glucose was consumed, there was a minor decline of the *L*-Tyr and *L*-Phe concentration, 0.409% and 0.237% for TyrOpt1, 0.328% and 0.163% for TyrOpt2 and 0.322% and 0.162% for TyrOpt3, respectively. This slight decline may be related to the fact that when there is a lack of glucose, some of the precursors stop being produced, their concentration drops to zero, and the organism consumes *L*-Tyr leading to a slight decline.

The higher production of *L*-Phe compared to L-Tyr in all models was experimentally confirmed by Kim and colleagues in a wild-type strain (Kim et al. 2018).

Regarding the biomass results, the difference between models was almost insignificant. The basis of the Jahan2016 model is quite different from the one used as an original base, Millard2017 in which the biomass equation was poorly explained. Hence, it is impossible to ensure that the biomass equation is correctly implemented in these models, which can help explain the nearly insignificant difference.

The results obtained were compared to the yields retrieved from the available literature. The models were used to simulate the synthesis of *L*-Tyr from a different concentration of glucose to recreate the studies found in the literature (Table 4.5).

Table 4.5 – Comparison of the yields obtained to available literature.

Paper	Initial [Glucose]	[*L*-Tyr] paper	[*L*-Tyr] TyrOpt1	[*L*-Tyr] TyrOpt2	[*L*-Tyr] TyrOpt3
Kim et al.. 2015	40 g/L	100 mg/L (value estimated from a graphic)	108.370 mg/L	147.515 mg/L	147.471 mg/L

The TyrOpt1 model was able to obtain a concentration of *L*-Tyr similar to the one obtained *in vivo* in the Kim et al. (2015) study. However, TyrOpt2 and TyrOpt3 obtained a concentration slightly higher than the documented one. This shows how more precise TyrOpt1 is when predicting *L*-Tyr concentration, probably due the more constrained parameter determination. No studies were found to compare the *L*-Phe production.

4.3 Optimisation

A stable steady-state must be found to obtain the best targets for optimisation through an MCA. However, in order to be able to find a steady-state, the search resolution was highly increased, rendering the results unreliable.

Hence, two different optimisation approaches were executed:

- Optimisation of targets obtained through the MCA and COPASI;
- Optimisation of targets used in strategies found in the literature.

Therefore, these optimisations' results should serve as a guide in the search for strain improvement strategies. Quantitative comparisons between different pathway designs should not be performed but should be rather regarded as a general idea of the best targets for increasing *L*-Tyr production *in vivo*.

4.3.1 Optimisation of the targets obtained through the MCA and COPASI

The first MCA was performed in the TyrOpt1_MCA_M0, TyrOpt2_MCA_M0 and TyrOpt3_MCA_M0 models (Appendix 4). The FCC obtained through this analysis were not significantly different between models. The reaction with higher control over *L*-Tyr production seemed to be the *L*-glutamate dehydrogenase (GluD) - highest positive FCC (Figure 4.4). As observed in Figure 3.1, GluD is the reversible reaction that converts *L*-Glu to α-KG. The positive FCC shows GluD as a potential bottleneck for *L*-Tyr production and, therefore, a target for overexpression. The models were optimised using COPASI's optimization task. The results and improved production yields obtained for the modified models are shown in Table 4.6.

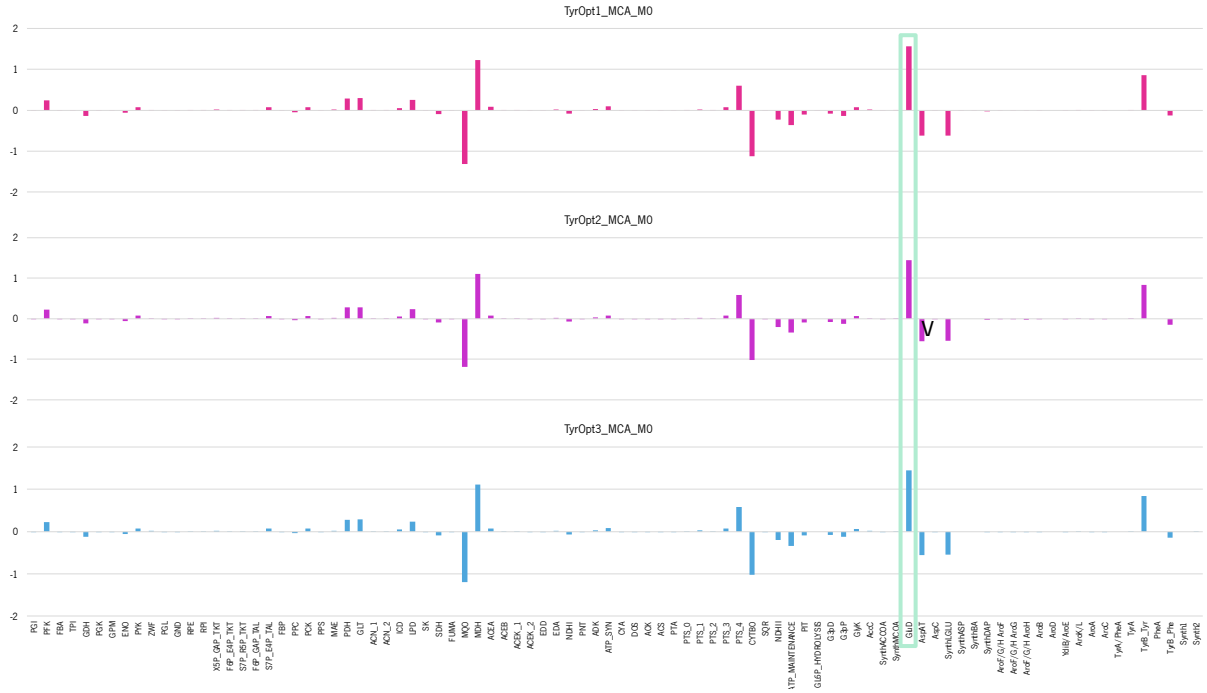

Figure 4.4 – Flux Control Coefficients for the mutant 0 of the three TyrOpt models, where the reaction with the most impact in the production of L-Tyr is highlighted in green correspondent to L-glutamate dehydrogenase (GluD).

Table 4.6 – Results obtained for the first optimisation (GluD reaction) of L-Tyr production.

Model	Original V_{max} (mM/s)	Optimised V_{max} (mM/s)	V_{max} Variation	Original [*L*-Tyr] (mg/L)	Optimised [*L*-Tyr] (mg/L)	[*L*-Tyr] Variation
TyrOpt1	0.1716	2.153	12.5 x ↑	29.395	30.451	3.59%
TyrOpt2	0.1716	0.592	3.5 x ↑	39.126	40.240	2.85%
TyrOpt3	0.1716	1.014	5.9 x ↑	39.112	40.407	3.31%

Although GluD was overexpressed, the variation in *L*-Tyr concentration was negligible, demonstrating that this reaction is not the ideal first target.

A second iteration using the Mutant1 models – TyrOpt1_MCA_M1, TyrOpt2_MCA_M1 and TyrOpt3_MCA_M1 – was performed (Appendix 4). Even though the targets showed in each model appeared to be the same, the FCC values obtained were different between models (Figure 4.5). The reaction that seemed to have higher control over *L*-Tyr production was the malate quinone oxidoreductase (MQO) reaction, with the lowest negative FCC (Figure 4.4). MQO, as observed in Figure 3.2, is the reaction that converts malate to oxaloacetate. Oxaloacetate is a metabolite present in the TCA, where α-KG is synthesised. Oxaloacetate also can be converted to *L*-aspartate in a reaction where *L*-Glu is converted to α-KG. Since *L*-Glu is necessary for the TyrB reaction, the underexpression of the MQO reaction was expected. The negative FCC shows that this reaction impairs *L*-Tyr's production, being therefore a target for underexpression. The models were optimized using COPASI's optimisation

task. The results obtained, as well as the improved production yield for the modified models are present in Table 4.7.

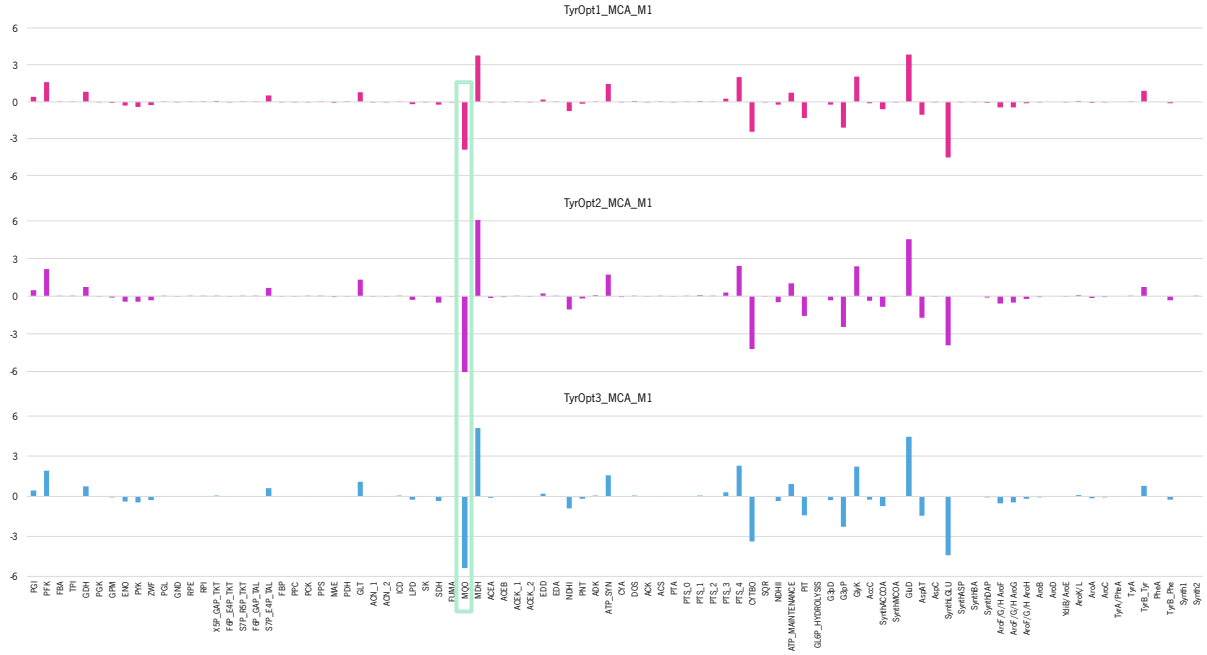

Figure 4.5 – Flux Control Coefficients for the mutant 1 of the three TyrOpt models, where the reaction with the most impact in the production of L-Tyr is highlighted in green correspondent to malate quinone oxidoreductase (MQO).

Table 4.7 – Results obtained for the second optimisation (MQO reaction) of the L-Tyr production.

Model	Original V_{max} (mM/s)	Optimised V_{max} (mM/s)	V_{max} Variation	Original [*L*-Tyr] (mg/L)	Optimised [*L*-Tyr] (mg/L)	[*L*-Tyr] Variation
TyrOpt1	4.623	7.627	1.6 x ↑	30.451	30.463	0.042%
TyrOpt2	4.623	84.513	18.3 x ↑	40.240	40.315	0.034%
TyrOpt3	4.623	21.035	4.6 x ↑	40.407	40.488	0.200%

Contrary to what was expected by the FCC value, MQO was overexpressed, but it barely increased *L*-Tyr production.

A third iteration using the Mutant2 models – TyrOpt1_MCA_M2, TyrOpt2_MCA_M2 and TyrOpt3_MCA_M2 – was performed to finalise the optimisation process through this approach (Appendix 4). Each model's targets seem to be the same, but the obtained FCC values were different, as previously observed (Figure 4.7). The reaction that seems to have higher control over *L*-Tyr production was the glycerol-3-phosphate phosphatase (G3pP) reaction, with the lowest negative FCC (Figure 4.4). GluD is a potential target, but the optimisation result is higher than 50-time fold the original V_{max} value, thus, it was discarded. G3pP deviates dihydroxyacetone phosphate that can be converted to glyceraldehyde-3-phosphate, a metabolite required at the beginning of the pathway that synthesises *L*-

Tyr (TktA reaction). Therefore, the negative FCC shows G3pP reaction as a negative effect for *L*-Tyr's production and consequently a target for underexpression. The models were optimized using COPASI's optimization task. The results obtained and the improved production yield for the modified models are shown in Table 4.8.

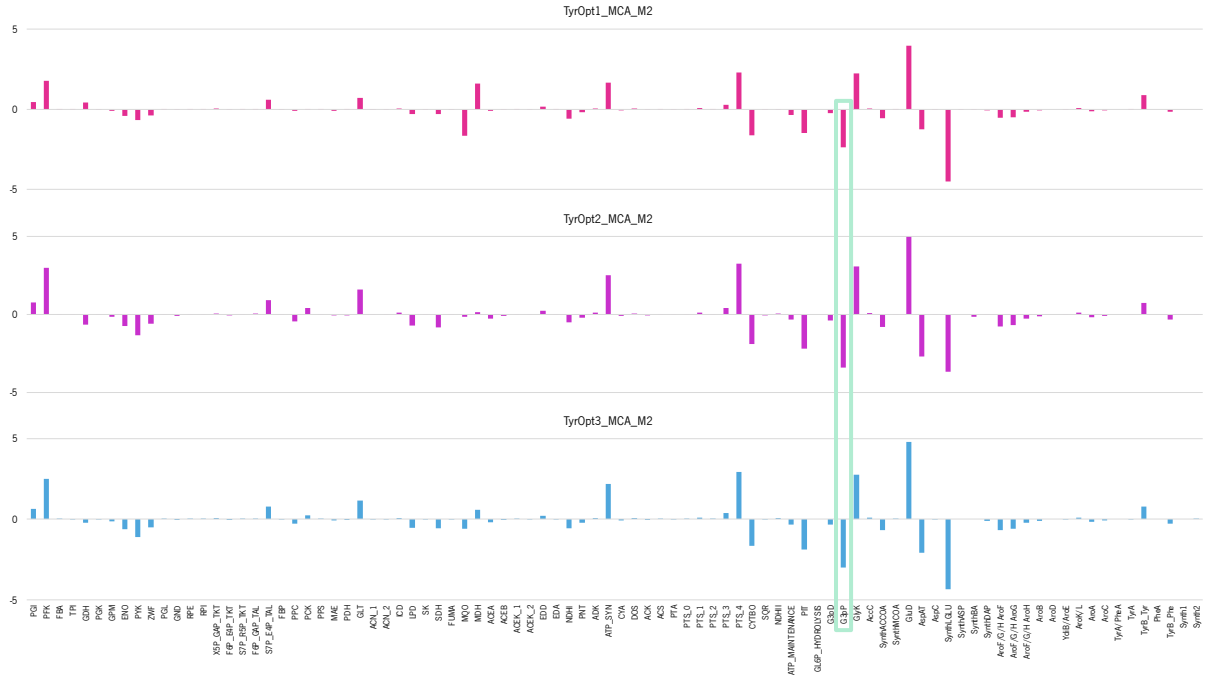

Figure 4.6 – Flux Control Coefficients for the mutant 2 of the three TyrOpt models, where the reaction with the most impact in the production of L-Tyr is highlighted in green correspondent to glycerol-3-phosphate phosphatase (G3pP).

Table 4.8 – Results obtained for the third optimisation (G3pP reaction) of the L-Tyr production.

Model	Original V_{max} (mM/s)	Optimised V_{max} (mM/s)	V_{max} Variation	Original [*L*-Tyr] (mg/L)	Optimised [*L*-Tyr] (mg/L)	[*L*-Tyr] Variation
TyrOpt1	0.7741	0.823	1.1 x ↑	30.463	30.463	0.001%
TyrOpt2	0.7741	0.205	3.8 x ↓	40.315	40.326	0.028%
TyrOpt3	0.7741	0.205	3.8 x ↓	40.488	40.492	0.009%

G3pP was underexpressed in two models, whereas in TyrOpt1 it was overexpressed. TyrOpt1 was the only model in which V_{max} values were calculated using an +/- 1% interval in the environmental conditions (the others used a +/- 10% interval was used). The use of a +/- 1% interval probably constrained the model so much, that the V_{max} of the G3pP reaction was already optimised. These modifications only led to a negligible increase in *L*-Tyr production.

These optimisations allowed an overall increase of 3.636%, 3.067% and 3.527% in the production of *L*-Tyr – TyrOpt1, TyrOpt2 and TyrOpt3, respectively. Most improvements were observed in the first

optimisation, causing an overlap of the production of *L*-Tyr for Mutant1, Mutant2 and Mutant3 of TyrOpt (Figure 4.7).

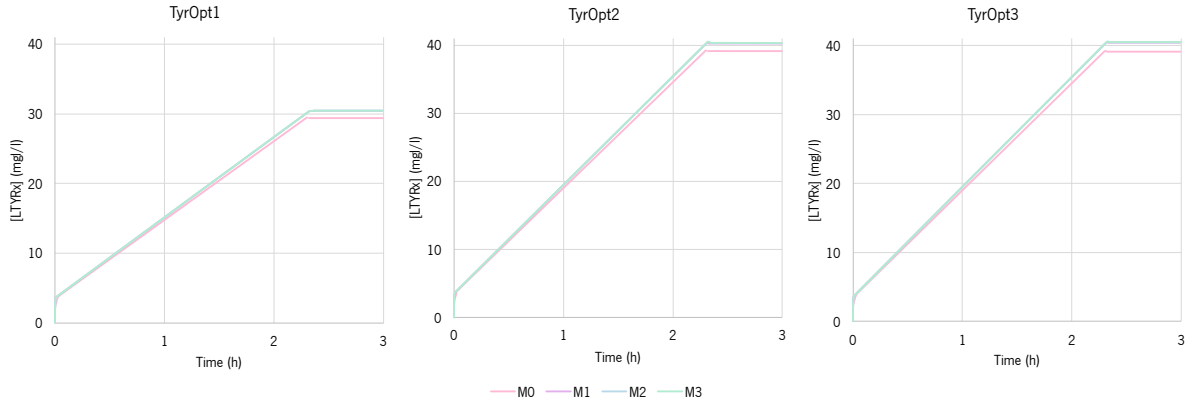

Figure 4.7 – L-Tyr production from the four mutants of each TyrOpt model. The simulations were conducted with 10 g/L of glucose for all the mutants. Mutant 0 - model with the heterologous pathway; Mutant 1 - increase in the V_{max} of the GluD; Mutant 2 - increase in the V_{max} of the MQO; Mutant 3 – increase/decrease in the V_{max} of the G3pP.

4.3.2 Optimisation of the targets used in strategies found in literature

Since the MCA did not allow identifying targets similar to the ones used in strategies described in literature, and the identified targets did not significantly improve the L-Tyr production, another approach was used. Here, the *L*-Tyr production pathway (Figure 2.6) and different strategies reported to improve *L*-Tyr production (Table 2.4) were analysed.

In the first optimisation, the selected targets were AroF/G/H (AroG), TyrB_Tyr, PheA and TyrB_Phe. AroF/G/H is catalysed by three isoenzymes, in which AroG was shown to have the highest impact on *L*-Tyr improvement (Rodriguez et al., 2014). TyrB_Tyr is the limiting last step in the pathway that produces *L*-Tyr. PheA and TyrB_Phe are reactions that deviate metabolites from the *L*-Tyr pathway to produce *L*-Phe.

The results obtained and the improved production yields for the modified models are shown in Table 4.9.

Table 4.9 – Results obtained for the first optimisation of the L-Tyr production using targets available in literature.

Model	Reaction	Original V_{max} (mM/s)	Optimised V_{max} (mM/s)	V_{max} Variation	Original [*L*-Tyr] (mg/L)	Optimised [*L*-Tyr] (mg/L)	[*L*-Tyr] Variation
TyrOpt1	AroF/G/H (AroG)	0.5183	3.148	6.1 x ↑	29.395	33.736	14.770%
	TyrB_Tyr	0.1504	0.751	5.0 x ↑			
	PheA	0.0037	8.074 E-05	45.6 x ↓			
	TyrB_Phe	0.1641	0.117	1.4 x ↓			

Table 4.9 – Results obtained for the first optimisation of the L-Tyr production using targets available in literature (continuation).

Model	Reaction	Original V_{max} (mM/s)	Optimised V_{max} (mM/s)	V_{max} Variation	Original [*L*-Tyr] (mg/L)	Optimised [*L*-Tyr] (mg/L)	[*L*-Tyr] Variation
TyrOpt2	AroF/G/H (AroG)	0.6371	3.002	4.7 x ↑	39.126	44.264	13.131%
	TyrB_Tyr	0.2072	8.082	39.0 x ↑			
	PheA	0.0052	1.270 E-04	40.8 x ↓			
	TyrB_Phe	0.2305	0.155	1.5 x ↓			
TyrOpt3	AroF/G/H (AroG)	0.6365	3.493	5.5 x ↑	39.112	47.416	21.232%
	TyrB_Tyr	0.2070	8.448	40.8 x ↑			
	PheA	0.0001	1.939 E-05	5.3 x ↓			
	TyrB_Phe	0.2303	0.217	1.1 x ↓			

As expected, AroF/G/H (AroG) and TyrB_Tyr were overexpressed, and PheA and TyrB_Phe under-expressed. The increase in *L*-Tyr concentration was more promising than in the previous approach.

In the second optimisation, the selected targets were YdiB/AroE, AroK/L, TyrA/PheA and TyrA. YdiB/AroE and AroK/L are two limiting steps of the SHK pathway. TyrA/PheA and TyrA are the two steps of the *L*-Phe pathway, that deviate Prephenate from the *L*-Tyr pathway.

The results obtained and the improved production yield for the modified models are shown in Table 4.10.

Table 4.10 – Results obtained for the second optimisation of the L-Tyr production using targets available in literature.

Model	Reaction	Original V_{max} (mM/s)	Optimised V_{max} (mM/s)	V_{max} Variation	Original [*L*-Tyr] (mg/L)	Optimised [*L*-Tyr] (mg/L)	[*L*-Tyr] Variation
TyrOpt1	YdiB/AroE	0.0445	0.094	2.1 x ↑	33.736	79.803	136.549%
	AroK/L	0.0231	0.165	7.1 x ↑			
	TyrA/PheA	0.0054	0.131	24.4 x ↑			
	TyrA	0.0021	5.282 E-03	2.6 x ↑			
TyrOpt2	YdiB/AroE	0.0547	0.434	7.9 x ↑	44.264	89.338	101.830%
	AroK/L	0.0284	1.370	48.2 x ↑			
	TyrA/PheA	0.0075	0.181	24.1 x ↑			
	TyrA	0.0029	6.056 E-03	2.1 x ↑			

Table 4.10 – Results obtained for the second optimisation of the L-Tyr production using targets available in literature (continuation).

Model	Reaction	Original V_{max} (mM/s)	Optimised V_{max} (mM/s)	V_{max} Variation	Original [*L*-Tyr] (mg/L)	Optimised [*L*-Tyr] (mg/L)	[*L*-Tyr] Variation
TyrOpt3	YdiB/AroE	0.0546	0.287	5.2 x ↑	47.416	82.614	74.231%
	AroK/L	0.0284	0.650	22.9 x ↑			
	TyrA/PheA	0.0075	0.227	30.2 x ↑			
	TyrA	0.0028	5.149 E-03	1.8 x ↑			

As expected, YdiB/AroE, AroK/L, TyrA/PheA and TyrA were overexpressed. The increase in *L*-Tyr concentration showed truly promising results.

These two optimisations allowed an overall increase of 171.488%, 128.332% and 111.222% in the production of *L*-Tyr – TyrOpt1, TyrOpt2 and TyrOpt3, respectively (Figure 4.8). When doing the same optimisations, but, with each reaction individually, TyrA reported the hightest impact in increasing the concentration of *L*-Tyr. These results confirmed the model's functionality, as the optimisation was done on targets already studied *in vivo*.

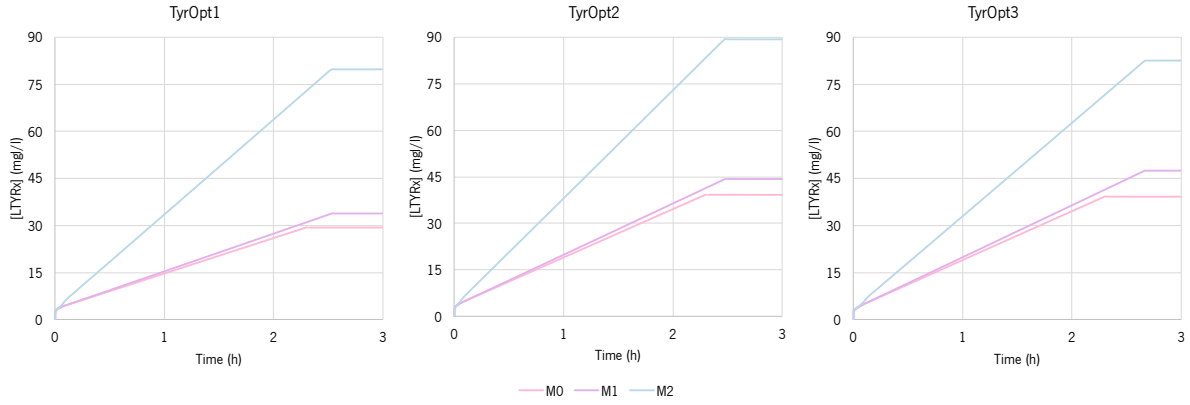

Figure 4.8 – L-Tyr production from the three mutants of each TyrOpt model. The simulations were conducted with 10 g/L of glucose for all the mutants. Mutant 0 - model with the heterologous pathway; Mutant 1 - increase in the V_{max} of the AroF/G/H (AroG) and TyrB_Tyr and decrease in the V_{max} of the PheA and TyrB_Phe; Mutant 2 - increase in the V_{max} of the YdiB/AroE, AroK/L, TyrA/PheA and TyrA.

5. Conclusion and Future Perspectives

5.1 Conclusions

The aim of this work was to perform the *in silico* insertion of the *L*-Tyr pathway in a kinetic model of the central carbon metabolism of *E. coli* and to identify the best target genes to design a *L*-Tyr overproducing strain.

In conclusion, it is possible to affirm that the main goal of this thesis was achieved. This work resulted in the development of three models that allow the production of *L*-Tyr and *L*-Phe using glucose as a carbon source (Table 4.1). Comparing the results provided from these models with published *in vivo* results, it seems that TyrOpt1 was more precise when predicting the concentration of *L*-Tyr than TyrOpt2 and TyrOpt3.

The parameter V_{max} is usually not available in the literature due to its high specificity for the enzyme concentration. Thus, a study on the impact of five variables – Objective Function, Optimisation Method, Kinetic Mechanism, Stoichiometric Models and Environmental Conditions Interval – on the reaction fluxes and the kinetic model was performed. A best set of variables was not found when analysing and comparing all 108 models. Yet it was possible to analyse the impact different variables had on parameter determination and in the designed model.

Finally, as the *L*-Tyr yield remains too low to be economically used and sustainably feasible in industrial-scale production, there is a need for optimisation strategies that allow an increase in *L*-Tyr synthesis, so two different approaches were conducted. A stable steady-state must be found to perform the MCA and obtain the best optimisation targets. However, the search resolution had to be highly increased. Therefore, the results obtained were not reliable. Nonetheless, the targets obtained in the MCA were tested but did not provide a significant increase in production. Thus, a different optimisation route was conducted. The expression of target genes already tested in literature, such as *aroG*, *aroE*, *aroL*, *tyrA* and *tyrB,* was optimised, and the results obtained using these targets provided a much more substantial increase in *L*-Tyr's production. The underexpression of the *L*-Phe production pathway, that deviates prephenate from the *L*-Tyr pathway, was able to increase the yield of *L*-Tyr.

5.2 Future Perpectives

In the future, more work is needed to enhance the designed kinetic models. It would be interesting to expand the model to contain the synthesis of different metabolites produced from *L*-Tyr, such as caffeic acid and curcuminoids.

Testing different tools for kinetic model optimisation, like MEWpy or OptimModels, would also be essential to search for new additional targets for *L*-Tyr maximisation.

Finally, the optimisation results should be validated. For that reason, these new designed strains should be implemented *in vivo*, to evaluate the validity of the obtained results.

BIBLIOGRAPHIC REFERENCES

Ahmad, S., Johnson, J. L., & Jensen, R. A. (1987). The recent evolutionary origin of the phenylalanine-sensitive isozyme of 3-deoxy-d-arabino-heptulosonate 7-phosphate synthase in the enteric lineage of bacteria. *Journal of Molecular Evolution*, *25*(2), 159–167. https://doi.org/10.1007/BF02101758

Akinwumi, B. C., Bordun, K. A. M., & Anderson, H. D. (2018). Biological activities of stilbenoids. *International Journal of Molecular Sciences*, *19*(3), 1–25. https://doi.org/10.3390/ijms19030792

Almquist, J., Cvijovic, M., Hatzimanikatis, V., Nielsen, J., & Jirstrand, M. (2014). Kinetic models in industrial biotechnology - Improving cell factory performance. *Metabolic Engineering*, *24*, 38–60. https://doi.org/10.1016/j.ymben.2014.03.007

Alper, H. S. (Ed.). (2013). *Systems Metabolic Engineering: Methods and Protocols*. Humana Press.

Bäck, T., & Schwefel, H.-P. (1993). An Overview of Evolutionary Algorithms for Parameter Optimization. *Evolutionary Computation*, *1*(1), 1–23. https://doi.org/10.1162/evco.1993.1.1.1

Bai, Y., Bi, H., Zhuang, Y., Liu, C., Cai, T., Liu, X., Zhang, X., Liu, T., & Ma, Y. (2014). Production of salidroside in metabolically engineered *Escherichia coli*. *Scientific Reports*, *4*, 1–8. https://doi.org/10.1038/srep06640

Bailey, J. E. (1991). Toward a science of metabolic engineering. *Science*, *252*(5013), 1668–1675. https://doi.org/10.1126/science.2047876

Bergmann, F. T., Hoops, S., Klahn, B., Kummer, U., Mendes, P., Pahle, J., & Sahle, S. (2017). COPASI and its applications in biotechnology. *Journal of Biotechnology*, *261*(June), 215–220. https://doi.org/10.1016/j.jbiotec.2017.06.1200

BiGG. (2019a). *Model iJO1366*. http://bigg.ucsd.edu/models/iJO1366

BiGG. (2019b). *Model iJR904*. http://bigg.ucsd.edu/models/iJR904

BiGG. (2019c). *Model iML1515*. http://bigg.ucsd.edu/models/iML1515

Brent, R. P. (1974). Algorithms for Minimization Without Derivatives. *IEEE Transactions on Automatic Control*, *19*(5), 632–633. https://doi.org/10.1109/TAC.1974.1100629

Briggs, G. E., & Haldane, J. B. S. (1925). A note on the kinetics of enzyme action. *Biochemical Journal*, *19*(2), 338. https://doi.org/10.7518/hxkq.2015.03.024

Brown, A. J. (1902). XXXVI.—Enzyme action. *J. Chem. Soc., Trans.*, *81*(81), 373–388. https://doi.org/10.1039/CT9028100373

Cao, Y., Gillespie, D. T., & Petzold, L. R. (2007). Adaptive explicit-implicit tau-leaping method with automatic tau selection. *Journal of Chemical Physics*, *126*(22). https://doi.org/10.1063/1.2745299

Chae, T. U., Choi, S. Y., Kim, J. W., Ko, Y. S., & Lee, S. Y. (2017). Recent advances in systems metabolic engineering tools and strategies. *Current Opinion in Biotechnology*, *47*, 67–82. https://doi.org/10.1016/j.copbio.2017.06.007

Chassagnole, C., Noisommit-Rizzi, N., Schmid, J. W., Mauch, K., & Reuss, M. (2002). Dynamic modeling of the central carbon metabolism of *Escherichia coli*. *Biotechnology and Bioengineering*, *79*(1), 53–73. https://doi.org/10.1002/bit.10288

Chávez-Béjar, M. I., Báez-Viveros, J. L., Martínez, A., Bolívar, F., & Gosset, G. (2012). Biotechnological production of *L*-tyrosine and derived compounds. *Process Biochemistry*, *47*(7), 1017–1026. https://doi.org/10.1016/j.procbio.2012.04.005

Chen, B.-S., & Wu, C.-C. (2013). Systems Biology as an Integrated Platform for Bioinformatics, Systems Synthetic Biology, and Systems Metabolic Engineering. In *Cells* (Vol. 2, Issue 4). https://doi.org/10.3390/cells2040635

Christendat, D., & Turnbull, J. L. (1999). Identifying groups involved in the binding of prephenate to prephenate dehydrogenase from *Escherichia coli*. *Biochemistry*, *38*(15), 4782–4793. https://doi.org/10.1021/bi982673o

Cooper, G. M. (2019). The Cell: A Molecular Approach. In Andrew D. Sinauer (Ed.), *Oxford University Press* (8th ed.). Oxford University Press.

COPASI. (2020a). *Deterministic Simulation*. http://copasi.org/Support/User_Manual/Methods/Time_Course_Calculation/Deterministic_Simulation/

COPASI. (2020b). *Hybrid Simulation*. http://copasi.org/Support/User_Manual/Methods/Time_Course_Calculation/Hybrid_Simulation/

COPASI. (2020c). *Metabolic Control Analysis (MCA)*. http://copasi.org/Support/User_Manual/Tasks/Metabolic_Control_Analysis_MCA/

COPASI. (2020d). *Optimization*. http://copasi.org/Support/User_Manual/Tasks/Optimization/

COPASI. (2020e). *Random Search*. http://copasi.org/Support/User_Manual/Methods/Optimization_Methods/Random_Search/

COPASI. (2020f). *Stochastic Simulation*. http://copasi.org/Support/User_Manual/Methods/Time_Course_Calculation/Stochastic_Simulation/

COPASI. (2020g). *Time Course Calculation*. http://copasi.org/Support/User_Manual/Methods/Time_Course_Calculation/

Correia, S., Lima, P., Rocha, M., & Rocha, I. (2017). *OptimModels: a framework for strain optimization using kinetic models*.

Cox, M. M., & Nelson, D. L. (2017). *Lehninger Principles of Biochemistry* (7th ed.). W. H. Freeman and Company.

Cuevas, D. A., Edirisinghe, J., Henry, C. S., Overbeek, R., O'Connell, T. G., & Edwards, R. A. (2016). From DNA to FBA: How to build your own genome-scale metabolic model. *Frontiers in Microbiology*, *7*(JUN), 1–12. https://doi.org/10.3389/fmicb.2016.00907

Dell, K. A., & Frost, J. W. (1993). Identification and Removal of Impediments to Biocatalytic Synthesis of Aromatics from D-Glucose: Rate-Limiting Enzymes in the Common Pathway of Aromatic Amino Acid Biosynthesis. *Journal of the American Chemical Society*, *115*(24), 11581–11589. https://doi.org/10.1021/ja00077a065

Dennis, J. E., Gay, D. M., & Walsh, R. E. (1981). An Adaptive Nonlinear Least-Squares Algorithm. *ACM Transactions on Mathematical Software (TOMS)*, *7*(3), 348–368. https://doi.org/10.1145/355958.355965

Edelstein-Keshet, L. (2005). *Mathematical models in biology*. Society for Industrial and Applied Mathematics.

Edwards, J. S., & Palsson, B. O. (1998). How Will Bioinformatics Influence Metabolic Engineering? *John Wiley & Sons, Inc.*, 647–658. https://doi.org/10.1016/B978-0-444-64046-8.00190-7

Flamholz, A., Noor, E., Bar-Even, A., & Milo, R. (2012). EQuilibrator - The biochemical thermodynamics calculator. *Nucleic Acids Research*, *40*(D1), 770–775. https://doi.org/10.1093/nar/gkr874

Fogel, D. B. (1994). Evolutionary programming: an introduction and some current directions. *Statistics and Computing*, *4*(2), 113–129. https://doi.org/10.1007/BF00175356

Fordjour, E., Adipah, F. K., Zhou, S., Du, G., & Zhou, J. (2019). Metabolic engineering of *Escherichia coli* BL21 (DE3) for de novo production of L-DOPA from D-glucose. *Microbial Cell Factories*, *18*(1), 1–10. https://doi.org/10.1186/s12934-019-1122-0

Foster, C. J., Wang, L., Dinh, H. V., Suthers, P. F., & Maranas, C. D. (2021). Building kinetic models for metabolic engineering. *Current Opinion in Biotechnology*, *67*, 35–41. https://doi.org/10.1016/j.copbio.2020.11.010

Gibson, M. A., & Bruck, J. (2000). Efficient exact stochastic simulation of chemical systems with many species and many channels. *Journal of Physical Chemistry A*, *104*(9), 1876–1889. https://doi.org/10.1021/jp993732q

Gillespie, D. T. (2001). Approximate accelerated stochastic simulation of chemically reacting systems. *Journal of Chemical Physics*, *115*(4), 1716–1733. https://doi.org/10.1063/1.1378322

Gillespie, Daniel T. (1976). A general method for numerically simulating the stochastic time evolution of coupled chemical reactions. *Journal of Computational Physics*, *22*(4), 403–434. https://doi.org/10.1016/0021-9991(76)90041-3

Goldberger, R. (Ed.). (2012). *Biological Regulation and Development: Gene Expression (Vol. 1)*. Springer Science & Business Media.

Hernández-Chávez, G., Martínez, A., & Gosset, G. (2019). Metabolic engineering strategies for caffeic acid production in *Escherichia coli. Electronic Journal of Biotechnology*, *38*, 19–26. https://doi.org/10.1016/j.ejbt.2018.12.004

Hindmarsh, A. C. (1983). ODEPACK, a systematized collection of ODE solvers. *Scientific Computing*, 55–64. https://www3.nd.edu/~powers/ame.60636/hindmarsh1983.pdf

Hooke, R., & Jeeves, T. A. (1961). "Direct Search" Solution of Numerical and Statistical Problems. *Journal of the ACM (JACM)*, *8*(2), 212–229. https://doi.org/10.1145/321062.321069

Hoops, S., Gauges, R., Lee, C., Pahle, J., Simus, N., Singhal, M., Xu, L., Mendes, P., & Kummer, U. (2006). COPASI - A COmplex PAthway SImulator. *Bioinformatics*, *22*(24), 3067–3074. https://doi.org/10.1093/bioinformatics/btl485

Jahan, N., Maeda, K., Matsuoka, Y., Sugimoto, Y., & Kurata, H. (2016). Development of an accurate kinetic model for the central carbon metabolism of *Escherichia coli*. *Microbial Cell Factories*, *15*(1), 1–19. https://doi.org/10.1186/s12934-016-0511-x

Jiang, J., Bi, H., Zhuang, Y., Liu, S., Liu, T., & Ma, Y. (2016). Engineered synthesis of rosmarinic acid in *Escherichia coli* resulting production of a new intermediate, caffeoyl-phenyllactate. *Biotechnology Letters*, *38*(1), 81–88. https://doi.org/10.1007/s10529-015-1945-7

Juminaga, D., Baidoo, E. E. K., Redding-Johanson, A. M., Batth, T. S., Burd, H., Mukhopadhyay, A., Petzold, C. J., & Keasling, J. D. (2012). Modular engineering of *L*-tyrosine production in *Escherichia coli*. *Applied and Environmental Microbiology*, *78*(1), 89–98. https://doi.org/10.1128/AEM.06017-11

Kadir, T. A. A., Mannan, A. A., Kierzek, A. M., McFadden, J., & Shimizu, K. (2010). Modeling and simulation of the main metabolism in *Escherichia coli* and its several single-gene knockout mutants with experimental verification. *Microbial Cell Factories*, *9*, 1–21. https://doi.org/10.1186/1475-2859-9-88

Kang, S. Y., Choi, O., Lee, J. K., Ahn, J. O., Ahn, J. S., Hwang, B. Y., & Hong, Y. S. (2015). Artificial de novo biosynthesis of hydroxystyrene derivatives in a tyrosine overproducing *Escherichia coli* strain. *Microbial Cell Factories*, *14*(1), 1–11. https://doi.org/10.1186/s12934-015-0268-7

Kang, S. Y., Choi, O., Lee, J. K., Hwang, B. Y., Uhm, T. B., & Hong, Y. S. (2012). Artificial biosynthesis of phenylpropanoic acids in a tyrosine overproducing *Escherichia coli* strain. *Microbial Cell Factories*, *11*, 1–9. https://doi.org/10.1186/1475-2859-11-153

Karp, P. D., Billington, R., Caspi, R., Fulcher, C. A., Latendresse, M., Kothari, A., Keseler, I. M., Krummenacker, M., Midford, P. E., Ong, Q., Ong, W. K., Paley, S. M., & Subhraveti, P. (2018). The BioCyc collection of microbial genomes and metabolic pathways. *Briefings in Bioinformatics*, *20*(4), 1085–1093. https://doi.org/10.1093/bib/bbx085

Keasling, J. D. (2010). Manufacturing molecules through metabolic engineering. *Science*, *330*(6009), 1355–1358. https://doi.org/10.1126/science.1193990

Kennedy, J., & Eberhart, R. (1963). Particle swarm optimization. *Proceedings of ICNN'95 - International Conference on Neural Networks*, *4*(2), 1942–1948. https://doi.org/10.1109/ICNN.1995.488968

Khodayari, A., Chowdhury, A., & Maranas, C. D. (2015). Succinate Overproduction: A Case Study of Computational Strain Design Using a Comprehensive *Escherichia coli* Kinetic Model. *Frontiers in Bioengineering and Biotechnology*, *2*(January). https://doi.org/10.3389/fbioe.2014.00076

Khodayari, A., Zomorrodi, A. R., Liao, J. C., & Maranas, C. D. (2014). A kinetic model of *Escherichia coli* core metabolism satisfying multiple sets of mutant flux data. *Metabolic Engineering*, *25*, 50–62. https://doi.org/10.1016/j.ymben.2014.05.014

Kim, B., Binkley, R., Kim, H. U., & Lee, S. Y. (2018). Metabolic engineering of *Escherichia coli* for the enhanced production of *L*-tyrosine. *Biotechnology and Bioengineering*, *115*(10), 2554–2564. https://doi.org/10.1002/bit.26797

Kim, S. C., Min, B. E., Hwang, H. G., Seo, S. W., & Jung, G. Y. (2015). Pathway optimization by re-design of untranslated regions for *L*-tyrosine production in *Escherichia coli*. *Scientific Reports*, *5*(August), 13853. https://doi.org/10.1038/srep13853

KiMoSys (https://kimosys.org). (2014a). *Model EntryID 13 (Escherichia coli)*. https://kimosys.org/repository/30/associated_models/13

KiMoSys (https://kimosys.org). (2014b). *Model EntryID 36 (Escherichia coli)*. https://kimosys.org/repository/35/associated_models/36

KiMoSys (https://kimosys.org). (2018a). *Model EntryID 16 (Escherichia coli)*. https://kimosys.org/repository/38/associated_models/16

KiMoSys (https://kimosys.org). (2018b). *Model EntryID 38 (Escherichia coli)*. https://kimosys.org/repository/38/associated_models/38

KiMoSys (https://kimosys.org). (2018c). *Model EntryID 42 (Escherichia coli)*. https://kimosys.org/repository/35/associated_models/42

KiMoSys (https://kimosys.org). (2018d). *Model EntryID 44 (Escherichia coli)*. https://www.kimosys.org/repository/108/associated_models/44

KiMoSys (https://kimosys.org). (2018e). *Model EntryID 45 (Escherichia coli)*. https://www.kimosys.org/repository/96/associated_models/45

King, Z. A., Lu, J., Dräger, A., Miller, P., Federowicz, S., Lerman, J. A., Ebrahim, A., Palsson, B. O., & Lewis, N. E. (2016). BiGG Models: A platform for integrating, standardizing and sharing genome-scale models. *Nucleic Acids Research*, *44*(D1), D515–D522. https://doi.org/10.1093/nar/gkv1049

Kirkpatrick, S., Gelatt, C. D., & Vecchi, M. P. (1983). Optimization by Simulated Annealing. *Science*, *220*(4598), 671–680. https://doi.org/10.1126/science.220.4598.671

Klipp, E., Liebermeister, W., Wierling, C., & Kowald, A. (2016). *Systems biology : a textbook* (2nd ed.). Wiley-VCH.

Koma, D., Kishida, T., Yoshida, E., Ohashi, H., Yamanaka, H., Moriyoshi, K., Nagamori, E., & Ohmoto, T. (2020). Chromosome Engineering To Generate Plasmid-Free Phenylalanine- and Tyrosine-Overproducing *Escherichia coli* Strains That Can Be Applied in the Generation of Aromatic-Compound-Producing Bacteria. *Applied and Environmental Microbiology*, *86*(14), 1–24. https://doi.org/10.1128/AEM.00525-20

Kurata, H., & Sugimoto, Y. (2018). Improved kinetic model of *Escherichia coli* central carbon metabolism in batch and continuous cultures. *Journal of Bioscience and Bioengineering*, *125*(2), 251–257. https://doi.org/10.1016/j.jbiosc.2017.09.005

Le Novère, N., Bornstein, B., Broicher, A., Courtot, M., Donizelli, M., Dharuri, H., Li, L., Sauro, H., Schilstra, M., Shapiro, B., Snoep, J. L., & Hucka, M. (2006). BioModels Database: a free, centralized database of curated, published, quantitative kinetic models of biochemical and cellular systems. *Nucleic Acids Research*, *34*(Database issue), 689–691. https://doi.org/10.1093/nar/gkj092

Levenberg, K. (1944). A method for the solution of certain non-linear problems in least squares. *Quarterly of Applied Mathematics*, *2*(2), 164–168. https://doi.org/10.1090/qam/10666

Liu, C., Liu, Y. M., Sun, Q. L., Jiang, C. Y., & Liu, S. J. (2015). Unraveling the kinetic diversity of microbial 3-dehydroquinate dehydratases of shikimate pathway. *AMB Express*, *5*(1), 1–9. https://doi.org/10.1186/s13568-014-0087-y

Long, M. R., Ong, W. K., & Reed, J. L. (2015). Computational methods in metabolic engineering for strain design. *Current Opinion in Biotechnology*, *34*, 135–141. https://doi.org/10.1016/j.copbio.2014.12.019

Machado, D., Rodrigues, L. R., & Rocha, I. (2014). A kinetic model for curcumin production in *Escherichia coli*. *BioSystems*, *125*, 16–21. https://doi.org/10.1016/j.biosystems.2014.09.001

Macheroux, P., Schmid, J., Amrhein, N., & Schaller, A. (1999). A unique reaction in a common pathway: mechanism and function of chorismate synthase in the shikimate pathway. *Planta*, *207*(3), 325–334. https://doi.org/10.1007/s004250050489

Mannan, A. A., Toya, Y., Shimizu, K., McFadden, J., Kierzek, A. M., & Rocco, A. (2015). Integrating kinetic model of *E. coli* with genome scale metabolic fluxes overcomes its open system problem and reveals bistability in central metabolism. *PLoS ONE*, *10*(10), 1–36. https://doi.org/10.1371/journal.pone.0139507

Maria, G. (2014). unIn silico Derivation of a Reduced Kinetic Model for Stationary or Oscillating Glycolysis in *Escherichia coli* Bacterium. *Chemical and Biochemical Engineering Quarterly Journal*, *28*(4), 509–529. https://doi.org/10.15255/CABEQ.2014.2002

Mehdi, S., Frost, J. W., & Knowles, J. R. (1987). *[39] Dehydroquinate synthase from Escherichia coli, and its substrate 3-deoxy-d-arabino-heptulosonic acid 7-phosphate* (Vol. 142, pp. 306–314). https://doi.org/10.1016/S0076-6879(87)42041-7

Mendes, P., & Kell, D. B. (1998). Non-linear optimization of biochemical pathways: Applications to metabolic engineering and parameter estimation. *Bioinformatics*, *14*(10), 869–883. https://doi.org/10.1093/bioinformatics/14.10.869

Mendes, P., Oliver, S. G., & Kell, D. B. (2015). Fitting Transporter Activities to Cellular Drug Concentrations and Fluxes: Why the Bumblebee Can Fly. *Trends in Pharmacological Sciences*, *36*(11), 710–723. https://doi.org/10.1016/j.tips.2015.07.006

Menéndez-Perdomo, I. M., & Facchini, P. J. (2018). Benzylisoquinoline alkaloids biosynthesis in sacred lotus. *Molecules*, *23*(11). https://doi.org/10.3390/molecules23112899

Michaelis, L., & Menten, M. L. (1913). Kinetik der Invertinwir-kung. *Biochem. Z*, *49*(333–369), 352. http://www.ncbi.nlm.nih.gov/pubmed/21888353

Millard, P., Smallbone, K., & Mendes, P. (2017). Metabolic regulation is sufficient for global and robust coordination of glucose uptake, catabolism, energy production and growth in *Escherichia coli. PLoS Computational Biology*, *13*(2), 1–24. https://doi.org/10.1371/journal.pcbi.1005396

Mitsuhashi, S., & Davis, B. D. (1954). Aromatic biosynthesis. XII. Conversion of 5-dehydroquinic acid to 5-dehydroshikimic acid dy 5-dehydroquinase. *Biochimica et Biophysica Acta*, *15*(1), 54–61. https://doi.org/10.1016/0006-3002(54)90093-1

Mochão, H., Barahona, P., & Costa, R. S. (2020). KiMoSys 2.0: an upgraded database for submitting, storing and accessing experimental data for kinetic modeling. *Database : The Journal of Biological Databases and Curation*, *2020*, 1–11. https://doi.org/10.1093/database/baaa093

Monk, J. M., Lloyd, C. J., Brunk, E., Mih, N., Sastry, A., King, Z., Takeuchi, R., Nomura, W., Zhang, Z., Mori, H., Feist, A. M., & Palsson, B. O. (2017). iML1515, a knowledgebase that computes *Escherichia coli* traits. *Nature Biotechnology*, *35*(10), 904–908. https://doi.org/10.1038/nbt.3956

Na, D., Yoo, S. M., Chung, H., Park, H., Park, J. H., & Lee, S. Y. (2013). Metabolic engineering of *Escherichia coli* using synthetic small regulatory RNAs. *Nature Biotechnology*, *31*(2), 170–174. https://doi.org/10.1038/nbt.2461

Nash, S. G. (1984). Newton-Type Minimization via the Lanczos Method. *SIAM Journal on Numerical Analysis*, *21*(4), 770–788. https://doi.org/10.1137/0721052

Nelder, J. A., & Mead, R. (1965). A Simplex Method for Function Minimization. *The Computer Journal*, *7*(4), 308–313. https://doi.org/10.1093/comjnl/7.4.308

Nielsen, J. (2001). Metabolic engineering. *Applied Microbiology and Biotechnology*, *55*(3), 263–283. https://doi.org/10.1007/s002530000511

Noble, M., Sinha, Y., Kolupaev, A., Demin, O., Earnshaw, D., Tobin, F., West, J., Martin, J. D., Qiu, C., Liu, W.-S., DeWolf, W. E., Tew, D., & Goryanin, I. I. (2006). The kinetic model of the shikimate pathway as a tool to optimize enzyme assays for high-throughput screening. *Biotechnology and Bioengineering*, *95*(4), 560–571. https://doi.org/10.1002/bit.20772

Noda, S., Shirai, T., Oyama, S., & Kondo, A. (2016). Metabolic design of a platform *Escherichia coli* strain producing various chorismate derivatives. *Metabolic Engineering*, *33*, 119–129. https://doi.org/10.1016/j.ymben.2015.11.007

Oliveira, A. (2020, October). *Oliveira2020 - Extended E. coli Central Carbon Metabolism from Glucose*. BioModels. https://doi.org/10.1371/journal.pcbi.1008704

Oliveira, A., Rodrigues, J., Ferreira, E. C., Rodrigues, L., & Dias, O. (2021). A kinetic model of the central carbon metabolism for acrylic acid production in *Escherichia coli*. *PLOS Computational Biology*, *17*(3), e1008704. https://doi.org/10.1371/journal.pcbi.1008704

Orth, J. D., Conrad, T. M., Na, J., Lerman, J. A., Nam, H., Feist, A. M., & Palsson, B. (2011). A comprehensive genome-scale reconstruction of *Escherichia coli* metabolism-2011. *Molecular Systems Biology*, *7*(535), 1–9. https://doi.org/10.1038/msb.2011.65

Orth, J. D., Thiele, I., & Palsson, B. O. (2010). What is flux balance analysis? *Nature Biotechnology*, *28*(3), 245–248. https://doi.org/10.1038/nbt.1614

Pahle, J. (2009). Biochemical simulations: Stochastic, approximate stochastic and hybrid approaches. *Briefings in Bioinformatics*, *10*(1), 53–64. https://doi.org/10.1093/bib/bbn050

Palsson, B. O. (2011). *Systems Biology: Simulation of dynamic network states*. Cambridge University Press.

Palsson, B. O. (2015). *Systems Biology Constraint-Based Reconstruction and Analysis* (2nd ed.). Cambridge University Press.

Panche, A. N., Diwan, A. D., & Chandra, S. R. (2016). Flavonoids: An overview. *Journal of Nutritional Science*, *5*. https://doi.org/10.1017/jns.2016.41

Park, J. H., & Lee, S. Y. (2008). Towards systems metabolic engineering of microorganisms for amino acid production. *Current Opinion in Biotechnology*, *19*(5), 454–460. https://doi.org/10.1016/j.copbio.2008.08.007

Patil, K. R., Rocha, I., Förster, J., & Nielsen, J. (2005). Evolutionary programming as a platform for in silico metabolic engineering. *BMC Bioinformatics*, *6*, 1–12. https://doi.org/10.1186/1471-2105-6-308

Pereira, V., Cruz, F., & Rocha, M. (2021). MEWpy: a computational strain optimization workbench in Python. *Bioinformatics*, *January*, 1–3. https://doi.org/10.1093/bioinformatics/btab013

Petzold, L. (1983). Automatic Selection of Methods for Solving Stiff and Nonstiff Systems of Ordinary Differential Equations. *SIAM Journal on Scientific and Statistical Computing*, *4*(1), 136–148. https://doi.org/10.1137/0904010

Placzek, S., Schomburg, I., Chang, A., Jeske, L., Ulbrich, M., Tillack, J., & Schomburg, D. (2017). BRENDA in 2017: new perspectives and new tools in BRENDA. *Nucleic Acids Research*, *45*(D1), D380–D388. https://doi.org/10.1093/nar/gkw952

Powell, J. T., & Morrison, J. F. (1978). The Purification and Properties of the Aspartate Aminotransferase and Aromatic-Amino-Acid Aminotransferase from *Escherichia coli*. *European Journal of Biochemistry*, *87*(2), 391–400. https://doi.org/10.1111/j.1432-1033.1978.tb12388.x

Reed, J. L., Vo, T. D., Schilling, C. H., & Palsson, B. O. (2003). An expanded genome-scale model of *Escherichia coli* K-12 (iJR904 GSM/GPR). *Genome Biology*, *4*(9), 1–12. https://doi.org/10.1186/gb-2003-4-9-r54

Riley, P. A. (1997). Melanin. *The International Journal of Biochemistry & Cell Biology*, *29*(11), 1235–1239. https://doi.org/10.1016/S1357-2725(97)00013-7

Rodrigues, J. L., Araújo, R. G., Prather, K. L. J., Kluskens, L. D., & Rodrigues, L. R. (2015). Heterologous production of caffeic acid from tyrosine in *Escherichia coli*. *Enzyme and Microbial Technology*, *71*, 36–44. https://doi.org/10.1016/j.enzmictec.2015.01.001

Rodrigues, J. L., Gomes, D., & Rodrigues, L. R. (2020). A Combinatorial Approach to Optimize the Production of Curcuminoids From Tyrosine in *Escherichia coli*. *Frontiers in Bioengineering and Biotechnology*, *8*(February), 1–15. https://doi.org/10.3389/fbioe.2020.00059

Rodrigues, J. L., Prather, K. L. J., Kluskens, L. D., & Rodrigues, L. R. (2015). Heterologous Production of Curcuminoids. *Microbiology and Molecular Biology Reviews*, *79*(1), 39–60. https://doi.org/10.1128/mmbr.00031-14

Rodriguez, A., Martínez, J. A., Flores, N., Escalante, A., Gosset, G., & Bolívar, F. (2014). Engineering *Escherichia coli* to overproduce aromatic amino acids and derived compounds. *Microbial Cell Factories*, *13*(1), 1–15. https://doi.org/10.1186/s12934-014-0126-z

Rosano, G. L., Morales, E. S., & Ceccarelli, E. A. (2019). New tools for recombinant protein production in *Escherichia coli*: A 5-year update. *Protein Science*, *28*(8), 1412–1422. https://doi.org/10.1002/pro.3668

Runarsson, T. P., & Yao, X. (2000). Stochastic ranking for constrained evolutionary optimization. *IEEE Transactions on Evolutionary Computation*, *4*(3), 284–294. https://doi.org/10.1109/4235.873238

Sá-Correia, I. (Ed.). (2019). *Yeasts in Biotechnology and Human Health* (Vol. 58). Springer International Publishing. https://doi.org/10.1007/978-3-030-13035-0

Saavedra, E., & Moreno-Sánchez, R. (2013). Flux Control Coefficient. In *Encyclopedia of Systems Biology* (pp. 752–752). Springer New York. https://doi.org/10.1007/978-1-4419-9863-7_1355

Shuttleworth, W. A., & Evans, J. N. S. (1996). The H385N Mutant of 5-Enolpyruvylshikimate-3-phosphate Synthase: Kinetics, Fluorescence, and Nuclear Magnetic Resonance Studies. *Archives of Biochemistry and Biophysics*, *334*(1), 37–42. https://doi.org/10.1006/abbi.1996.0426

Singh, V. K., & Ghosh, I. (2006). Kinetic modeling of tricarboxylic acid cycle and glyoxylate bypass in Mycobacterium tuberculosis, and its application to assessment of drug targets. *Theoretical Biology and Medical Modelling*, *3*(1), 27. https://doi.org/10.1186/1742-4682-3-27

Stephanopoulos, G. N., Aristidou, A. A., & Nielsen, J. (1998). *Metabolic Engineering: Principles and Methodologies* (1st ed.). Elsevier Science (USA).

Tepper, N., & Shlomi, T. (2009). Predicting metabolic engineering knockout strategies for chemical production: Accounting for competing pathways. *Bioinformatics*, *26*(4), 536–543. https://doi.org/10.1093/bioinformatics/btp704

Trantas, E., Navakoudis, E., Pavlidis, T., Nikou, T., Halabalaki, M., & Skaltsounis, L. (2019). Correction: Dual pathway for metabolic engineering of *Escherichia coli* to produce the highly valuable hydroxytyrosol. *PLOS ONE*, *14*(12), e0226760. https://doi.org/10.1371/journal.pone.0226760

Vilaça, P., Maia, P., Giesteira, H., Rocha, I., & Rocha, M. (2018). Analyzing and designing cell factories with OptFlux. In *Methods in Molecular Biology* (Vol. 1716). https://doi.org/10.1007/978-1-4939-7528-0_2

Wei, T., Cheng, B. Y., & Liu, J. Z. (2016). Genome engineering *Escherichia coli* for L-DOPA overproduction from glucose. *Scientific Reports*, *6*(July), 1–9. https://doi.org/10.1038/srep30080

Wilson, David B.; Sahm, Hermann; Stahmann, Klaus-Peter; Koffas, M. (Ed.). (2019). *Industrial Microbiology*. John Wiley & Sons.

Wittmann, C., & Lee, S. Y. (Eds.). (2012). *Systems Metabolic Engineering* (1st ed.). Springer Netherlands.

Xu, S., Wang, Q., Zeng, W., Li, Y., Shi, G., & Zhou, J. (2020). Construction of a heat-inducible *Escherichia coli* strain for efficient de novo biosynthesis of *L*-tyrosine. *Process Biochemistry*, *92*(January), 85–92. https://doi.org/10.1016/j.procbio.2020.02.023

Yang, D., Park, S. Y., Park, Y. S., Eun, H., & Lee, S. Y. (2020). Metabolic Engineering of *Escherichia coli* for Natural Product Biosynthesis. *Trends in Biotechnology*, *38*(7), 745–765. https://doi.org/10.1016/j.tibtech.2019.11.007

Yao, Y. F., Wang, C. S., Qiao, J., & Zhao, G. R. (2013). Metabolic engineering of *Escherichia coli* for production of salvianic acid A via an artificial biosynthetic pathway. *Metabolic Engineering*, *19*, 79–87. https://doi.org/10.1016/j.ymben.2013.06.001

Zhang, C., Zhang, J., Kang, Z., Du, G., Yu, X., Wang, T., & Chen, J. (2013). Enhanced production of *L*-phenylalanine in Corynebacterium glutamicum due to the introduction of *Escherichia coli* wild-type gene aroH. *Journal of Industrial Microbiology and Biotechnology*, *40*(6), 643–651. https://doi.org/10.1007/s10295-013-1262-x

Zhang, S., Wilson, D. B., & Ganem, B. (2000). Probing the catalytic mechanism of prephenate dehydratase by site- directed mutagenesis of the *Escherichia coli* P-protein dehydratase domain. *Biochemistry*, *39*(16), 4722–4728. https://doi.org/10.1021/bi9926680

Zhang, S., Wilson, D. B., & Ganem, B. (2003). An engineered chorismate mutase with allosteric regulation. *Bioorganic and Medicinal Chemistry*, *11*(14), 3109–3114. https://doi.org/10.1016/S0968-0896(03)00242-6

Zhou, L., Ding, Q., Jiang, G. Z., Liu, Z. N., Wang, H. Y., & Zhao, G. R. (2017). Chromosome engineering of *Escherichia coli* for constitutive production of salvianic acid A. *Microbial Cell Factories*, *16*(1), 1–11. https://doi.org/10.1186/s12934-017-0700-2

SUPPLEMENTARY INFORMATION

Appendix 1

Set of models designed to evaluate the impact of certain variables – Objective Function, Optimisation Method, Kinetic Mechanism, Stoichiometric Models and Environmental Conditions Interval – in parameter determination.

Appendix 2

V_{max} values calculated for the reactions necessary to produce *L*-Tyr and *L*-Phe for all 108 models.

Appendix 3

Observations made and *L*-Tyr concentration from each kinetic model designed on the study of the impact that different variables have on parameter determination.

Appendix 4

Heatmaps made from the FCC values from each MCA performed in all models.

Appendix 1 – Set of models designed to evaluate the impact of certain variables in parameter determination. Mass Action (MA), Michaelis–Menten (MM), Flux Balance Analysis (FBA), Parsimonious Flux Balance Analysis (pFBA), L-Tyrosine (L-Tyr)

Environmental Conditions Interval	Stoichiometric Model	Kinetic Mechanism	FBA			pFBA		
			Biomass	**[*L*-Tyr]**	**[Chorismate]**	**Biomass**	**[*L*-Tyr]**	**[Chorismate]**
+/- 1%	**iML1515**	**MA**	TyrOpt_1A_Bi_a	TyrOpt_1A_Ti_a	TyrOpt_1A_Ci_a	TyrOpt_1B_Bi_a	TyrOpt_1B_Ti_a	TyrOpt_1B_Ci_a
		MM	TyrOpt_1A_Bii_a	TyrOpt_1A_Tii_a	TyrOpt_1A_Cii_a	TyrOpt_1B_Bii_a	TyrOpt_1B_Tii_a	TyrOpt_1B_Cii_a
	iJO1366	**MA**	TyrOpt_2A_Bi_a	TyrOpt_2A_Ti_a	TyrOpt_2A_Ci_a	TyrOpt_2B_Bi_a	TyrOpt_2B_Ti_a	TyrOpt_2B_Ci_a
		MM	TyrOpt_2A_Bii_a	TyrOpt_2A_Tii_a	TyrOpt_2A_Cii_a	TyrOpt_2B_Bii_a	TyrOpt_2B_Tii_a	TyrOpt_2B_Cii_a
	iJR904	**MA**	TyrOpt_3A_Bi_a	TyrOpt_3A_Ti_a	TyrOpt_3A_Ci_a	TyrOpt_3B_Bi_a	TyrOpt_3B_Ti_a	TyrOpt_3B_Ci_a
		MM	TyrOpt_3A_Bii_a	TyrOpt_3A_Tii_a	TyrOpt_3A_Cii_a	TyrOpt_3B_Bii_b	TyrOpt_3B_Tii_a	TyrOpt_3B_Cii_a
+/- 0.1mM	**iML1515**	**MA**	TyrOpt_1A_Bi_b	TyrOpt_1A_Ti_b	TyrOpt_1A_Ci_b	TyrOpt_1B_Bi_b	TyrOpt_1B_Ti_b	TyrOpt_1B_Ci_b
		MM	TyrOpt_1A_Bii_b	TyrOpt_1A_Tii_b	TyrOpt_1A_Cii_b	TyrOpt_1B_Bii_b	TyrOpt_1B_Tii_b	TyrOpt_1B_Cii_b
	iJO1366	**MA**	TyrOpt_2A_Bi_b	TyrOpt_2A_Ti_b	TyrOpt_2A_Ci_b	TyrOpt_2B_Bi_b	TyrOpt_2B_Ti_b	TyrOpt_2B_Ci_b
		MM	TyrOpt_2A_Bii_b	TyrOpt_2A_Tii_b	TyrOpt_2A_Cii_b	TyrOpt_2B_Bii_b	TyrOpt_2B_Tii_b	TyrOpt_2B_Cii_b
	iJR904	**MA**	TyrOpt_3A_Bi_b	TyrOpt_3A_Ti_b	TyrOpt_3A_Ci_b	TyrOpt_3B_Bi_b	TyrOpt_3B_Ti_b	TyrOpt_3B_Ci_b
		MM	TyrOpt_3A_Bii_b	TyrOpt_3A_Tii_b	TyrOpt_3A_Cii_b	TyrOpt_3B_Bii_b	TyrOpt_3B_Tii_b	TyrOpt_3B_Cii_b
+/- 10%	**iML1515**	**MA**	TyrOpt_1A_Bi_c	TyrOpt_1A_Ti_c	TyrOpt_1A_Ci_c	TyrOpt_1B_Bi_c	TyrOpt_1B_Ti_c	TyrOpt_1B_Ci_c
		MM	TyrOpt_1A_Bii_c	TyrOpt_1A_Tii_c	TyrOpt_1A_Cii_c	TyrOpt_1B_Bii_c	TyrOpt_1B_Tii_c	TyrOpt_1B_Cii_c
	iJO1366	**MA**	TyrOpt_2A_Bi_c	TyrOpt_2A_Ti_c	TyrOpt_2A_Ci_c	TyrOpt_2B_Bi_c	TyrOpt_2B_Ti_c	TyrOpt_2B_Ci_c
		MM	TyrOpt_2A_Bii_c	TyrOpt_2A_Tii_c	TyrOpt_2A_Cii_c	TyrOpt_2B_Bii_c	TyrOpt_2B_Tii_c	TyrOpt_2B_Cii_c
	iJR904	**MA**	TyrOpt_3A_Bi_c	TyrOpt_3A_Ti_c	TyrOpt_3A_Ci_c	TyrOpt_3B_Bi_c	TyrOpt_3B_Ti_c	TyrOpt_3B_Ci_c
		MM	TyrOpt_3A_Bii_c	TyrOpt_3A_Tii_c	TyrOpt_3A_Cii_c	TyrOpt_3B_Bii_c	TyrOpt_3B_Tii_c	TyrOpt_3B_Cii_c

Appendix 2 – V_{max} values calculated for the reactions necessary to produce L-Tyr and L-Phe for all 108 models.

	TyrOpt_1A_Bi_a	**TyrOpt_1A_Bii_a**	**TyrOpt_1B_Bi_a**	**TyrOpt_1B_Bii_a**
Reaction	V_{max} (mM/s)	V_{max} (mM/s)	V_{max} (mM/s)	V_{max} (mM/s)
AroF/G/H (AroF)	0.1283	0.1283	0.1283	0.1283
AroF/G/H (AroG)	0.5496	0.5496	0.5496	0.5496
AroF/G/H (AroH)	0.0119	0.0119	0.0119	0.0119
AroB	0.0061	0.0061	0.0061	0.0061
AroD	0.0070	0.0070	0.0070	0.0070
YdiB/AroE	0.0472	0.0472	0.0472	0.0472
AroK/L	0.0245	0.0245	0.0245	0.0245
AroA	0.0699	0.0699	0.0699	0.0699
AroC	0.0059	0.0059	0.0059	0.0059
TyrA/PheA	0.0068	0.0068	0.0068	0.0068
TyrA	0.0035	0.0035	0.0035	0.0035
TyrB_Tyr	0.2523	0.2523	0.2523	0.2523
PheA	0.0034	0.0034	0.0034	0.0034
TyrB_Phe	0.1523	0.1523	0.1523	0.1523
Synth Reaction	k_1 (1/s)	V_{max} (mM/s)	k_1 (1/s)	V_{max} (mM/s)
Synth 3-Dehydroquinate	0	0	0	0
Synth Chorismate	0.0007	0.0014	0.0007	0.0014
Synth Prephenate	0	0	0	0
Synth *L*-Tyrosine	0.0014	0.0028	0.0014	0.0028
Synth Phenylpyruvate	0	0	0	0

Appendix 2 – V_{max} values calculated for the reactions necessary to produce L-Tyr and L-Phe for all 108 models (continuation).

	TyrOpt_1A_Ti_a	**TyrOpt_1A_Tii_a**	**TyrOpt_1B_Ti_a**	**TyrOpt_1B_Tii_a**
Reaction	V_{max} (mM/s)	V_{max} (mM/s)	V_{max} (mM/s)	V_{max} (mM/s)
AroF/G/H (AroF)	0.1283	0.1283	0.1198	0.1198
AroF/G/H (AroG)	0.5496	0.5496	0.5131	0.5131
AroF/G/H (AroH)	0.0119	0.0119	0.0111	0.0111
AroB	0.0061	0.0061	0.0057	0.0057
AroD	0.0070	0.0070	0.0065	0.0065
YdiB/AroE	0.0472	0.0472	0.0440	0.0440
AroK/L	0.0245	0.0245	0.0229	0.0229
AroA	0.0699	0.0699	0.0653	0.0653
AroC	0.0059	0.0059	0.0055	0.0055
TyrA/PheA	0.0068	0.0068	0.0063	0.0063
TyrA	0.0035	0.0035	0.0031	0.0031
TyrB_Tyr	0.2547	0.2547	0.2219	0.2219
PheA	0.0034	0.0034	0.0034	0.0034
TyrB_Phe	0.1508	0.1508	0.1508	0.1508
Synth Reaction	k_1 (1/s)	V_{max} (mM/s)	k_1 (1/s)	V_{max} (mM/s)
Synth 3-Dehydroquinate	0	0	0	0
Synth Chorismate	0.0007	0.0014	0.0007	0.0014
Synth Prephenate	0	0	0	0
Synth *L*-Tyrosine	0.0010	0.0021	0.0010	0.0021
Synth Phenylpyruvate	0	0	0	0

Appendix 2 – V_{max} values calculated for the reactions necessary to produce L-Tyr and L-Phe for all 108 models (continuation).

	TyrOpt_1A_Ci_a	**TyrOpt_1A_Cii_a**	**TyrOpt_1B_Ci_a**	**TyrOpt_1B_Cii_a**
Reaction	V_{max} (mM/s)	V_{max} (mM/s)	V_{max} (mM/s)	V_{max} (mM/s)
AroF/G/H (AroF)	0.1283	0.1283	0.1198	0.1198
AroF/G/H (AroG)	0.5496	0.5496	0.5131	0.5131
AroF/G/H (AroH)	0.0119	0.0119	0.0111	0.0111
AroB	0.0061	0.0061	0.0057	0.0057
AroD	0.0070	0.0070	0.0065	0.0065
YdiB/AroE	0.0472	0.0472	0.0440	0.0440
AroK/L	0.0245	0.0245	0.0229	0.0229
AroA	0.0699	0.0699	0.0653	0.0653
AroC	0.0059	0.0059	0.0055	0.0055
TyrA/PheA	0.0063	0.0063	0.0063	0.0063
TyrA	0.0031	0.0031	0.0031	0.0031
TyrB_Tyr	0.2219	0.2219	0.2219	0.2219
PheA	0.0034	0.0034	0.0034	0.0034
TyrB_Phe	0.1508	0.1508	0.1508	0.1508
Synth Reaction	k_1 (1/s)	V_{max} (mM/s)	k_1 (1/s)	V_{max} (mM/s)
Synth 3-Dehydroquinate	0	0	0	0
Synth Chorismate	0.0007	0.0014	0.0007	0.0014
Synth Prephenate	0	0	0	0
Synth *L*-Tyrosine	0.0010	0.0021	0.0010	0.0021
Synth Phenylpyruvate	0	0	0	0

Appendix 2 – V_{max} values calculated for the reactions necessary to produce L-Tyr and L-Phe for all 108 models (continuation).

	TyrOpt_2A_Bi_a	**TyrOpt_2A_Bii_a**	**TyrOpt_2B_Bi_a**	**TyrOpt_2B_Bii_a**
Reaction	V_{max} (mM/s)	V_{max} (mM/s)	V_{max} (mM/s)	V_{max} (mM/s)
AroF/G/H (AroF)	0.1234	0.1234	0.1234	0.1234
AroF/G/H (AroG)	0.5285	0.5285	0.5285	0.5285
AroF/G/H (AroH)	0.0115	0.0115	0.0115	0.0115
AroB	0.0059	0.0059	0.0059	0.0059
AroD	0.0051	0.0051	0.0051	0.0051
YdiB/AroE	0.0347	0.0347	0.0347	0.0347
AroK/L	0.0181	0.0181	0.0181	0.0181
AroA	0.0514	0.0514	0.0514	0.0514
AroC	0.0043	0.0043	0.0043	0.0043
TyrA/PheA	0.0048	0.0048	0.0048	0.0048
TyrA	0.0018	0.0018	0.0018	0.0018
TyrB_Tyr	0.1315	0.1315	0.1315	0.1315
PheA	0.0033	0.0033	0.0033	0.0033
TyrB_Phe	0.1463	0.1463	0.1463	0.1463
Synth Reaction	k_1 (1/s)	V_{max} (mM/s)	k_1 (1/s)	V_{max} (mM/s)
Synth 3-Dehydroquinate	-0.0013	-0.0027	-0.0013	-0.0027
Synth Chorismate	0.0007	0.0013	0.0007	0.0013
Synth Prephenate	0	0	0	0
Synth *L*-Tyrosine	2.54 E-06	5.07 E-06	2.54 E-06	5.07 E-06
Synth Phenylpyruvate	0	0	0	0

Appendix 2 – V_{max} values calculated for the reactions necessary to produce L-Tyr and L-Phe for all 108 models (continuation).

	TyrOpt_2A_Ti_a	**TyrOpt_2A_Tii_a**	**TyrOpt_2B_Ti_a**	**TyrOpt_2B_Tii_a**
Reaction	V_{max} (mM/s)	V_{max} (mM/s)	V_{max} (mM/s)	V_{max} (mM/s)
AroF/G/H (AroF)	0.1283	0.1283	0.1283	0.1283
AroF/G/H (AroG)	0.5496	0.5496	0.5496	0.5496
AroF/G/H (AroH)	0.0119	0.0119	0.0119	0.0119
AroB	0.0061	0.0061	0.0061	0.0061
AroD	0.0070	0.0070	0.0070	0.0070
YdiB/AroE	0.0472	0.0472	0.0472	0.0472
AroK/L	0.0245	0.0245	0.0245	0.0245
AroA	0.0699	0.0699	0.0699	0.0699
AroC	0.0059	0.0059	0.0059	0.0059
TyrA/PheA	0.0068	0.0068	0.0068	0.0068
TyrA	0.0036	0.0036	0.0036	0.0036
TyrB_Tyr	0.2642	0.2642	0.2642	0.2642
PheA	0.0033	0.0033	0.0033	0.0033
TyrB_Phe	0.1448	0.1448	0.1448	0.1448
Synth Reaction	k_1 (1/s)	V_{max} (mM/s)	k_1 (1/s)	V_{max} (mM/s)
Synth 3-Dehydroquinate	-1.55 E-20	-3.10 E-20	0	0
Synth Chorismate	0.0007	0.0013	0.0007	0.0013
Synth Prephenate	0	0	0	0
Synth *L*-Tyrosine	2.51 E-06	5.02 E-06	2.51 E-06	5.02 E-06
Synth Phenylpyruvate	0	0	0	0

Appendix 2 – V_{max} values calculated for the reactions necessary to produce L-Tyr and L-Phe for all 108 models (continuation).

	TyrOpt_2A_Ci_a	**TyrOpt_2A_Cii_a**	**TyrOpt_2B_Ci_a**	**TyrOpt_2B_Cii_a**
Reaction	V_{max} (mM/s)	V_{max} (mM/s)	V_{max} (mM/s)	V_{max} (mM/s)
AroF/G/H (AroF)	0.1283	0.1283	0.1283	0.1283
AroF/G/H (AroG)	0.5496	0.5496	0.5496	0.5496
AroF/G/H (AroH)	0.0119	0.0119	0.0119	0.0119
AroB	0.0061	0.0061	0.0061	0.0061
AroD	0.0070	0.0070	0.0070	0.0070
YdiB/AroE	0.0472	0.0472	0.0472	0.0472
AroK/L	0.0245	0.0245	0.0245	0.0245
AroA	0.0699	0.0699	0.0699	0.0699
AroC	0.0059	0.0059	0.0059	0.0059
TyrA/PheA	0.0047	0.0068	0.0047	0.0068
TyrA	0.0018	0.0036	0.0018	0.0036
TyrB_Tyr	0.1302	0.2642	0.1302	0.2642
PheA	0.0033	0.0033	0.0033	0.0033
TyrB_Phe	0.1448	0.1448	0.1448	0.1448
Synth Reaction	k_1 (1/s)	V_{max} (mM/s)	k_1 (1/s)	V_{max} (mM/s)
Synth 3-Dehydroquinate	0	0	0	0
Synth Chorismate	0.0007	0.0013	0.0007	0.0013
Synth Prephenate	0	0	0	0
Synth *L*-Tyrosine	2.51 E-06	5.02 E-06	2.51 E-06	5.02 E-06
Synth Phenylpyruvate	0	0	0	0

Appendix 2 – V_{max} values calculated for the reactions necessary to produce L-Tyr and L-Phe for all 108 models (continuation).

	TyrOpt_3A_Bi_a	**TyrOpt_3A_Bii_a**	**TyrOpt_3B_Bi_a**	**TyrOpt_3B_Bii_a**
Reaction	V_{max} (mM/s)	V_{max} (mM/s)	V_{max} (mM/s)	V_{max} (mM/s)
AroF/G/H (AroF)	0.1210	0.1210	0.1210	0.1210
AroF/G/H (AroG)	0.5183	0.5183	0.5183	0.5183
AroF/G/H (AroH)	0.0112	0.0112	0.0112	0.0112
AroB	0.0058	0.0058	0.0058	0.0058
AroD	0.0066	0.0066	0.0066	0.0066
YdiB/AroE	0.0445	0.0445	0.0445	0.0445
AroK/L	0.0231	0.0231	0.0231	0.0231
AroA	0.0660	0.0660	0.0660	0.0660
AroC	0.0056	0.0056	0.0056	0.0056
TyrA/PheA	0.0054	0.0054	0.0054	0.0054
TyrA	0.0021	0.0021	0.0021	0.0021
TyrB_Tyr	0.1504	0.1504	0.1504	0.1504
PheA	0.0037	0.0037	0.0037	0.0037
TyrB_Phe	0.1641	0.1641	0.1641	0.1641
Synth Reaction	k_1 (1/s)	V_{max} (mM/s)	k_1 (1/s)	V_{max} (mM/s)
Synth 3-Dehydroquinate	0	0	0	0
Synth Chorismate	0.0014	0.0028	0.0014	0.0028
Synth Prephenate	0	0	0	0
Synth *L*-Tyrosine	0	0	0	0
Synth Phenylpyruvate	0	0	0	0

Appendix 2 – V_{max} values calculated for the reactions necessary to produce L-Tyr and L-Phe for all 108 models (continuation).

	TyrOpt_3A_Ti_a	**TyrOpt_3A_Tii_a**	**TyrOpt_3B_Ti_a**	**TyrOpt_3B_Tii_a**
Reaction	V_{max} (mM/s)	V_{max} (mM/s)	V_{max} (mM/s)	V_{max} (mM/s)
AroF/G/H (AroF)	0.1211	0.1211	0.1211	0.1211
AroF/G/H (AroG)	0.5186	0.5186	0.5186	0.5186
AroF/G/H (AroH)	0.0112	0.0112	0.0112	0.0112
AroB	0.0058	0.0058	0.0058	0.0058
AroD	0.0066	0.0066	0.0066	0.0066
YdiB/AroE	0.0445	0.0445	0.0445	0.0445
AroK/L	0.0232	0.0232	0.0232	0.0232
AroA	0.0660	0.0660	0.0660	0.0660
AroC	0.0056	0.0056	0.0056	0.0056
TyrA/PheA	0.0054	0.0054	0.0054	0.0054
TyrA	0.0021	0.0021	0.0021	0.0021
TyrB_Tyr	0.1538	0.1538	0.1538	0.1538
PheA	0.0036	0.0036	0.0036	0.0036
TyrB_Phe	0.1624	0.1624	0.1624	0.1624
Synth Reaction	k_1 (1/s)	V_{max} (mM/s)	k_1 (1/s)	V_{max} (mM/s)
Synth 3-Dehydroquinate	0	0	0	0
Synth Chorismate	0.0014	0.0028	0.0014	0.0028
Synth Prephenate	0	0	0	0
Synth *L*-Tyrosine	0	0	0	0
Synth Phenylpyruvate	0	0	0	0

Appendix 2 – V_{max} values calculated for the reactions necessary to produce L-Tyr and L-Phe for all 108 models (continuation).

	TyrOpt_3A_Ci_a	**TyrOpt_3A_Cii_a**	**TyrOpt_3B_Ci_a**	**TyrOpt_3B_Cii_a**
Reaction	V_{max} (mM/s)	V_{max} (mM/s)	V_{max} (mM/s)	V_{max} (mM/s)
AroF/G/H (AroF)	0.1211	0.1211	0.1211	0.1211
AroF/G/H (AroG)	0.5186	0.5186	0.5186	0.5186
AroF/G/H (AroH)	0.0112	0.0112	0.0112	0.0112
AroB	0.0058	0.0058	0.0058	0.0058
AroD	0.0066	0.0066	0.0066	0.0066
YdiB/AroE	0.0445	0.0445	0.0445	0.0445
AroK/L	0.0232	0.0232	0.0232	0.0232
AroA	0.0660	0.0660	0.0660	0.0660
AroC	0.0056	0.0056	0.0056	0.0056
TyrA/PheA	0.0053	0.0053	0.0053	0.0053
TyrA	0.0020	0.0020	0.0020	0.0020
TyrB_Tyr	0.1458	0.1458	0.1458	0.1458
PheA	0.0036	0.0036	0.0036	0.0036
TyrB_Phe	0.1624	0.1624	0.1624	0.1624
Synth Reaction	k_1 (1/s)	V_{max} (mM/s)	k_1 (1/s)	V_{max} (mM/s)
Synth 3-Dehydroquinate	0	0	0	0
Synth Chorismate	0.0007	0.0013	0.0014	0.0028
Synth Prephenate	0	0	0	0
Synth *L*-Tyrosine	0	0	0	0
Synth Phenylpyruvate	0	0	0	0

Appendix 2 – V_{max} values calculated for the reactions necessary to produce L-Tyr and L-Phe for all 108 models (continuation).

	TyrOpt_1A_Bi_b	**TyrOpt_1A_Bii_b**	**TyrOpt_1B_Bi_b**	**TyrOpt_1B_Bii_b**
Reaction	V_{max} (mM/s)	V_{max} (mM/s)	V_{max} (mM/s)	V_{max} (mM/s)
AroF/G/H (AroF)	0.3135	0.3135	0.3135	0.3135
AroF/G/H (AroG)	1.3428	1.3428	1.3428	1.3428
AroF/G/H (AroH)	0.0291	0.0291	0.0291	0.0291
AroB	0.0150	0.0150	0.0150	0.0150
AroD	0.0171	0.0171	0.0171	0.0171
YdiB/AroE	0.1153	0.1153	0.1153	0.1153
AroK/L	0.0600	0.0600	0.0600	0.0600
AroA	0.1709	0.1709	0.1709	0.1709
AroC	0.0144	0.0144	0.0144	0.0144
TyrA/PheA	0.0158	0.0158	0.0158	0.0158
TyrA	0.0060	0.0060	0.0060	0.0060
TyrB_Tyr	0.4367	0.4367	0.4367	0.4367
PheA	0.0109	0.0109	0.0109	0.0109
TyrB_Phe	0.4858	0.4858	0.4858	0.4858
Synth Reaction	k_1 (1/s)	V_{max} (mM/s)	k_1 (1/s)	V_{max} (mM/s)
Synth 3-Dehydroquinate	0	0	0	0
Synth Chorismate	0.0022	0.0044	0.0022	0.0044
Synth Prephenate	0	0	0	0
Synth *L*-Tyrosine	8.43 E-06	1.69 E-05	8.43 E-06	1.69 E-05
Synth Phenylpyruvate	0	0	0	0

Appendix 2 – V_{max} values calculated for the reactions necessary to produce L-Tyr and L-Phe for all 108 models (continuation).

	TyrOpt_1A_Ti_b	**TyrOpt_1A_Tii_b**	**TyrOpt_1B_Ti_b**	**TyrOpt_1B_Tii_b**
Reaction	V_{max} (mM/s)	V_{max} (mM/s)	V_{max} (mM/s)	V_{max} (mM/s)
AroF/G/H (AroF)	1.8730	1.8730	1.8730	1.8730
AroF/G/H (AroG)	8.0230	8.0230	8.0230	8.0230
AroF/G/H (AroH)	0.1739	0.1739	0.1739	0.1739
AroB	0.0896	0.0896	0.0896	0.0896
AroD	0.1022	0.1022	0.1022	0.1022
YdiB/AroE	0.6888	0.6888	0.6888	0.6888
AroK/L	0.3582	0.3582	0.3582	0.3582
AroA	1.0209	1.0209	1.0209	1.0209
AroC	0.0862	0.0862	0.0862	0.0862
TyrA/PheA	0.1090	0.1090	0.1090	0.1090
TyrA	0.0896	0.0896	0.0896	0.0896
TyrB_Tyr	6.5081	6.5081	6.5081	6.5081
PheA	0.0098	0.0098	0.0098	0.0098
TyrB_Phe	0.4373	0.4373	0.4373	0.4373
Synth Reaction	k_1 (1/s)	V_{max} (mM/s)	k_1 (1/s)	V_{max} (mM/s)
Synth 3-Dehydroquinate	0	0	0	0
Synth Chorismate	0.0020	0.0039	0.0020	0.0039
Synth Prephenate	0	0	0	0
Synth *L*-Tyrosine	7.58 E-06	1.52 E-05	7.58 E-06	1.52 E-05
Synth Phenylpyruvate	0	0	0	0

Appendix 2 – V_{max} values calculated for the reactions necessary to produce L-Tyr and L-Phe for all 108 models (continuation).

	TyrOpt_1A_Ci_b	**TyrOpt_1A_Cii_b**	**TyrOpt_1B_Ci_b**	**TyrOpt_1B_Cii_b**
Reaction	V_{max} (mM/s)	V_{max} (mM/s)	V_{max} (mM/s)	V_{max} (mM/s)
AroF/G/H (AroF)	1.8730	1.8730	1.8730	1.8730
AroF/G/H (AroG)	8.0230	8.0230	8.0230	8.0230
AroF/G/H (AroH)	0.1739	0.1739	0.1739	0.1739
AroB	0.0896	0.0896	0.0896	0.0896
AroD	0.1022	0.1022	0.1022	0.1022
YdiB/AroE	0.6888	0.6888	0.6888	0.6888
AroK/L	0.3582	0.3582	0.3582	0.3582
AroA	1.0209	1.0209	1.0209	1.0209
AroC	0.0862	0.0862	0.0862	0.0862
TyrA/PheA	0.0143	0.0143	0.0143	0.0143
TyrA	0.0054	0.0054	0.0054	0.0054
TyrB_Tyr	0.3930	0.3930	0.3930	0.3930
PheA	0.0098	0.0098	0.0098	0.0098
TyrB_Phe	0.4373	0.4373	0.4373	0.4373
Synth Reaction	k_1 (1/s)	V_{max} (mM/s)	k_1 (1/s)	V_{max} (mM/s)
Synth 3-Dehydroquinate	0	0	0	0
Synth Chorismate	0.0020	0.0039	0.0020	0.0039
Synth Prephenate	0	0	0	0
Synth *L*-Tyrosine	7.58 E-06	1.52 E-05	7.58 E-06	1.52 E-05
Synth Phenylpyruvate	0	0	0	0

Appendix 2 – V_{max} values calculated for the reactions necessary to produce L-Tyr and L-Phe for all 108 models (continuation).

	TyrOpt_2A_Bi_b	**TyrOpt_2A_Bii_b**	**TyrOpt_2B_Bi_b**	**TyrOpt_2B_Bii_b**
Reaction	V_{max} (mM/s)	V_{max} (mM/s)	V_{max} (mM/s)	V_{max} (mM/s)
AroF/G/H (AroF)	0.8472	0.8472	0.8472	0.8472
AroF/G/H (AroG)	3.6290	3.6290	3.6290	3.6290
AroF/G/H (AroH)	0.0787	0.0787	0.0787	0.0787
AroB	0.0405	0.0405	0.0405	0.0405
AroD	0.0462	0.0462	0.0462	0.0462
YdiB/AroE	0.3115	0.3115	0.3115	0.3115
AroK/L	0.1620	0.1620	0.1620	0.1620
AroA	0.4618	0.4618	0.4618	0.4618
AroC	0.0390	0.0390	0.0390	0.0390
TyrA/PheA	0.0428	0.0428	0.0428	0.0428
TyrA	0.0162	0.0162	0.0162	0.0162
TyrB_Tyr	1.1802	1.1802	1.1802	1.1802
PheA	0.0295	0.0295	0.0295	0.0295
TyrB_Phe	1.3131	1.3131	1.3131	1.3131
Synth Reaction	k_1 (1/s)	V_{max} (mM/s)	k_1 (1/s)	V_{max} (mM/s)
Synth 3-Dehydroquinate	0	0	0	0
Synth Chorismate	0.0059	0.0118	0.0059	0.0118
Synth Prephenate	0	0	0	0
Synth *L*-Tyrosine	2.28 E-05	4.55 E-05	2.28 E-05	4.55 E-05
Synth Phenylpyruvate	0	0	0	0

Appendix 2 – V_{max} values calculated for the reactions necessary to produce L-Tyr and L-Phe for all 108 models (continuation).

	TyrOpt_2A_Ti_b	**TyrOpt_2A_Tii_b**	**TyrOpt_2B_Ti_b**	**TyrOpt_2B_Tii_b**
Reaction	V_{max} (mM/s)	V_{max} (mM/s)	V_{max} (mM/s)	V_{max} (mM/s)
AroF/G/H (AroF)	3.6386	3.6386	3.6386	3.6386
AroF/G/H (AroG)	15.5862	15.5862	15.5862	15.5862
AroF/G/H (AroH)	0.3378	0.3378	0.3378	0.3378
AroB	0.1741	0.1741	0.1741	0.1741
AroD	0.1985	0.1985	0.1985	0.1985
YdiB/AroE	1.3380	1.3380	1.3380	1.3380
AroK/L	0.6960	0.6960	0.6960	0.6960
AroA	1.9834	1.9834	1.9834	1.9834
AroC	0.1674	0.1674	0.1674	0.1674
TyrA/PheA	0.2165	0.2165	0.2165	0.2165
TyrA	0.1919	0.1919	0.1919	0.1919
TyrB_Tyr	13.9436	13.9436	13.9436	13.9436
PheA	0.0006	0.0006	0.0006	0.0006
TyrB_Phe	0.0272	0.0272	0.0272	0.0272
Synth Reaction	k_1 (1/s)	V_{max} (mM/s)	k_1 (1/s)	V_{max} (mM/s)
Synth 3-Dehydroquinate	0	0	0	0
Synth Chorismate	0.0001	0.0002	0.0001	0.0002
Synth Prephenate	0	0	0	0
Synth *L*-Tyrosine	4.72 E-07	9.43 E-07	4.72 E-07	9.43 E-07
Synth Phenylpyruvate	0	0	0	0

Appendix 2 – V_{max} values calculated for the reactions necessary to produce L-Tyr and L-Phe for all 108 models (continuation).

	TyrOpt_2A_Ci_b	TyrOpt_2A_Cii_b	TyrOpt_2B_Ci_b	TyrOpt_2B_Cii_b
Reaction	V_{max} (mM/s)	V_{max} (mM/s)	V_{max} (mM/s)	V_{max} (mM/s)
AroF/G/H (AroF)	3.6386	3.6386	3.6386	3.6386
AroF/G/H (AroG)	15.5862	15.5862	15.5862	15.5862
AroF/G/H (AroH)	0.3378	0.3378	0.3378	0.3378
AroB	0.1741	0.1741	0.1741	0.1741
AroD	0.1985	0.1985	0.1985	0.1985
YdiB/AroE	1.3380	1.3380	1.3380	1.3380
AroK/L	0.6960	0.6960	0.6960	0.6960
AroA	1.9834	1.9834	1.9834	1.9834
AroC	0.1674	0.1674	0.1674	0.1674
TyrA/PheA	0.0009	0.0009	0.0009	0.0009
TyrA	0.0003	0.0003	0.0003	0.0003
TyrB_Tyr	0.0244	0.0244	0.0244	0.0244
PheA	0.0006	0.0006	0.0006	0.0006
TyrB_Phe	0.0272	0.0272	0.0272	0.0272
Synth Reaction	k_1 (1/s)	V_{max} (mM/s)	k_1 (1/s)	V_{max} (mM/s)
Synth 3-Dehydroquinate	0	0	0	0
Synth Chorismate	0.0001	0.0002	0.0001	0.0002
Synth Prephenate	0	0	0	0
Synth *L*-Tyrosine	4.72 E-07	9.43 E-07	4.72 E-07	9.43 E-07
Synth Phenylpyruvate	0	0	0	0

Appendix 2 – V_{max} values calculated for the reactions necessary to produce L-Tyr and L-Phe for all 108 models (continuation).

	TyrOpt_3A_Bi_b	**TyrOpt_3A_Bii_b**	**TyrOpt_3B_Bi_b**	**TyrOpt_3B_Bii_b**
Reaction	V_{max} (mM/s)	V_{max} (mM/s)	V_{max} (mM/s)	V_{max} (mM/s)
AroF/G/H (AroF)	0.5858	0.5858	0.5858	0.5858
AroF/G/H (AroG)	2.5092	2.5092	2.5092	2.5092
AroF/G/H (AroH)	0.0544	0.0544	0.0544	0.0544
AroB	0.0280	0.0280	0.0280	0.0280
AroD	0.0320	0.0320	0.0320	0.0320
YdiB/AroE	0.2154	0.2154	0.2154	0.2154
AroK/L	0.1120	0.1120	0.1120	0.1120
AroA	0.3193	0.3193	0.3193	0.3193
AroC	0.0270	0.0270	0.0270	0.0270
TyrA/PheA	0.0260	0.0260	0.0260	0.0260
TyrA	0.0099	0.0099	0.0099	0.0099
TyrB_Tyr	0.7177	0.7177	0.7177	0.7177
PheA	0.0180	0.0180	0.0180	0.0180
TyrB_Phe	0.7998	0.7998	0.7998	0.7998
Synth Reaction	k_1 (1/s)	V_{max} (mM/s)	k_1 (1/s)	V_{max} (mM/s)
Synth 3-Dehydroquinate	0	0	0	0
Synth Chorismate	0.0068	0.0136	0.0068	0.0136
Synth Prephenate	0	0	0	0
Synth *L*-Tyrosine	0	0	0	0
Synth Phenylpyruvate	0	0	0	0

Appendix 2 – V_{max} values calculated for the reactions necessary to produce L-Tyr and L-Phe for all 108 models (continuation).

	TyrOpt_3A_Ti_b	**TyrOpt_3A_Tii_b**	**TyrOpt_3B_Ti_b**	**TyrOpt_3B_Tii_b**
Reaction	V_{max} (mM/s)	V_{max} (mM/s)	V_{max} (mM/s)	V_{max} (mM/s)
AroF/G/H (AroF)	2.3583	2.3583	2.3583	2.3583
AroF/G/H (AroG)	10.1018	10.1018	10.1018	10.1018
AroF/G/H (AroH)	0.2190	0.2190	0.2190	0.2190
AroB	0.1128	0.1128	0.1128	0.1128
AroD	0.1287	0.1287	0.1287	0.1287
YdiB/AroE	0.8672	0.8672	0.8672	0.8672
AroK/L	0.4511	0.4511	0.4511	0.4511
AroA	1.2855	1.2855	1.2855	1.2855
AroC	0.1085	0.1085	0.1085	0.1085
TyrA/PheA	0.1325	0.1325	0.1325	0.1325
TyrA	0.1057	0.1057	0.1057	0.1057
TyrB_Tyr	7.6845	7.6845	7.6845	7.6845
PheA	0.0162	0.0162	0.0162	0.0162
TyrB_Phe	0.7198	0.7198	0.7198	0.7198
Synth Reaction	k_1 (1/s)	V_{max} (mM/s)	k_1 (1/s)	V_{max} (mM/s)
Synth 3-Dehydroquinate	0	0	0	0
Synth Chorismate	0.0061	0.0123	0.0061	0.0123
Synth Prephenate	0	0	0	0
Synth *L*-Tyrosine	0	0	0	0
Synth Phenylpyruvate	0	0	0	0

Appendix 2 – V_{max} values calculated for the reactions necessary to produce L-Tyr and L-Phe for all 108 models (continuation).

	TyrOpt_3A_Ci_b	**TyrOpt_3A_Cii_b**	**TyrOpt_3B_Ci_b**	**TyrOpt_3B_Cii_b**
Reaction	V_{max} (mM/s)	V_{max} (mM/s)	V_{max} (mM/s)	V_{max} (mM/s)
AroF/G/H (AroF)	2.6635	2.6635	2.6635	2.6635
AroF/G/H (AroG)	11.4091	11.4091	11.4091	11.4091
AroF/G/H (AroH)	0.2473	0.2473	0.2473	0.2473
AroB	0.1274	0.1274	0.1274	0.1274
AroD	0.1453	0.1453	0.1453	0.1453
YdiB/AroE	0.9794	0.9794	0.9794	0.9794
AroK/L	0.5094	0.5094	0.5094	0.5094
AroA	1.4518	1.4518	1.4518	1.4518
AroC	0.1226	0.1226	0.1226	0.1226
TyrA/PheA	0.0234	0.0234	0.0234	0.0234
TyrA	0.0089	0.0089	0.0089	0.0089
TyrB_Tyr	0.6459	0.6459	0.6459	0.6459
PheA	0.0162	0.0162	0.0162	0.0162
TyrB_Phe	0.7198	0.7198	0.7198	0.7198
Synth Reaction	k_1 (1/s)	V_{max} (mM/s)	k_1 (1/s)	V_{max} (mM/s)
Synth 3-Dehydroquinate	0	0	0	0
Synth Chorismate	0.0061	0.0123	0.0061	0.0123
Synth Prephenate	0	0	0	0
Synth *L*-Tyrosine	0	0	0	0
Synth Phenylpyruvate	0	0	0	0

Appendix 2 – V_{max} values calculated for the reactions necessary to produce L-Tyr and L-Phe for all 108 models (continuation).

	TyrOpt_1A_Bi_c	**TyrOpt_1A_Bii_c**	**TyrOpt_1B_Bi_c**	**TyrOpt_1B_Bii_c**
Reaction	V_{max} (mM/s)	V_{max} (mM/s)	V_{max} (mM/s)	V_{max} (mM/s)
AroF/G/H (AroF)	0.1487	0.1487	0.1487	0.1487
AroF/G/H (AroG)	0.6371	0.6371	0.6371	0.6371
AroF/G/H (AroH)	0.0138	0.0138	0.0138	0.0138
AroB	0.0071	0.0071	0.0071	0.0071
AroD	0.0081	0.0081	0.0081	0.0081
YdiB/AroE	0.0547	0.0547	0.0547	0.0547
AroK/L	0.0284	0.0284	0.0284	0.0284
AroA	0.0811	0.0811	0.0811	0.0811
AroC	0.0068	0.0068	0.0068	0.0068
TyrA/PheA	0.0075	0.0075	0.0075	0.0075
TyrA	0.0029	0.0029	0.0029	0.0029
TyrB_Tyr	0.2072	0.2072	0.2072	0.2072
PheA	0.0052	0.0052	0.0052	0.0052
TyrB_Phe	0.2305	0.2305	0.2305	0.2305
Synth Reaction	k_1 (1/s)	V_{max} (mM/s)	k_1 (1/s)	V_{max} (mM/s)
Synth 3-Dehydroquinate	0	0	0	0
Synth Chorismate	0.0010	0.0021	0.0010	0.0021
Synth Prephenate	0	0	0	0
Synth *L*-Tyrosine	4.00 E-06	8.00 E-06	4.00 E-06	8.00 E-06
Synth Phenylpyruvate	0	0	0	0

Appendix 2 – V_{max} values calculated for the reactions necessary to produce L-Tyr and L-Phe for all 108 models (continuation).

	TyrOpt_1A_Ti_c	**TyrOpt_1A_Tii_c**	**TyrOpt_1B_Ti_c**	**TyrOpt_1B_Tii_c**
Reaction	V_{max} (mM/s)	V_{max} (mM/s)	V_{max} (mM/s)	V_{max} (mM/s)
AroF/G/H (AroF)	0.1677	0.1677	0.1677	0.1677
AroF/G/H (AroG)	0.7184	0.7184	0.7184	0.7184
AroF/G/H (AroH)	0.0156	0.0156	0.0156	0.0156
AroB	0.0080	0.0080	0.0080	0.0080
AroD	0.0091	0.0091	0.0091	0.0091
YdiB/AroE	0.0617	0.0617	0.0617	0.0617
AroK/L	0.0321	0.0321	0.0321	0.0321
AroA	0.0914	0.0914	0.0914	0.0914
AroC	0.0077	0.0077	0.0077	0.0077
TyrA/PheA	0.0088	0.0088	0.0088	0.0088
TyrA	0.0044	0.0044	0.0044	0.0044
TyrB_Tyr	0.3166	0.3166	0.3166	0.3166
PheA	0.0047	0.0047	0.0047	0.0047
TyrB_Phe	0.2075	0.2075	0.2075	0.2075
Synth Reaction	k_1 (1/s)	V_{max} (mM/s)	k_1 (1/s)	V_{max} (mM/s)
Synth 3-Dehydroquinate	0	0	0	0
Synth Chorismate	0.0009	0.0019	0.0009	0.0019
Synth Prephenate	0	0	0	0
Synth *L*-Tyrosine	3.60 E-06	7.20 E-06	3.60 E-06	7.20 E-06
Synth Phenylpyruvate	0	0	0	0

Appendix 2 – V_{max} values calculated for the reactions necessary to produce L-Tyr and L-Phe for all 108 models (continuation).

	TyrOpt_1A_Ci_c	**TyrOpt_1A_Cii_c**	**TyrOpt_1B_Ci_c**	**TyrOpt_1B_Cii_c**
Reaction	V_{max} (mM/s)	V_{max} (mM/s)	V_{max} (mM/s)	V_{max} (mM/s)
AroF/G/H (AroF)	0.1677	0.1677	0.1677	0.1677
AroF/G/H (AroG)	0.7184	0.7184	0.7184	0.7184
AroF/G/H (AroH)	0.0156	0.0156	0.0156	0.0156
AroB	0.0080	0.0080	0.0080	0.0080
AroD	0.0091	0.0091	0.0091	0.0091
YdiB/AroE	0.0617	0.0617	0.0617	0.0617
AroK/L	0.0321	0.0321	0.0321	0.0321
AroA	0.0914	0.0914	0.0914	0.0914
AroC	0.0077	0.0077	0.0077	0.0077
TyrA/PheA	0.0068	0.0068	0.0068	0.0068
TyrA	0.0026	0.0026	0.0026	0.0026
TyrB_Tyr	0.1865	0.1865	0.1865	0.1865
PheA	0.0047	0.0047	0.0047	0.0047
TyrB_Phe	0.2075	0.2075	0.2075	0.2075
Synth Reaction	k_1 (1/s)	V_{max} (mM/s)	k_1 (1/s)	V_{max} (mM/s)
Synth 3-Dehydroquinate	0	0	0	0
Synth Chorismate	0.0009	0.0019	0.0009	0.0019
Synth Prephenate	0	0	0	0
Synth *L*-Tyrosine	3.60 E-06	7.20 E-06	3.60 E-06	7.20 E-06
Synth Phenylpyruvate	0	0	0	0

Appendix 2 – V_{max} values calculated for the reactions necessary to produce L-Tyr and L-Phe for all 108 models (continuation).

	TyrOpt_2A_Bi_c	**TyrOpt_2A_Bii_c**	**TyrOpt_2B_Bi_c**	**TyrOpt_2B_Bii_c**
Reaction	V_{max} (mM/s)	V_{max} (mM/s)	V_{max} (mM/s)	V_{max} (mM/s)
AroF/G/H (AroF)	0.1486	0.1486	0.1486	0.1486
AroF/G/H (AroG)	0.6365	0.6365	0.6365	0.6365
AroF/G/H (AroH)	0.0138	0.0138	0.0138	0.0138
AroB	0.0071	0.0071	0.0071	0.0071
AroD	0.0081	0.0081	0.0081	0.0081
YdiB/AroE	0.0546	0.0546	0.0546	0.0546
AroK/L	0.0284	0.0284	0.0284	0.0284
AroA	0.0810	0.0810	0.0810	0.0810
AroC	0.0068	0.0068	0.0068	0.0068
TyrA/PheA	0.0075	0.0075	0.0075	0.0075
TyrA	0.0028	0.0028	0.0028	0.0028
TyrB_Tyr	0.2070	0.2070	0.2070	0.2070
PheA	0.0052	0.0052	0.0052	0.0052
TyrB_Phe	0.2303	0.2303	0.2303	0.2303
Synth Reaction	k_1 (1/s)	V_{max} (mM/s)	k_1 (1/s)	V_{max} (mM/s)
Synth 3-Dehydroquinate	0	0	0	0
Synth Chorismate	0.0010	0.0021	0.0010	0.0021
Synth Prephenate	0	0	0	0
Synth *L*-Tyrosine	3.99 E-06	7.99 E-06	3.99 E-06	7.99 E-06
Synth Phenylpyruvate	0	0	0	0

Appendix 2 – V_{max} values calculated for the reactions necessary to produce L-Tyr and L-Phe for all 108 models (continuation).

	TyrOpt_2A_Ti_c	**TyrOpt_2A_Tii_c**	**TyrOpt_2B_Ti_c**	**TyrOpt_2B_Tii_c**
Reaction	V_{max} (mM/s)	V_{max} (mM/s)	V_{max} (mM/s)	V_{max} (mM/s)
AroF/G/H (AroF)	0.1676	0.1676	0.1676	0.1676
AroF/G/H (AroG)	0.7178	0.7178	0.7178	0.7178
AroF/G/H (AroH)	0.0156	0.0156	0.0156	0.0156
AroB	0.0080	0.0080	0.0080	0.0080
AroD	0.0091	0.0091	0.0091	0.0091
YdiB/AroE	0.0616	0.0616	0.0616	0.0616
AroK/L	0.0321	0.0321	0.0321	0.0321
AroA	0.0913	0.0913	0.0913	0.0913
AroC	0.0077	0.0077	0.0077	0.0077
TyrA/PheA	0.0088	0.0088	0.0088	0.0088
TyrA	0.0044	0.0044	0.0044	0.0044
TyrB_Tyr	0.3164	0.3164	0.3164	0.3164
PheA	0.0047	0.0047	0.0047	0.0047
TyrB_Phe	0.2073	0.2073	0.2073	0.2073
Synth Reaction	k_1 (1/s)	V_{max} (mM/s)	k_1 (1/s)	V_{max} (mM/s)
Synth 3-Dehydroquinate	0	0	0	0
Synth Chorismate	0.0009	0.0021	0.0009	0.0021
Synth Prephenate	0	0	0	0
Synth *L*-Tyrosine	3.59 E-06	7.19 E-06	3.59 E-06	7.19 E-06
Synth Phenylpyruvate	0	0	0	0

Appendix 2 – V_{max} values calculated for the reactions necessary to produce L-Tyr and L-Phe for all 108 models (continuation).

	TyrOpt_2A_Ci_c	**TyrOpt_2A_Cii_c**	**TyrOpt_2B_Ci_c**	**TyrOpt_2B_Cii_c**
Reaction	V_{max} (mM/s)	V_{max} (mM/s)	V_{max} (mM/s)	V_{max} (mM/s)
AroF/G/H (AroF)	0.1676	0.1676	0.1676	0.1676
AroF/G/H (AroG)	0.7178	0.7178	0.7178	0.7178
AroF/G/H (AroH)	0.0156	0.0156	0.0156	0.0156
AroB	0.0080	0.0080	0.0080	0.0080
AroD	0.0091	0.0091	0.0091	0.0091
YdiB/AroE	0.0616	0.0616	0.0616	0.0616
AroK/L	0.0321	0.0321	0.0321	0.0321
AroA	0.0913	0.0913	0.0913	0.0913
AroC	0.0077	0.0077	0.0077	0.0077
TyrA/PheA	0.0068	0.0068	0.0068	0.0068
TyrA	0.0026	0.0026	0.0026	0.0026
TyrB_Tyr	0.1863	0.1863	0.1863	0.1863
PheA	0.0047	0.0047	0.0047	0.0047
TyrB_Phe	0.2073	0.2073	0.2073	0.2073
Synth Reaction	k_1 (1/s)	V_{max} (mM/s)	k_1 (1/s)	V_{max} (mM/s)
Synth 3-Dehydroquinate	0	0	0	0
Synth Chorismate	0.0009	0.0021	0.0009	0.0021
Synth Prephenate	0	0	0	0
Synth *L*-Tyrosine	3.59 E-06	7.19 E-06	3.59 E-06	7.19 E-06
Synth Phenylpyruvate	0	0	0	0

Appendix 2 – V_{max} values calculated for the reactions necessary to produce L-Tyr and L-Phe for all 108 models (continuation).

	TyrOpt_3A_Bi_c	TyrOpt_3A_Bii_c	TyrOpt_3B_Bi_c	TyrOpt_3B_Bii_c
Reaction	V_{max} (mM/s)	V_{max} (mM/s)	V_{max} (mM/s)	V_{max} (mM/s)
AroF/G/H (AroF)	0.1495	0.1495	0.1495	0.1495
AroF/G/H (AroG)	0.6403	0.6403	0.6403	0.6403
AroF/G/H (AroH)	0.0139	0.0139	0.0139	0.0139
AroB	0.0072	0.0072	0.0072	0.0072
AroD	0.0082	0.0082	0.0082	0.0082
YdiB/AroE	0.0550	0.0550	0.0550	0.0550
AroK/L	0.0286	0.0286	0.0286	0.0286
AroA	0.0815	0.0815	0.0815	0.0815
AroC	0.0069	0.0069	0.0069	0.0069
TyrA/PheA	0.0066	0.0066	0.0066	0.0066
TyrA	0.0025	0.0025	0.0025	0.0025
TyrB_Tyr	0.1831	0.1831	0.1831	0.1831
PheA	0.0046	0.0046	0.0046	0.0046
TyrB_Phe	0.2041	0.2041	0.2041	0.2041
Synth Reaction	k_1 (1/s)	V_{max} (mM/s)	k_1 (1/s)	V_{max} (mM/s)
Synth 3-Dehydroquinate	0	0	0	0
Synth Chorismate	0.0017	0.0035	0.0017	0.0035
Synth Prephenate	0	0	0	0
Synth *L*-Tyrosine	0	0	0	0
Synth Phenylpyruvate	0	0	0	0

Appendix 2 – V_{max} values calculated for the reactions necessary to produce L-Tyr and L-Phe for all 108 models (continuation).

	TyrOpt_3A_Ti_c	**TyrOpt_3A_Tii_c**	**TyrOpt_3B_Ti_c**	**TyrOpt_3B_Tii_c**
Reaction	V_{max} (mM/s)	V_{max} (mM/s)	V_{max} (mM/s)	V_{max} (mM/s)
AroF/G/H (AroF)	0.1677	0.1677	0.1591	0.1591
AroF/G/H (AroG)	0.7184	0.7184	0.6814	0.6814
AroF/G/H (AroH)	0.0156	0.0156	0.0148	0.0148
AroB	0.0080	0.0080	0.0076	0.0076
AroD	0.0091	0.0091	0.0087	0.0087
YdiB/AroE	0.0617	0.0617	0.0585	0.0585
AroK/L	0.0321	0.0321	0.0304	0.0304
AroA	0.0914	0.0914	0.0867	0.0867
AroC	0.0077	0.0077	0.0073	0.0073
TyrA/PheA	0.0088	0.0088	0.0074	0.0074
TyrA	0.0044	0.0044	0.0036	0.0036
TyrB_Tyr	0.3166	0.3166	0.2591	0.2591
PheA	0.0047	0.0047	0.0041	0.0041
TyrB_Phe	0.2075	0.2075	0.1837	0.1837
Synth Reaction	k_1 (1/s)	V_{max} (mM/s)	k_1 (1/s)	V_{max} (mM/s)
Synth 3-Dehydroquinate	0	0	0	0
Synth Chorismate	0.0016	0.0031	0.0016	0.0031
Synth Prephenate	0	0	0	0
Synth *L*-Tyrosine	0	0	0	0
Synth Phenylpyruvate	0	0	0	0

Appendix 2 – V_{max} values calculated for the reactions necessary to produce L-Tyr and L-Phe for all 108 models (continuation).

	TyrOpt_3A_Ci_c	**TyrOpt_3A_Cii_c**	**TyrOpt_3B_Ci_c**	**TyrOpt_3B_Cii_c**
Reaction	V_{max} (mM/s)	V_{max} (mM/s)	V_{max} (mM/s)	V_{max} (mM/s)
AroF/G/H (AroF)	0.1591	0.1591	0.1591	0.1591
AroF/G/H (AroG)	0.6814	0.6814	0.6814	0.6814
AroF/G/H (AroH)	0.0148	0.0148	0.0148	0.0148
AroB	0.0076	0.0076	0.0076	0.0076
AroD	0.0087	0.0087	0.0087	0.0087
YdiB/AroE	0.0585	0.0585	0.0585	0.0585
AroK/L	0.0304	0.0304	0.0304	0.0304
AroA	0.0867	0.0867	0.0867	0.0867
AroC	0.0073	0.0073	0.0073	0.0073
TyrA/PheA	0.0060	0.0060	0.0060	0.0060
TyrA	0.0023	0.0023	0.0023	0.0023
TyrB_Tyr	0.1648	0.1648	0.1648	0.1648
PheA	0.0041	0.0041	0.0041	0.0041
TyrB_Phe	0.1837	0.1837	0.1837	0.1837
Synth Reaction	k_1 (1/s)	V_{max} (mM/s)	k_1 (1/s)	V_{max} (mM/s)
Synth 3-Dehydroquinate	0	0	0	0
Synth Chorismate	0.0016	0.0031	0.0016	0.0031
Synth Prephenate	0	0	0	0
Synth *L*-Tyrosine	0	0	0	0
Synth Phenylpyruvate	0	0	0	0

Appendix 3 – Observations made and L-Tyr concentration from each kinetic model designed on the study of the impact that different variables have on parameter determination.

Model	Observations	[*L*-Tyr] (mM/L)	[*L*-Tyr] (mg/L)
TyrOpt_1A_Bi_a	*L*-Tyrosine does not stabilise and there is an error at 9844.36s	0.245	44.423
TyrOpt_1A_Bii_a	*L*-Tyrosine does not stabilise and there is an error at 9848.49s	0.235	42.596
TyrOpt_2A_Bi_a	*L*-Tyrosine stabilises and there is no error	0.144	26.101
TyrOpt_2A_Bii_a	*L*-Tyrosine stabilises and there is no error	0.144	26.092
TyrOpt_3A_Bi_a	*L*-Tyrosine stabilises and there is no error	0.162	29.395
TyrOpt_3A_Bii_a	*L*-Tyrosine stabilises and there is no error	0.162	29.386
TyrOpt_1A_Ti_a	*L*-Tyrosine does not stabilise and there is an error at 9832.59s	0.251	45.475
TyrOpt_1A_Tii_a	*L*-Tyrosine does not stabilise and there is an error at 9743.35s	0.243	44.066
TyrOpt_2A_Ti_a	*L*-Tyrosine stabilises and there is an error at 9791.94s	0.270	49.005
TyrOpt_2A_Tii_a	*L*-Tyrosine stabilises and there is an error at 9791.81s	0.270	48.987
TyrOpt_3A_Ti_a	*L*-Tyrosine stabilises and there is no error	0.166	29.987
TyrOpt_3A_Tii_a	*L*-Tyrosine stabilises and there is no error	0.165	29.978
TyrOpt_1A_Ci_a	*L*-Tyrosine does not stabilise and there is no error	0.223	40.343
TyrOpt_1A_Cii_a	*L*-Tyrosine does not stabilise and there is no error	0.216	39.104
TyrOpt_2A_Ci_a	*L*-Tyrosine stabilises and there is no error	0.145	26.275
TyrOpt_2A_Cii_a	*L*-Tyrosine stabilises and there is no error	0.145	26.331
TyrOpt_3A_Ci_a	*L*-Tyrosine stabilises and there is no error	0.160	28.912

Appendix 3 – Observations made and L-Tyr concentration from each kinetic model designed on the study of the impact that different variables have on parameter determination (continuation).

Model	Observations	[*L*-Tyr] (mM/L)	[*L*-Tyr] (mg/L)
TyrOpt_3A_Cii_a	*L*-Tyrosine stabilises and there is no error	0.160	28.977
TyrOpt_1B_Bi_a	*L*-Tyrosine does not stabilise and there is an error at 9844.36s	0.245	44.423
TyrOpt_1B_Bii_a	*L*-Tyrosine does not stabilise and there is an error at 9848.49s	0.235	42.596
TyrOpt_2B_Bi_a	*L*-Tyrosine stabilises and there is no error	0.144	26.101
TyrOpt_2B_Bii_a	*L*-Tyrosine stabilises and there is no error	0.144	26.092
TyrOpt_3B_Bi_a	*L*-Tyrosine stabilises and there is no error	0.162	29.395
TyrOpt_3B_Bii_b	*L*-Tyrosine stabilises and there is no error	0.162	29.386
TyrOpt_1B_Ti_a	*L*-Tyrosine does not stabilise and there is no error	0.221	40.074
TyrOpt_1B_Tii_a	*L*-Tyrosine does not stabilise and there is an error at 9899.62s	0.214	38.773
TyrOpt_2B_Ti_a	*L*-Tyrosine stabilises and there is an error at 9791.94s	0.270	49.005
TyrOpt_2B_Tii_a	*L*-Tyrosine stabilises and there is an error at 9721.81s	0.270	48.987
TyrOpt_3B_Ti_a	*L*-Tyrosine stabilises and there is no error	0.166	29.987
TyrOpt_3B_Tii_a	*L*-Tyrosine stabilises and there is no error	0.165	29.978
TyrOpt_1B_Ci_a	*L*-Tyrosine does not stabilise and there is no error	0.221	40.074
TyrOpt_1B_Cii_a	*L*-Tyrosine does not stabilise and there is an error at 9899.62s	0.214	38.773
TyrOpt_2B_Ci_a	*L*-Tyrosine stabilises and there is no error	0.145	26.275
TyrOpt_2B_Cii_a	*L*-Tyrosine stabilises and there is no error	0.145	26.331

Appendix 3 – Observations made and L-Tyr concentration from each kinetic model designed on the study of the impact that different variables have on parameter determination (continuation).

Model	Observations	[*L*-Tyr] (mM/L)	[*L*-Tyr] (mg/L)
TyrOpt_3B_Ci_a	*L*-Tyrosine stabilises and there is no error	0.158	28.634
TyrOpt_3B_Cii_a	*L*-Tyrosine stabilises and there is no error	0.158	28.640
TyrOpt_1A_Bi_b	*L*-Tyrosine stabilises and there is no error	0.431	78.075
TyrOpt_1A_Bii_b	*L*-Tyrosine stabilises and there is no error	0.431	78.029
TyrOpt_2A_Bi_b	*L*-Tyrosine stabilises and there is an error at 145.747s	0.017	3.108
TyrOpt_2A_Bii_b	*L*-Tyrosine stabilises and there is an error at 144.732s	0.017	3.108
TyrOpt_3A_Bi_b	*L*-Tyrosine stabilises and there is an error at 371.097s	0.019	3.481
TyrOpt_3A_Bii_b	*L*-Tyrosine stabilises and there is an error at 366.645s	0.019	3.481
TyrOpt_1A_Ti_b	*L*-Tyrosine stabilises and there is an error at 61.1497s	0.020	3.671
TyrOpt_1A_Tii_b	*L*-Tyrosine stabilises and there is an error at 61.0875s	0.020	3.671
TyrOpt_2A_Ti_b	*L*-Tyrosine stabilises and there is an error at 36.0282s	0.023	4.143
TyrOpt_2A_Tii_b	*L*-Tyrosine stabilises and there is an error at 36.0271s	0.023	4.143
TyrOpt_3A_Ti_b	*L*-Tyrosine stabilises and there is an error at 52.1449s	0.020	3.629
TyrOpt_3A_Tii_b	*L*-Tyrosine stabilises and there is an error at 52.0143s	0.020	3.629
TyrOpt_1A_Ci_b	*L*-Tyrosine stabilises and there is an error at 49.9199s	0.015	2.808
TyrOpt_1A_Cii_b	*L*-Tyrosine stabilises and there is an error at 49.9199s	0.015	2.808

Appendix 3 – Observations made and L-Tyr concentration from each kinetic model designed on the study of the impact that different variables have on parameter determination (continuation).

Model	Observations	[*L*-Tyr] ($\mathrm{mM/L}$)	[*L*-Tyr] ($\mathrm{mg/L}$)
TyrOpt_2A_Cii_b	*L*-Tyrosine stabilises and there is an error at 28.9382s	0.011	2.005
TyrOpt_3A_Ci_b	*L*-Tyrosine stabilises and there is an error at 41.2039s	0.016	2.877
TyrOpt_3A_Cii_b	*L*-Tyrosine stabilises and there is an error at 41.2041s	0.016	2.877
TyrOpt_1B_Bi_b	*L*-Tyrosine stabilises and there is no error	0.431	78.075
TyrOpt_1B_Bii_b	*L*-Tyrosine stabilises and there is no error	0.431	78.029
TyrOpt_2B_Bi_b	*L*-Tyrosine stabilises and there is an error at 145.747s	0.017	3.108
TyrOpt_2B_Bii_b	*L*-Tyrosine stabilises and there is an error at 144.732s	0.017	3.108
TyrOpt_3B_Bi_b	*L*-Tyrosine stabilises and there is an error at 371.097s	0.019	3.481
TyrOpt_3B_Bii_b	*L*-Tyrosine stabilises and there is an error at 366.645s	0.019	3.481
TyrOpt_1B_Ti_b	*L*-Tyrosine stabilises and there is an error at 61.1497s	0.020	3.671
TyrOpt_1B_Tii_b	*L*-Tyrosine stabilises and there is an error at 61.0875s	0.020	3.671
TyrOpt_2B_Ti_b	*L*-Tyrosine stabilises and there is an error at 36.0282s	0.023	4.143
TyrOpt_2B_Tii_b	*L*-Tyrosine stabilises and there is an error at 36.0271s	0.023	4.143
TyrOpt_3B_Ti_b	*L*-Tyrosine stabilises and there is an error at 52.1449s	0.020	3.629
TyrOpt_3B_Tii_b	*L*-Tyrosine stabilises and there is an error at 52.0143s	0.020	3.629
TyrOpt_1B_Ci_b	*L*-Tyrosine stabilises and there is an error at 49.9199s	0.015	2.808

Appendix 3 – Observations made and L-Tyr concentration from each kinetic model designed on the study of the impact that different variables have on parameter determination (continuation).

Model	Observations	[*L*-Tyr] (mM/L)	[*L*-Tyr] (mg/L)
TyrOpt_2B_Ci_b	*L*-Tyrosine stabilises and there is an error at 28.9382s	0.011	2.005
TyrOpt_2B_Cii_b	*L*-Tyrosine stabilises and there is an error at 28.9382s	0.011	2.005
TyrOpt_3B_Ci_b	*L*-Tyrosine stabilises and there is an error at 41.2039s	0.016	2.877
TyrOpt_3B_Cii_b	*L*-Tyrosine stabilises and there is an error at 41.2041s	0.016	2.877
TyrOpt_1A_Bi_c	*L*-Tyrosine stabilises and there is no error	0.216	39.144
TyrOpt_1A_Bii_c	*L*-Tyrosine stabilises and there is no error	0.216	39.126
TyrOpt_2A_Bi_c	*L*-Tyrosine stabilises and there is no error	0.216	39.112
TyrOpt_2A_Bii_c	*L*-Tyrosine stabilises and there is no error	0.216	39.095
TyrOpt_3A_Bi_c	*L*-Tyrosine stabilises and there is no error	0.193	34.990
TyrOpt_3A_Bii_c	*L*-Tyrosine stabilises and there is no error	0.193	34.979
TyrOpt_1A_Ti_c	*L*-Tyrosine stabilises and there is no error	0.320	57.908
TyrOpt_1A_Tii_c	*L*-Tyrosine stabilises and there is an error at 9472.71s	0.319	57.887
TyrOpt_2A_Ti_c	*L*-Tyrosine stabilises and there is no error	0.319	57.880
TyrOpt_2A_Tii_c	*L*-Tyrosine stabilises and there is an error at 9473.24s	0.319	57.859
TyrOpt_3A_Ti_c	*L*-Tyrosine stabilises and there is an error at 9201.59s	0.316	57.296
TyrOpt_3A_Tii_c	*L*-Tyrosine stabilises and there is an error at 9144.24s	0.315	57.095

Appendix 3 – Observations made and L-Tyr concentration from each kinetic model designed on the study of the impact that different variables have on parameter determination (continuation).

Model	Observations	[*L*-Tyr] ($\mathrm{mM/L}$)	[*L*-Tyr] ($\mathrm{mg/L}$)
TyrOpt_1A_Cii_c	*L*-Tyrosine stabilises and there is no error	0.200	36.152
TyrOpt_2A_Ci_c	*L*-Tyrosine stabilises and there is no error	0.199	36.011
TyrOpt_2A_Cii_c	*L*-Tyrosine stabilises and there is no error	0.199	36.122
TyrOpt_3A_Ci_c	*L*-Tyrosine stabilises and there is no error	0.177	32.119
TyrOpt_3A_Cii_c	*L*-Tyrosine stabilises and there is no error	0.178	32.236
TyrOpt_1B_Bi_c	*L*-Tyrosine stabilises and there is no error	0.216	39.144
TyrOpt_1B_Bii_c	*L*-Tyrosine stabilises and there is no error	0.216	39.126
TyrOpt_2B_Bi_c	*L*-Tyrosine stabilises and there is no error	0.216	39.112
TyrOpt_2B_Bii_c	*L*-Tyrosine stabilises and there is no error	0.216	39.095
TyrOpt_3B_Bi_c	*L*-Tyrosine stabilises and there is no error	0.193	34.990
TyrOpt_3B_Bii_c	*L*-Tyrosine stabilises and there is no error	0.193	34.979
TyrOpt_1B_Ti_c	*L*-Tyrosine stabilises and there is no error	0.320	57.908
TyrOpt_1B_Tii_c	*L*-Tyrosine stabilises and there is an error at 9472.71s	0.319	57.887
TyrOpt_2B_Ti_c	*L*-Tyrosine stabilises and there is no error	0.319	57.880
TyrOpt_2B_Tii_c	*L*-Tyrosine stabilises and there is an error at 9473.24s	0.319	57.859
TyrOpt_3B_Ti_c	*L*-Tyrosine stabilises and there is no error	0.265	48.053

Appendix 3 – Observations made and L-Tyr concentration from each kinetic model designed on the study of the impact that different variables have on parameter determination (continuation).

Model	Observations	[*L*-Tyr] ($\mathrm{mM/L}$)	[*L*-Tyr] ($\mathrm{mg/L}$)
TyrOpt_1B_Ci_c	*L*-Tyrosine stabilises and there is no error	0.199	36.040
TyrOpt_1B_Cii_c	*L*-Tyrosine stabilises and there is no error	0.200	36.152
TyrOpt_2B_Ci_c	*L*-Tyrosine stabilises and there is no error	0.199	36.011
TyrOpt_2B_Cii_c	*L*-Tyrosine stabilises and there is no error	0.199	36.122
TyrOpt_3B_Ci_c	*L*-Tyrosine stabilises and there is no error	0.177	32.119
TyrOpt_3B_Cii_c	*L*-Tyrosine stabilises and there is no error	0.178	32.236

Appendix 4

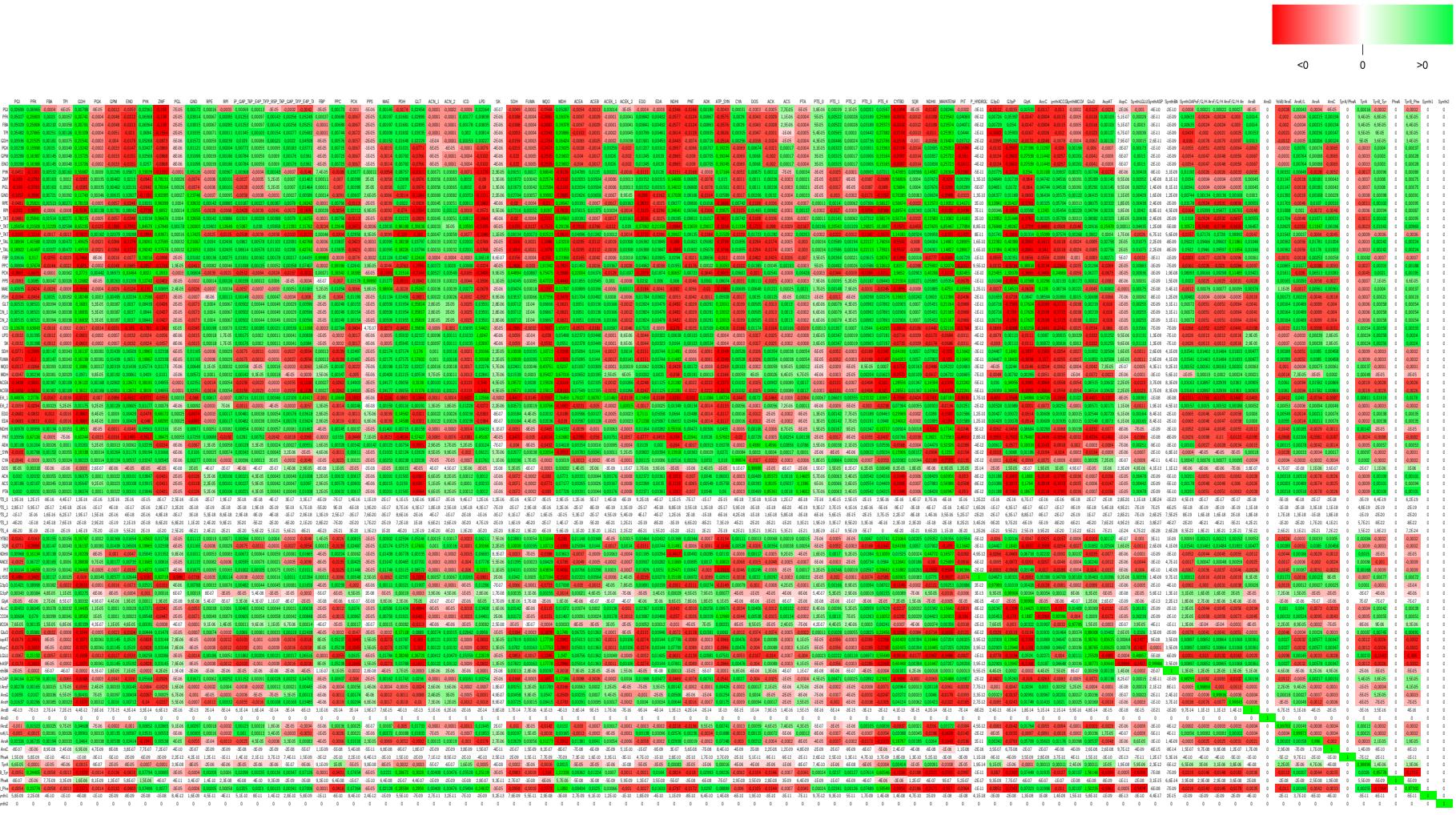

Appendix 4. 1 – Heatmap obtained with the values of Flux Control Coefficients from the Metabolic Course Reaction performed on TyrOpt1_MCA_M0.

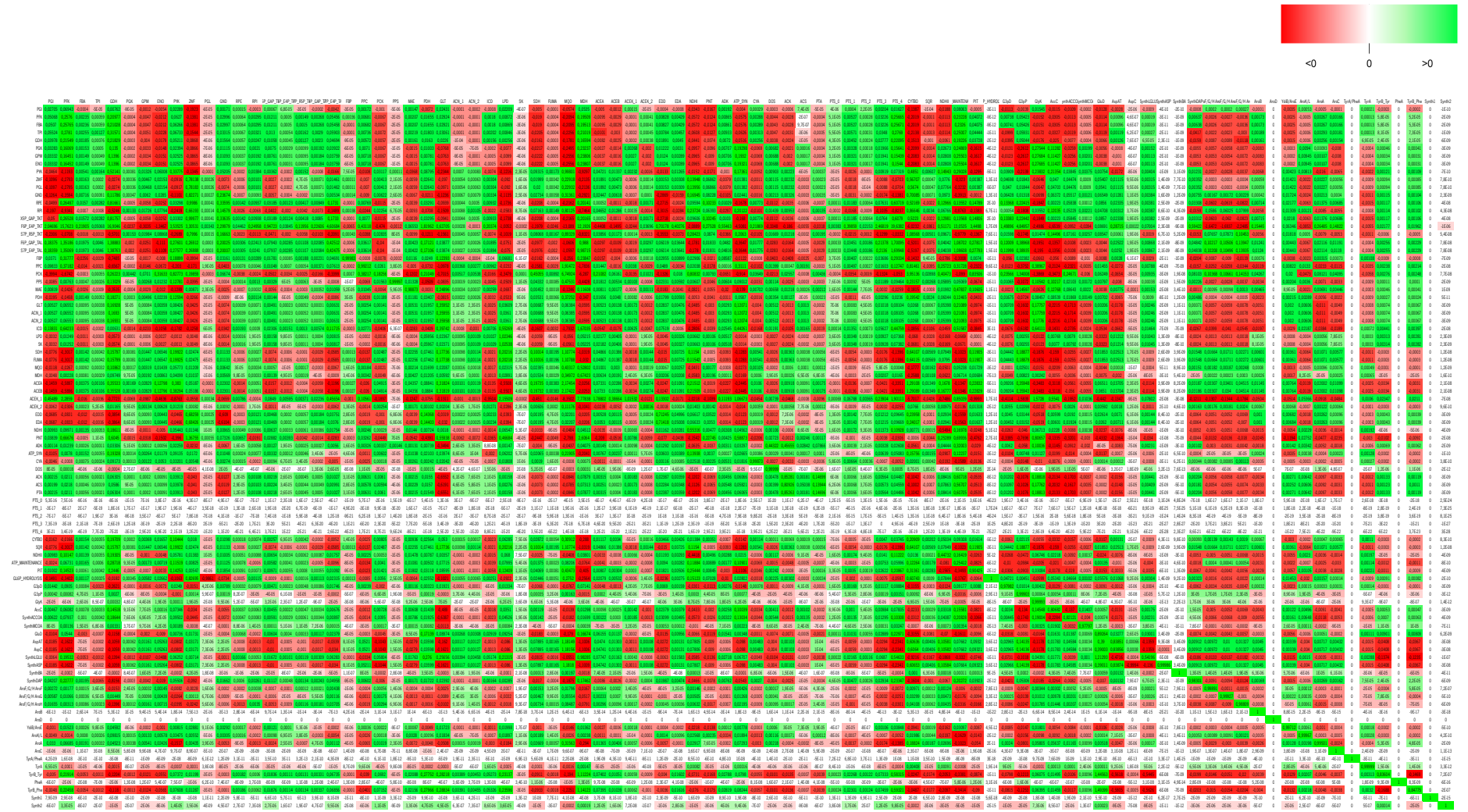

Appendix 4. 2 – Heatmap obtained with the values of Flux Control Coefficients from the Metabolic Course Reaction performed on TyrOpt2_MCA_M0.

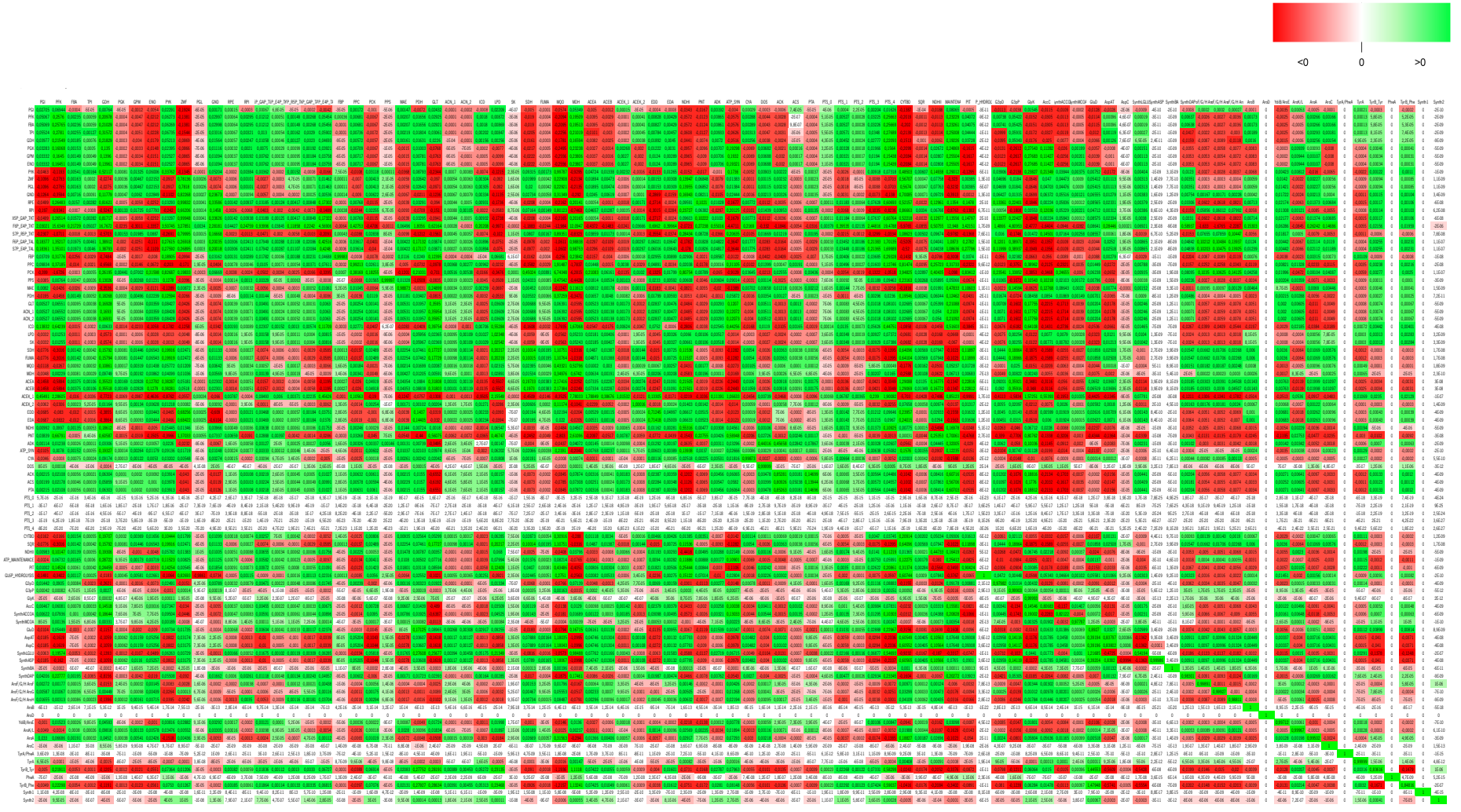

Appendix 4. 3 – Heatmap obtained with the values of Flux Control Coefficients from the Metabolic Course Reaction performed on TyrOpt3_MCA_M0.

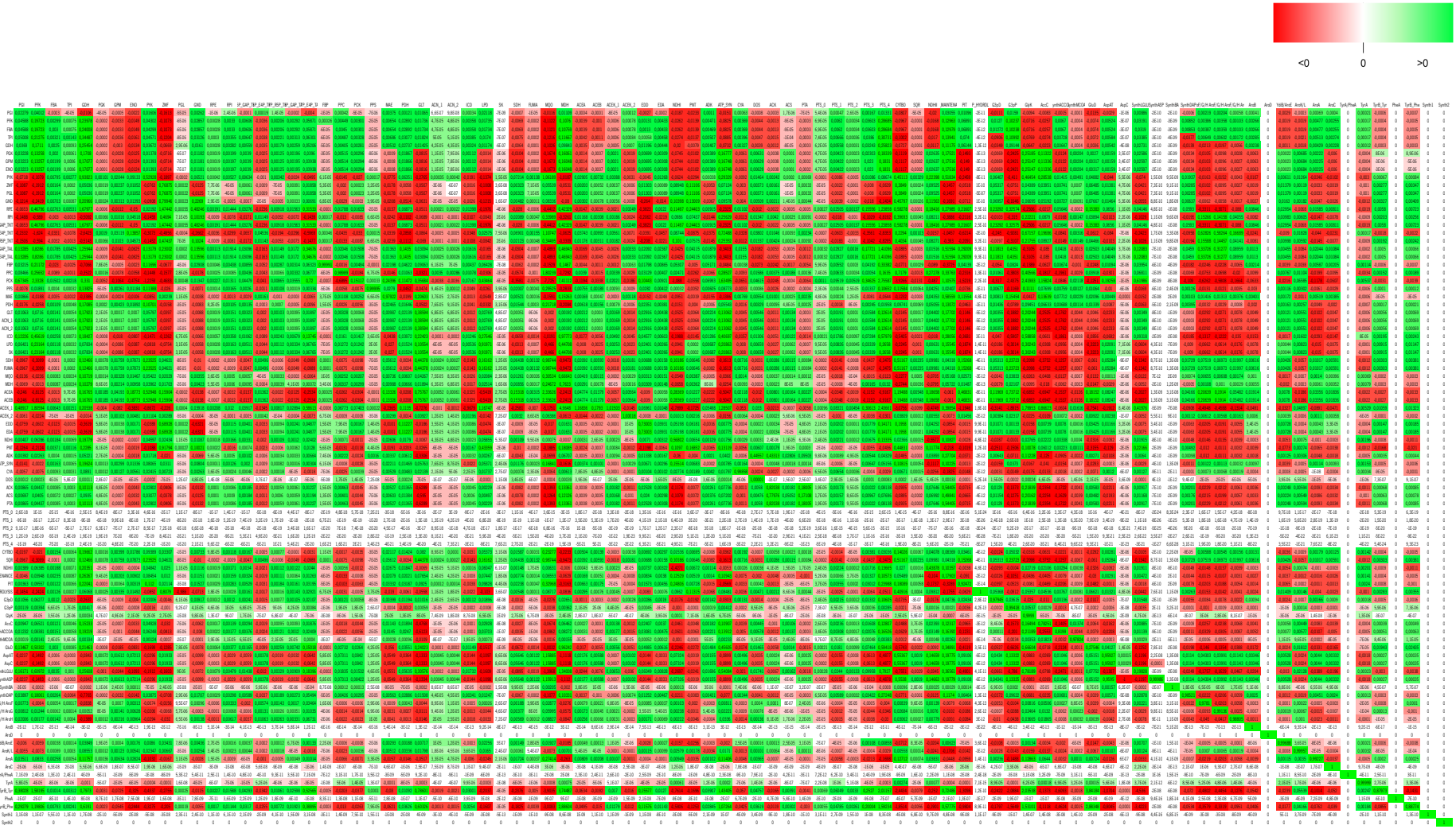

Appendix 4. 4 – Heatmap obtained with the values of Flux Control Coefficients from the Metabolic Course Reaction performed on TyrOpt1_MCA_M1.

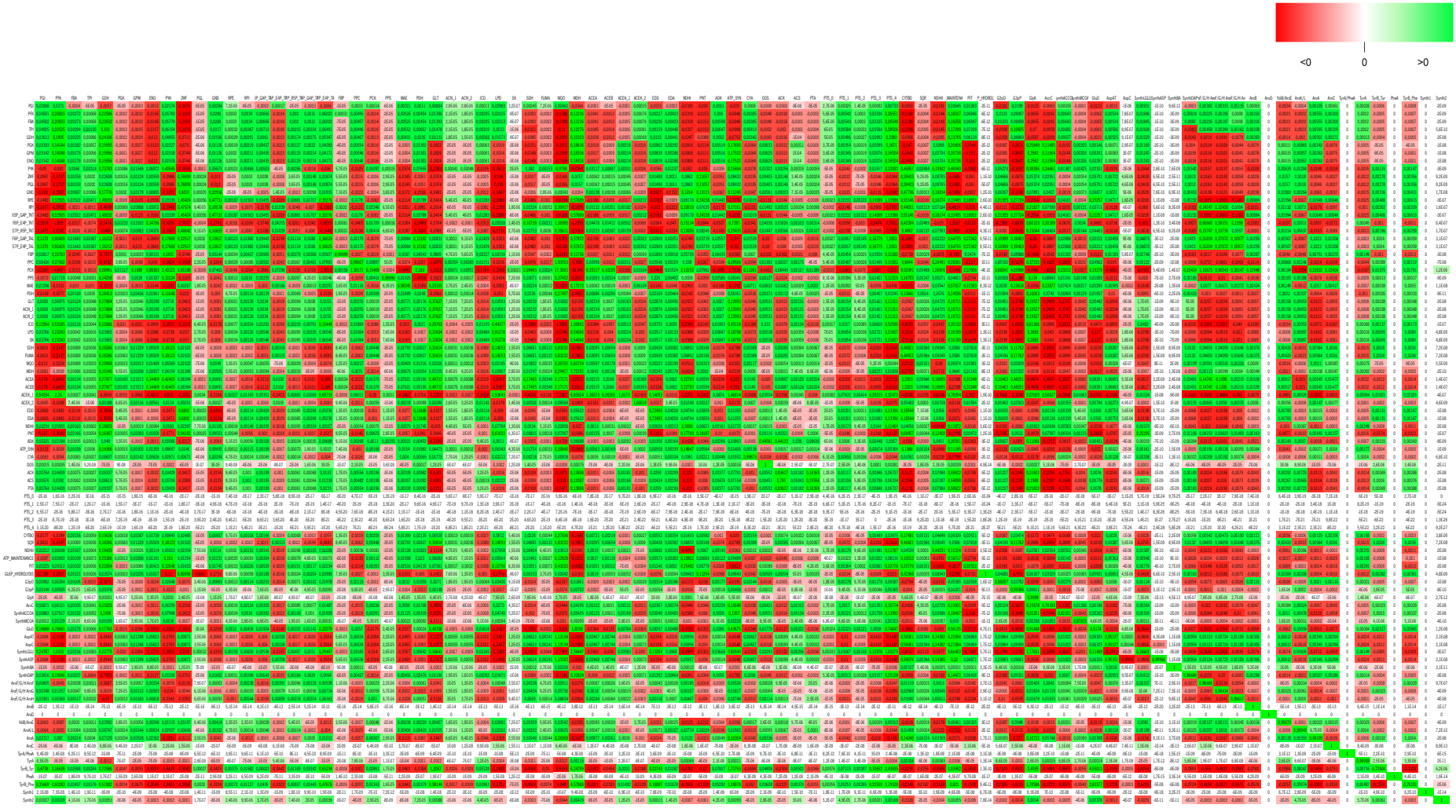

Appendix 4. 5 – Heatmap obtained with the values of Flux Control Coefficients from the Metabolic Course Reaction performed on TyrOpt2_MCA_M1.

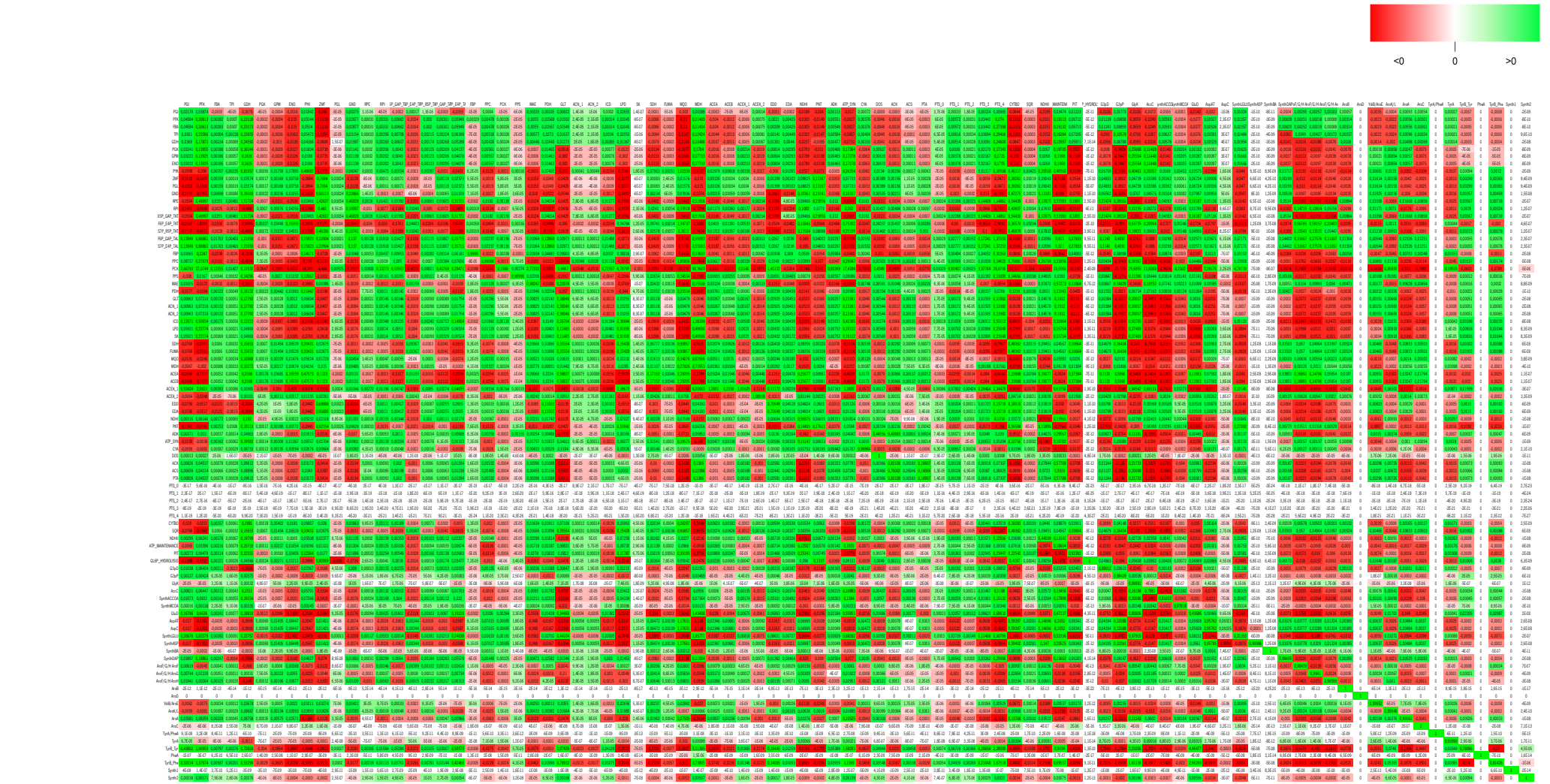

Appendix 4. 6 – Heatmap obtained with the values of Flux Control Coefficients from the Metabolic Course Reaction performed on TyrOpt3_MCA_M1.

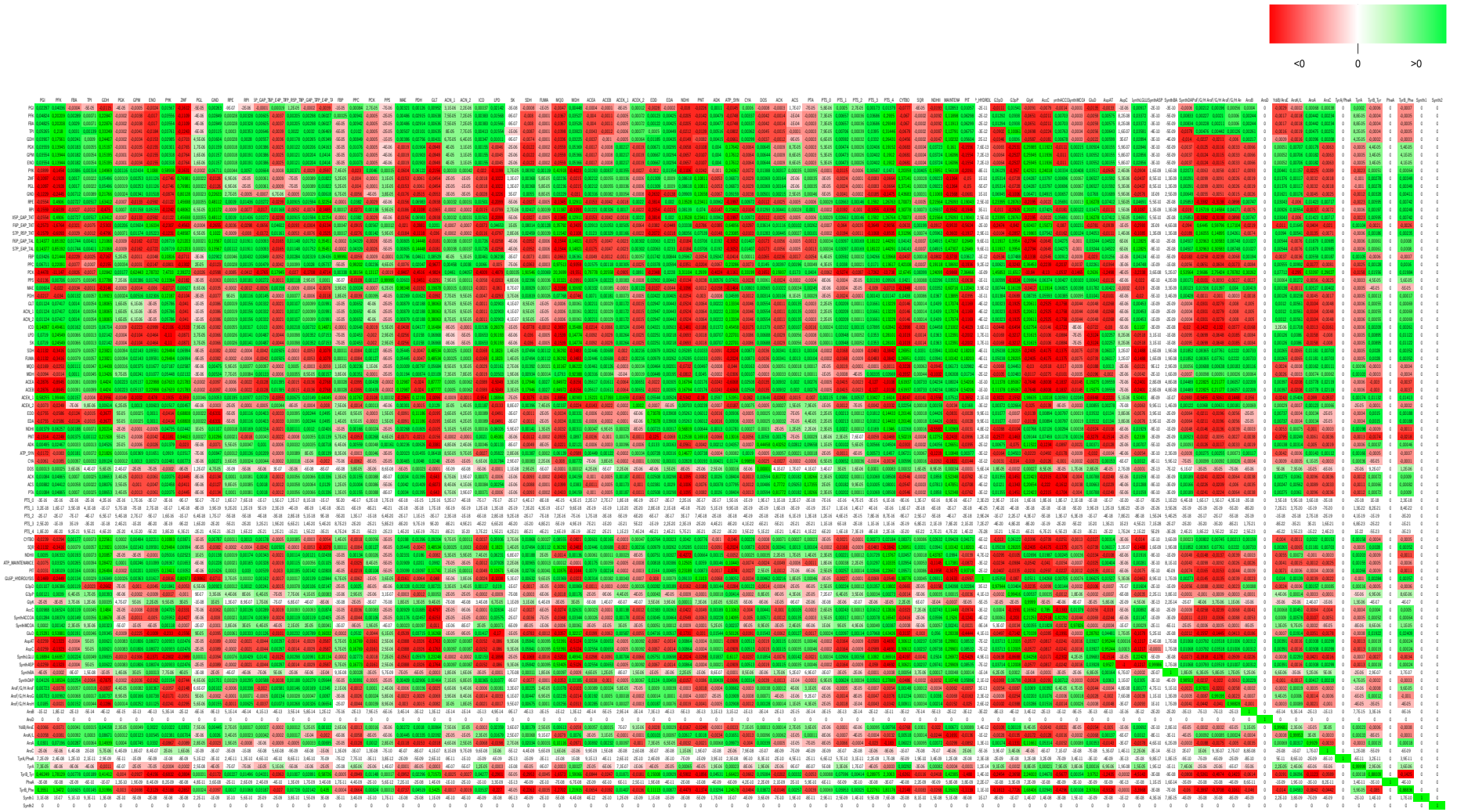

Appendix 4. 7 – Heatmap obtained with the values of Flux Control Coefficients from the Metabolic Course Reaction performed on TyrOpt1_MCA_M2.

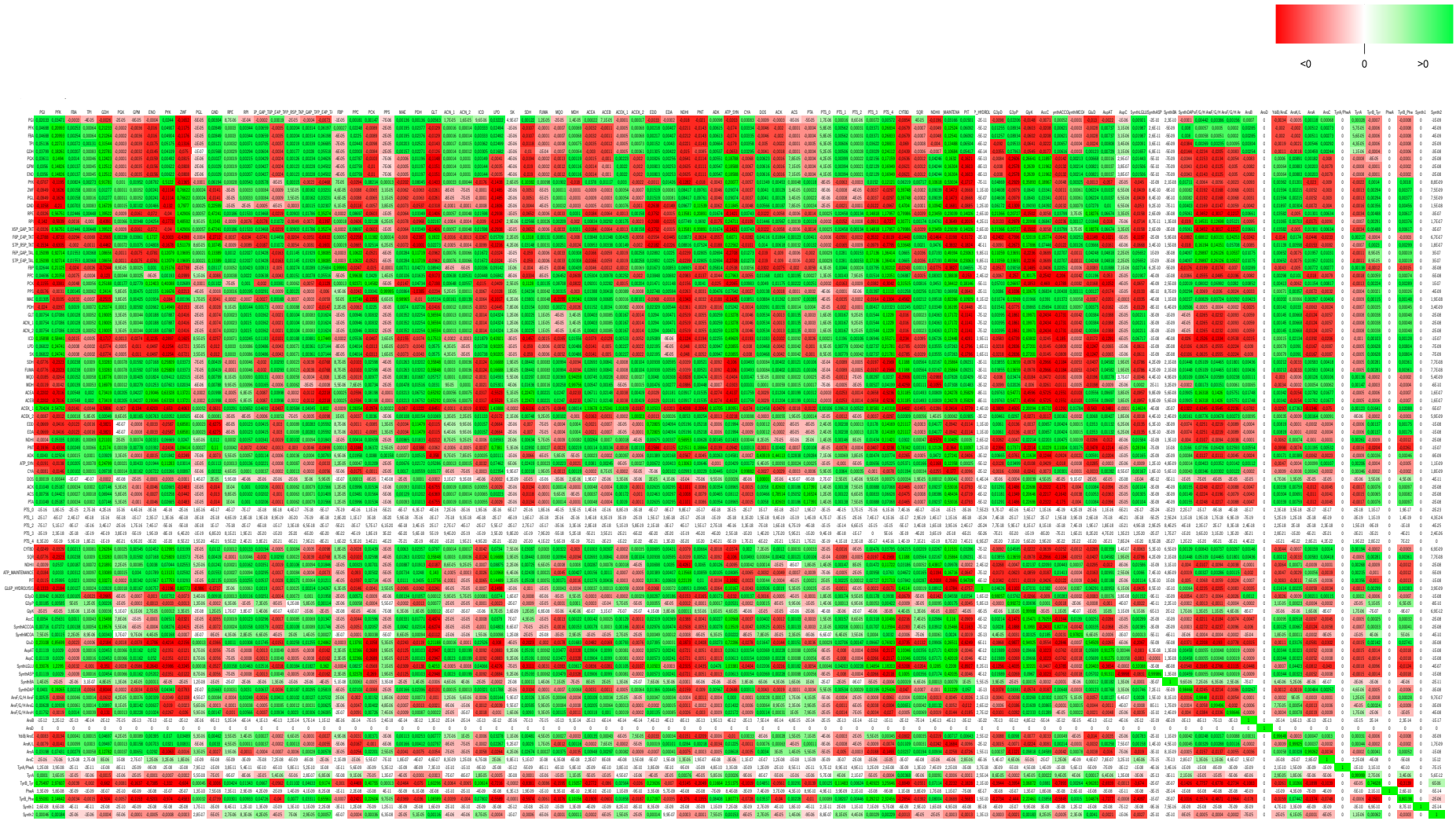

Appendix 4. 8 – Heatmap obtained with the values of Flux Control Coefficients from the Metabolic Course Reaction performed on TyrOpt2_MCA_M2.

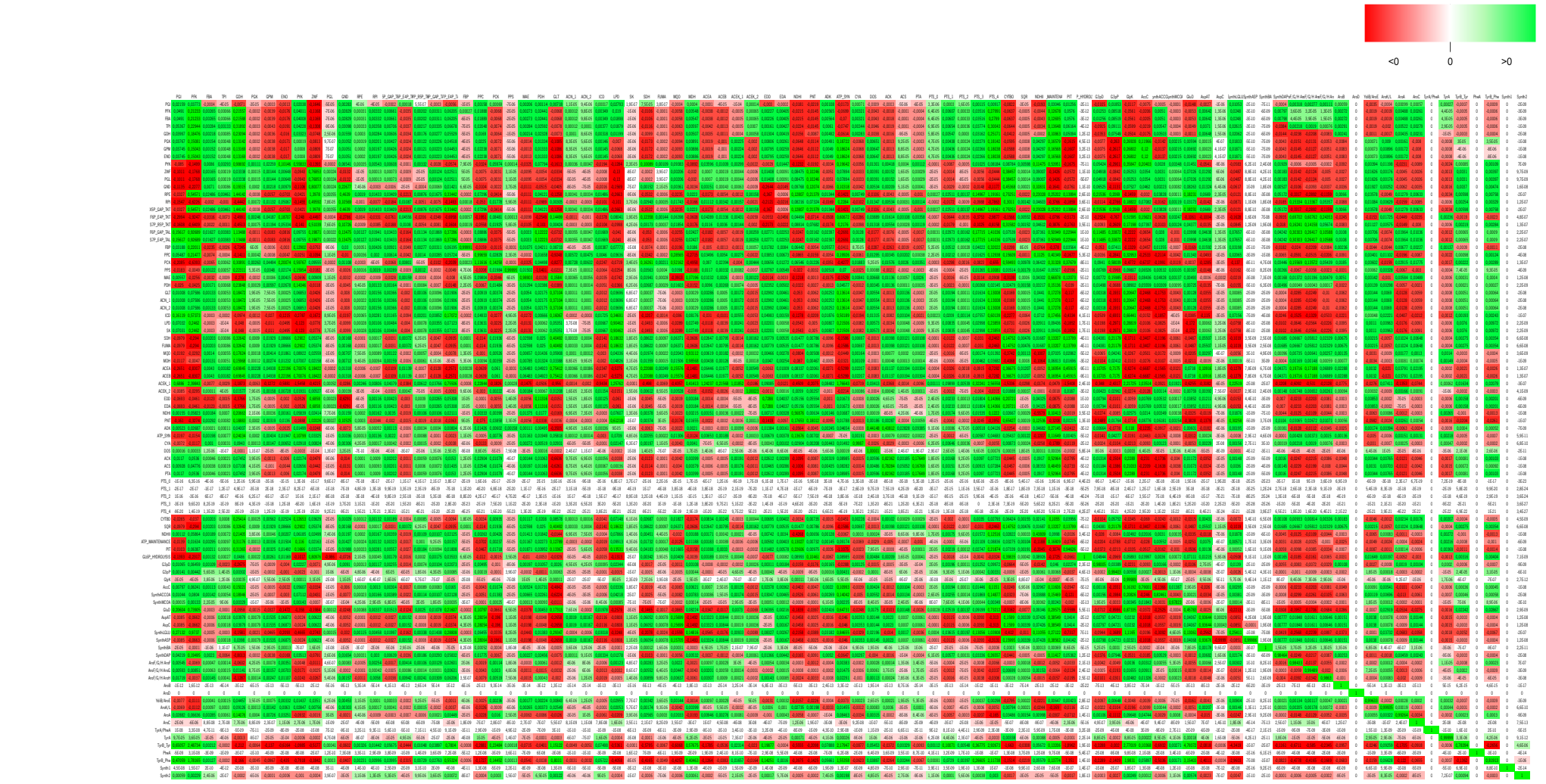

Appendix 4. 9 – Heatmap obtained with the values of Flux Control Coefficients from the Metabolic Course Reaction performed on TyrOpt3_MCA_M2.